Survival Thresholds for Convex Renewal Under Non-Ergodic Dynamics

A GameStop Case Study (2021–2025)

Carlos O. Hunter

carlosohunter.com
carlos@ontologiclabs.com

Ontologic Labs
ontologiclabs.com

Faculty of Physics, University of Barcelona

May 3, 2026

MANUSCRIPT DRAFT

Abstract

GameStop shareholders have held for five years through a stock split, multiple equity offerings, and sustained ridicule. They are regarded widely as irrational by conventional finance. The community's thesis centres on an extreme rare-regime payoff of unknown timing, and participants must survive the wait to obtain it. In multiplicative dynamics with absorbing exit, the cost of waiting can destroy a position before the payoff arrives, framing the operative question: whether persistence is *time-rational*, meaning whether time-average growth stays nonnegative through the wait. For a rare structural event that has not resolved, the success probability cannot be credibly estimated. Kelly optimization therefore requires an input the data cannot supply, and a relevant object is the zero-growth contour: the boundary of the viable region. The *survival threshold* applies this contour to repeated option renewal, where implied volatility jointly determines burn rate, payoff leverage, and touch probability, yielding the minimum success probability below which the gamble destroys time-average wealth. That probability is never directly observed. Evaluated against daily GME data from January 2021 through December 2025, the ergodicity wedge (the realised Jensen gap between arithmetic and geometric returns) concentrates sharply, with two burst episodes spanning roughly 8% of trading days accounting for approximately 59% of cumulative compounding drag. Because Black–Scholes maps higher IV to a more expensive call at the same strike, the survival threshold is highest when options cost the most. Under static implied volatility and zero physical log-drift (median-neutral: the median price path is flat, but level drift is positive; the window vanishes under risk-neutral drift and widens under positive drift), the comparison between Black–Scholes renewal cost and the model-implied touch probability produces a bounded growth-positive region for call renewal at high IV, with the onset shifting by tenor and sizing; this is a structural benchmark that depends on the assumed physical diffusion, static volatility, zero frictions, and renewal convention. Risk-neutral pricing holds under the pricing measure; positive time-average growth arises under the specified physical hitting probabilities. Realised IV is not static, but near-term GME contracts traded at IVs exceeding 1,000% during the January 2021 burst, inside the weekly static-IV growth-positive window, while at the IV levels prevailing over the rest of the five-year period the static benchmark is negative at every tenor. The participation ecology operates through two channels—direct shareholding and registration that lower exit hazard, and repeated short-dated call purchases—sustained by a decentralised community. The social account is interpretive; the formal results are invariant to it. Claims are separated into four evidentiary tiers. The survival threshold applies wherever wealth is multiplicative and exit is absorbing; the renewal margin additionally requires a feasibility model. GameStop supplies the test case; the structural conditions are not unique to it.

Contents

1 Introduction

In late 2020, GameStop (GME) carried reported short interest exceeding 100% of its free float. In January 2021, a broad surge of retail buying—catalysed in part by the publicly shared analysis of Keith Gill, known by the artistic name Roaring Kitty[1]—sent the stock from roughly $5 to an after-hours high near $500 (pre-split) over approximately three weeks; the SEC

[1] Not a cat.

staff report attributes the move primarily to buying pressure and intermediary constraints rather than to confirmed short covering [9]. On January 28, multiple brokers restricted buying [46], and the price collapsed. The community's thesis—referred to internally as "MOASS" (Mother of All Short Squeezes)—is that the squeeze was incomplete: that although reported short interest fell back to conventional levels, obligation-like exposure persists in forms not fully captured by standard reporting, and that a second, larger repricing is structurally possible if effective supply is sufficiently constrained when a catalyst arrives. Appendix A details the mechanism.

Five years on, the shareholders are still here—evidenced by issuer-reported DRS (Direct Registration System) counts, sustained options activity, and continued community participation—through a 4:1 stock split, multiple at-the-market equity offerings, adverse price action, and sustained media scepticism and ridicule. The community's collective infrastructure has persisted through platform disruptions, internal conflicts, and regulatory attention. Conventional finance can explain why people entered; those who stayed are *regarded* widely as irrational. Expectation-based ranking becomes unreliable once a rare-regime payoff enters the picture. What remains is a different question: what does it cost to stay in long enough—in compounding drag, premium burn, and survival capacity—for the rare payoff to have a chance of arriving? The structural conditions, in their view, remain intact, and the community sustains the wait. We ask what it costs to hold that belief through time, in an environment that is effectively non-ergodic for bounded participants: wealth evolves multiplicatively, and exit is absorbing at the agent level.[2]

Infinities and ranking collapse. The St. Petersburg paradox isolates the core difficulty: when a gamble's expected value is dominated by a rare tail, the expectation criterion becomes unreliable for participants constrained by time and survival.[3] A payoff story dominated by a rare jackpot produces long realised stretches in which the jackpot does not arrive. Under multiplicative dynamics, those stretches are costly: remaining exposed through *not-yet time* carries compounding drag and a persistent risk of forced exit. *Diamond hands*, anti-selling norms, and direct registration practices address the core difficulty: staying exposed is nontrivial. Once MOASS is assigned positive probability, expectation-based ranking among nonzero-exposure tactics becomes uninformative: many strategies inherit the same tail-dominated payoff story, so finite differences in premia, leverage, or implementation details no longer separate them on expected-value grounds. The relevant comparative question shifts from expected payoff to *time-embedded performance*: persistence, participation costs, and exposure survival along a realised path [4, 5, 6]. Not everyone in the GME ecology assigns positive probability to the rare regime (the constraint-dominant repricing described above as MOASS). We distinguish *tail-concerned shareholders*: participants who assign decision-relevant probability to the rare regime and evaluate tactics accordingly [14, 15]. Community artefacts sometimes make the unbounded-tail intuition explicit.[4] Within this group, members differ in how much, if at all, they burn on short-dated call renewal, how large they estimate the conditional payoff to be, and how exposed they are to absorbing exit—margin calls, brokerage risks, capital depletion. In a non-ergodic setting these differences govern access: what matters along a realised path can diverge sharply from what an ensemble average would suggest [4].

Two channels and collective infrastructure. In practice, the ecology operates through two participation channels. Buying and holding shares, and the direct registration of those shares, form a *slow persistence channel*—they plausibly lower exit hazard and extend exposure survival. Repeated purchases of short-dated call options form a *fast renewal channel*—participants pay theta to maintain convex access to the conditional payoff [8]. Both channels may serve the same rare-regime thesis, but they carry different costs: *theta burn* (the explicit premium for short-dated convex exposure) and the *ergodicity wedge* (a realised Jensen gap between arithmetic and log returns that measures the implicit compounding penalty of remaining exposed through high-dispersion periods [4, 7]). When dispersion is high—when time is expensive—the *survival threshold* for call renewal rises: the minimum success probability at which repeated buying still grows time-average wealth. Dispersion and implied volatility move together: when IV is elevated, the premium burn per renewal increases, time is expensive, and the cost of each renewal cycle is highest. The wedge measures a separate compounding penalty on the equity sleeve, but the call survival threshold is driven by the burn rate and the conditional payoff multiple.

Shared infrastructure is a plausible account of why participants stayed. The community developed practices associated with preserving shareholding through perceived intermediary and systemic risks: direct registration to remove shares from street-name custody, and holding norms that reduce voluntary exit (Section 5). Without these, individual attrition would plausibly have been faster; with them, people held long enough for time costs—premium burn and compounding drag—to become the binding constraint rather than loss of conviction.

The survival threshold. Standard Kelly optimization maximises growth given a known success probability; when the success probability cannot be credibly estimated—as with a rare structural event that has not resolved—Kelly optimization requires an input the data cannot supply, and the relevant object is the zero-growth contour itself: the boundary between configurations that survive repeated play and those that do not. GameStop is the natural test case because the probability of the rare regime is not credibly estimable by any party: The survival threshold surface (Section 3) maps this contour across strike, sizing, and payoff leverage, producing a landscape that tells a participant what call renewal costs at any configuration. Any model that assigns a conditional probability to the payoff event occurring within the option's life can be evaluated against the threshold

[2] An observable is ergodic if its time average along a single realised trajectory equals its expectation value taken over an ensemble of hypothetical realisations. In many economic settings—especially those involving growth and compounding—wealth is non-ergodic, so ensemble expectations do not describe what happens to a typical individual over time. See Peters [4].

[3] The St. Petersburg paradox concerns gambles with divergent expected payoff for which expectation-based decision criteria become ill-posed. Modern treatments embed such gambles in time and evaluate time-average growth rates rather than ensemble averages; see Peters [3, 4]. The intuition also appears in community artefacts, including a publicly available web game (http://sirlondon.com/) that presents itself as entertainment with unbounded price dynamics.

[4] A prominent example is https://gmefloor.com/, which displays an ever-increasing notional floor price. We cite such artefacts only as evidence of how unbounded-tail intuitions are stabilised in community discourse.

surface: the surface determines which contracts are time-rational under that probability and which are not, and the multi-period framework (Section 3.6) generates testable predictions across horizons that can falsify the assumed probability. Evaluated against daily GME data (Section 4), the dispersion cost concentrates: two burst episodes carry the bulk of the compounding drag, and the threshold spikes during the same windows because IV lifts the premium burn. Whether any volatility regime exists where renewal pays for itself at the prevailing IV is a separate theoretical question, addressed in Section 6.

Episode markers. Post-2020 GME is intermittent: long quiet intervals are interrupted by short episodes of extreme activity. We focus on two salient burst episodes—January–March 2021 and May–June 2024—as descriptive anchors. The 2021 episode is anchored to the SEC staff report on early-2021 market structure conditions [9]; a precondition is unusually high reported short interest prior to January 2021 and purchase restrictions at some brokers during the peak [11, 12]. The 2024 episode is anchored to contemporaneous coverage of the May–June 2024 resurgence [27, 28, 29], coinciding with the public reappearance of Roaring Kitty, whose social-media return and disclosed purchases coincided with the 2024 burst. The quantitative analysis does not model his activity as a separate input, but the episode is a primary object of study.

Contribution. The core contribution is a quantitative framework—centred on the survival threshold—that measures what repeated call renewal costs in time-average terms. The threshold is state-dependent: it classifies call renewal as growth-positive or growth-negative given premium burn, conditional payoff magnitude, and the realised compounding penalty. GameStop is the case study; the framework applies wherever agents pay a recurring cost to maintain exposure to rare payoffs. We assemble a real-time constraint stress checklist from four observable gauges: (i) capacity relevance (call open interest scaled by tradeable float), (ii) the expensive-time wedge, (iii) the survival threshold, and (iv) OI persistence across expiry cycles and connect to Peters and Adamou's [1] result that cooperation can be ergodicity-rational even when it is expectation-irrational: the GME ecology exhibits a related structure, with participants producing a public good—collective infrastructure that plausibly lowers exit hazard—through decentralised contributions (Section 7). The formal framework derives the survival threshold (Proposition 1), extends it to correlated multi-period sequences where positive dependence tightens the survival constraint (Proposition 6), shows that the ergodicity wedge and the threshold share the same Jensen-tax structure (Section 3.7), and establishes that a collective relay can sustain arithmetic viability in regimes where individual compounding is time-irrational (Section 3.5). The rationality of leveraged renewal depends on drift, implied volatility, tenor, and sizing, with computable boundaries that shift across regimes.

Structure. The mathematics says what persistence costs (Section 3). The empirics say where those costs concentrated (Section 4). The ethnography describes the collective infrastructure that sustained exposure long enough for the costs to matter (Section 5). The formal results are invariant to the social interpretation, but the case study as a whole draws on all three layers: the community account supplies the mechanism that connects cost structure to observed duration. The order is: time lens and ergodicity wedge (Section 2), survival threshold for convex exposure (Section 3), empirical pattern (Section 4), community infrastructure (Section 5), static renewal margin and asymptotic bounds (Section 6), discussion (Section 7). A reader interested only in the formal results can read Sections 2, 3, and 6 and skip Section 5 entirely; a reader interested in the empirical cost landscape should focus on Sections 4–6; the community account in Section 5 is interpretive and all formal results are stated and proved before it appears.

Scope boundaries. The framework does not assert that the rare regime (MOASS) will occur, does not identify historical feasibility, and does not causally identify the social channel. The survival threshold is derived in closed form, but the success probability it must be compared against is never directly observed. This is a feature of the design: the framework identifies what exposure costs even when the success probability governing the payoff is not directly observable, and maps those costs against publicly available data. Whether the system was historically above or below the threshold at any given moment is deliberately left as a conditional question, parametrised by scenario grids and bounded by the feasibility sandwich (Section 7.10). As Roaring Kitty once remarked, "absence of evidence is not evidence of absence."[5] The natural question is what it costs to remain exposed through time. The constraint mechanism, the coupled externality between the two participation channels, and proxy construction are detailed in Appendices A–C.

Evidentiary architecture. The claims carry different epistemic weight, and we flag the tier explicitly so the reader can track it throughout. *Tier 1 (exact within stated assumptions):* the survival threshold (Proposition 1), the static renewal margin formula (Section 6), asymptotic convergence rates (Proposition 4)—mathematical results whose derivations are exact given their premises. *Tier 2 (measured):* the ergodicity wedge, wedge concentration in burst episodes, survival-threshold scenarios, capacity relevance B_t, risk-neutral touch probabilities, and the repricing state summary—computed from publicly available daily data, independent of the collective-infrastructure interpretation. *Tier 3 (embedded observation):* the community-infrastructure account of Section 5, grounded by issuer-reported DRS counts, options data, and longitudinal participant observation from January 2021 through early 2026. *Tier 4 (theoretical / forward-looking):* the positive-Φ window (a zero-friction, drift-conditional structural benchmark whose full-commitment peak is fragile to transaction costs) and the Kelly-optimal growth-positive region (onset dependent on strike, target, and tenor; Figure 11), more robust to friction; these have not been tested against historical data. Each section's results are tagged to these tiers; where a claim crosses tiers (e.g. the feasibility sandwich combines Tier 1 thresholds with Tier 2 touch probabilities), the crossing is noted. The strongest empirical results run along the intensity axis (wedge concentration, repricing-state clustering); the persistence axis is suggestive and conditional on a noisy daily proxy. The two-channel ecology is observed at low frequency; the claim that the

[5] The aphorism is a standard epistemological principle, widely attributed to Martin Rees and Carl Sagan among others.

Table 1: Principal notation.

Symbol	Meaning	Ref.
Volatility and price		
σ, σ_0, σ_t	implied vol.; entry IV; current IV	§2, 3
σ_c, σ_u	positive-Φ window boundaries	§6
g	physical log-price drift ($g = 0$: zero log drift, our physical baseline; $g = -\sigma^2/2$: risk-neutral)	§6
S, F	stock price; effective free float	§4
Renewal framework		
A_{t+1}	success indicator ($= C_{t+1} I_{t+1}$)	§3
κ, L	burn rate; payoff-to-premium multiple	§3
$\pi^*(\kappa, L)$	survival threshold	§3
P^{touch}	barrier-contact probability	§3
$\Phi(\sigma_0, \sigma_t)$	renewal margin $= P^{\text{touch}} - \pi^*$	§3
$\Phi_{\text{static}}(\sigma)$	static margin ($\sigma_0 = \sigma_t$)	§6
$\tilde{\kappa}$	effective burn rate, mixed portfolio: $\alpha_c\,\kappa$	§3
π^*_{mix}	mixed-portfolio survival threshold (exact, share-equiv.)	§3
f^*	Kelly-optimal commitment fraction	§6
Empirical diagnostics		
$\widehat{\Delta}(t;T)$	ergodicity wedge (rolling Jensen gap)	§2
γ_t	options intensity ($\ln V_t^{\text{opt}}$, log total opt. vol.)†	§4
q_t	persistence proxy (norm. OBV slope)	§3.4
B_t	boundary relevance $= \text{OI}_t^{\text{call}}/F$	§4
$\hat{p}_t^{\text{ign}}$	repricing state summary (classifier score)	§4
Persistence		
h_t	exit hazard	§3.4

†Split-adjusted; construction in Appendix C.

channels complement each other in the specific way the model describes remains interpretive.

2 Time embedding

Volatility compounds. A stock that swings +50% then −50% does not return to where it started—it ends at 75% of where it started. The bigger the swings, the wider the gap between the average return you see and the growth your account actually experiences. We call that gap the ergodicity wedge. When the wedge is large, time is expensive: staying in the trade costs more in compounding drag per unit of calendar time. This section defines the wedge (Tier 1: exact given stated assumptions), computes it from daily returns alone (Tier 2: measured), and maps out when holding GME was cheaper and when it was most costly under dispersion.

Ergodicity economics enforces a discipline: evaluation criteria must match object dynamics [4, 5]. In finance, wealth is multiplicative. Returns compound, losses shrink the base, exit is absorbing (e.g. capital depletion, forced exit). The relevant criterion is wealth compounding along the realised path—what actually happens to a participant's account through time.

Let $R_{t+1} > 0$ be the gross return factor, so that $W_{t+1} = W_t R_{t+1}$. The time-embedded criterion is time-average log growth:

$$\bar{g}_{\log} := \frac{1}{T} \sum_{t=0}^{T-1} \ln R_{t+1}. \tag{1}$$

Unlike expected returns, log growth encodes survivability: without some mechanism that keeps participants in the trade, near-zero outcomes tend to dominate individual trajectories. A tactic is *time-rational* if its time-average log growth rate is non-negative along the realised path; *time-irrational* otherwise. In the renewal model below, "time-rational" refers to nonnegative expected log growth under the stated renewal law, the standard repeated-play proxy for long-run time-average growth.

2.1 The ergodicity wedge

Over a rolling window of T trading days ending at t, define the time-embedded compounding estimate and an arithmetic-mean summary:

$$\widehat{g}_{\text{time}}(t;T) = \frac{1}{T} \sum_{j=0}^{T-1} \ln(1 + r_{t-j}), \tag{2}$$

$$\widehat{g}_{\text{ens}}(t;T) = \ln\left(\frac{1}{T} \sum_{j=0}^{T-1} (1 + r_{t-j}) \right), \tag{3}$$

where r_t is the simple return with $r_t > -1$. The first quantity, $\widehat{g}_{\text{time}}$, measures how wealth actually compounds along the realised path; the second, $\widehat{g}_{\text{ens}}$, is the log of the arithmetic-mean gross return over the same window.[6] Their difference is the realised arithmetic-geometric gap:

$$\widehat{\Delta}(t;T) := \widehat{g}_{\text{ens}}(t;T) - \widehat{g}_{\text{time}}(t;T) \geq 0, \tag{4}$$

with nonnegativity from Jensen's inequality. At leading order, $\widehat{\Delta} \approx \frac{1}{2} \widehat{\text{Var}}_T(r;t)$: the wedge is a realised-dispersion statistic.

A participant who stays exposed through volatile periods compounds wealth along one path. The arithmetic mean of gross returns is always at least as large as the geometric mean, by Jensen's inequality; the gap between them grows with dispersion. The wedge measures this gap: the compounding penalty paid by anyone who lives through the volatility rather than averaging over it. Under multiplicative dynamics with lognormal returns ($\ln R \sim N(\mu, \sigma^2)$), the log of the arithmetic-mean gross return exceeds the mean log return by $\sigma^2/2$ [4, 7]; dispersion is a direct cost of staying exposed.

2.2 "Expensive time": volatility as a compounding cost

When the wedge is large, time is *expensive*: steep compounding penalties for remaining exposed. When near zero, time is cheap. During GameStop's quiet stretches, the wedge is near zero (approximately 0.001, negligible drag). During burst windows (January–March 2021, May–June 2024), the daily wedge (computed over a $T = 20$ trading-day rolling window) rises to roughly 15–70 times baseline depending on the episode—a nontrivial per-day penalty that accumulates over multi-week episodes (Section 4). The ratio compresses at longer T and sharpens at shorter T. But cheap time is not free time: small daily drag compounding over years of quiet holding adds up, and cumulatively the long stretches exact a cost comparable to the bursts themselves.

Premium burn (theta) and the wedge are the two taxes on participation.[7] For call buyers, the survival threshold (Section 3) specifies when the convex gamble can sustain premium burn; the wedge compounds the cost by eroding the wealth base available for future renewal.

Renewal analysis matters because each call purchase repeats the gamble. Repeated call renewal can have $\mathbb{E}[R] > 1$ while $\mathbb{E}[\ln R] < 0$ if premium burn is steady and rare payoffs too infrequent: a strategy profitable under arithmetic-mean evaluation depletes the options sleeve until participants can no longer afford

[6] Or, ensemble-average growth rate in the terminology of Peters [4].
[7] Death and taxes, as it were.

it, because time-average wealth growth is negative. Premium burn drives depletion directly; the wedge compounds it.

Both the survival threshold π^* derived in the next section and the touch probability P^{touch} that measures renewal feasibility depend on the same implied volatility σ. Whether P^{touch} can ever catch π^*—whether the gamble can sustain itself at a single volatility level—is a question Section 6 will address.

Wedge concentration in short calendar windows is expected for any asset with intermittent volatility[8]: the Jensen gap is mechanically large when dispersion spikes and near-zero otherwise. What is not generic is that participants kept showing up for five years between bursts.

3 Survival threshold

Every call option expires. A participant who wants to stay exposed through convex instruments has to keep buying new ones—and most of them may expire worthless. The question is: how often does a rare win need to arrive for the strategy to break even in time-average terms? This section derives that boundary (Proposition 1, Tier 1). Below it, renewal destroys time-average wealth. Above it, renewal is growth-positive. We call this boundary the *survival threshold*.

Holding shares costs dispersion (the wedge from Section 2). Buying short-dated calls costs premium burn—theta eats the position every day the payoff does not arrive. The threshold tells the participant how much burn the strategy can absorb as a function of what each round costs and what the win pays.[9] Its evaluation against empirical configurations follows in Section 4.

The core result is in Sections 3.1–3.2: the renewal model and the survival threshold (Proposition 1). Sections 3.3–3.5 develop the conceptual extensions: intermittent participation, persistence and access for the slow channel, and the collective relay. A reader primarily interested in the empirical results can proceed to Section 4 after Section 3.5. The remaining two subsections are technical: Section 3.6 separates per-round viability from finite-horizon survival and shows how positive dependence tightens the constraint (formal model in Appendix B.5), and Section 3.7 shows that the threshold and the ergodicity wedge share the same Jensen-tax structure.

3.1 A minimal renewal model

Fix a renewal interval (e.g. weekly, biweekly, monthly) over which a participant renews convex exposure by purchasing calls. Let $\kappa \in (0,1)$ denote the fraction of the convex sleeve spent on premium per interval (burn rate), and let $L \geq 1$ denote the gross multiple on that spend conditional on a payoff-relevant success event occurring within the exposure horizon. The convex sleeve's one-interval gross return factor is

$$R^{\text{cx}}_{t+1} = 1 - \kappa + \kappa L\, A_{t+1}, \tag{5}$$

where $A_{t+1} \in \{0,1\}$ indicates whether a payoff-relevant event occurs within the interval. The return is a unit-free gross factor on the convex sleeve's value at the start of each interval—it applies whether the sleeve is denominated in dollars, shares, or any other unit. A losing round returns $1-\kappa$ (the sleeve minus the premium burned) and a winning round returns $1-\kappa+\kappa L$ (the sleeve minus the premium plus L times the premium). Success can be modelled as requiring both (i) a catalyst arrival $C_{t+1} \in \{0,1\}$ (an exogenous trigger—corporate action, regulatory event, or the reappearance of a focal actor) and (ii) market-structure ignition $I_{t+1} \in \{0,1\}$ conditional on the catalyst (positioning, hedging feedback, and float conditions converting the catalyst into a payoff-relevant price move through strikes):

$$A_{t+1} = C_{t+1}\, I_{t+1}. \tag{6}$$

Let $\mathcal{G}_t$ denote the information available at time t. Define the one-interval *success feasibility*:

$$\begin{aligned}\pi^{\text{succ}}_t &:= \Pr(A_{t+1}=1 \mid \mathcal{G}_t) \\ &= \Pr(C_{t+1}=1 \mid \mathcal{G}_t)\ \Pr(I_{t+1}=1 \mid C_{t+1}=1, \mathcal{G}_t).\end{aligned} \tag{7}$$

The state variables in Section 4 and Appendix C—intensity, persistence, boundary relevance—speak to the second gate (ignition conditional on catalyst) rather than to the catalyst itself. The catalyst is deliberately unmodelled. The survival threshold disciplines whether the compounding cost of keeping the gamble running is time-rational given the ignition conditions. Because $\Pr(C_{t+1}=1 \mid \mathcal{G}_t) \leq 1$, ignition feasibility conditional on catalyst is an upper bound on the full success feasibility π^{succ}_t. The empirically estimated $\hat{p}^{\text{ign}}_t$ (Section 4) targets this gate, though its label (IV-repricing shock) differs from the payoff-trigger sense used here; the bound is therefore approximate (Section 4 qualifies the mapping). When the diagnostic barely clears the threshold even under this generous reading, the finding is informative because the true π^{succ}_t is weakly lower.

In the case we study, the typical portfolio is mostly shares, with calls as a convex sleeve sized as a fraction of total wealth. The pair (κ, L) is an effective description of the repeated gamble within that sleeve. In practice, κ varies with implied volatility, strike/tenor selection, and frictions; L is the net payoff multiple conditional on the success event, reflecting how far the stock moves past the strike, how IV reprices, and how quickly the move occurs. A clarification: L is conditioned on the success event $A_{t+1}=1$, not on normal market dynamics. During an ignition event, moves can be fast (hours to days), implied volatility tends to reprice sharply upward (amplifying option value beyond delta alone), and hedging feedback can compress the time over which the payoff is realised. We therefore treat L as a scenario parameter and compute the threshold across a grid of (κ, L) combinations rather than attempting to identify single "true" values.

The participant has more control over L than the scenario framing suggests. For OTM calls, the burn rate κ equals the call premium divided by the spot price, a dimensionless ratio that is the same whether the sleeve is priced in dollars or shares. Its reciprocal $1/\kappa$ gives the gearing ratio at purchase: a call costing 5% of spot buys 20× the notional exposure per unit of premium. The scale of the gamble is set by κ at entry, not by the eventual payoff. As the stock moves past the strike, the call goes deeper in the money, delta approaches one, and the position's effective convexity diminishes toward zero: gamma shrinks, vega exposure falls, and the call increasingly behaves like shares. For large price moves, L is well approximated by intrinsic value at exit divided by the premium paid, because option value converges to intrinsic value once the call is deep in the money. For a target move that leaves the call closer to the money, L also depends

[8] The S&P 500 exhibits the same pattern around market panics; the mechanism is not specific to GME.

[9] In plain terms: how many losing rounds can the participant absorb before a rare win stops compensating?

on the remaining time value and implied volatility at exit. The calibration grid (Appendix B.1) computes L; OTM strikes sit in the high-L corner of Figure 1.

3.2 The survival threshold

The baseline model assumes each round resolves at expiry: the participant pays κ upfront and either loses it entirely ($A = 0$) or collects κL ($A = 1$). Early exit replaces κ with the realised effective burn κ_{eff}; the mathematics are identical, and hold-to-expiry is the conservative case (maximum per-round loss). Throughout the calibration, $\kappa = C/S_0$ is a share-equivalent burn rate: one unit of account is one spot unit, the call premium C is spent, and the unspent $S_0 - C$ remains in the sleeve.

Proposition 1 (Survival threshold)**.** *The convex sleeve has nonnegative time-embedded growth if and only if*

$$\pi_t^{\text{succ}} \;\geq\; \pi^*(\kappa, L) := \frac{-\ln(1-\kappa)}{\ln(1-\kappa+\kappa L) - \ln(1-\kappa)}. \tag{8}$$

Proof. After one renewal interval, the convex sleeve returns $R = 1 - \kappa + \kappa L$ with probability $\pi := \pi_t^{\text{succ}}$ (event fires) and $R = 1 - \kappa$ with probability $1 - \pi$ (event does not fire). The per-interval growth rate under multiplicative compounding is

$$G(\pi; \kappa, L) \;:=\; \mathbb{E}[\ln R] \;=\; \pi \,\ln(1-\kappa+\kappa L) \;+\; (1-\pi)\,\ln(1-\kappa). \tag{9}$$

This is affine in π with slope $\ln(1-\kappa+\kappa L) - \ln(1-\kappa) > 0$ (since $L \geq 1$ and $\kappa > 0$) and intercept $\ln(1-\kappa) < 0$. Setting $G(\pi^*) = 0$:

$$\pi^* \big[\ln(1-\kappa+\kappa L) - \ln(1-\kappa)\big] \;=\; -\ln(1-\kappa),$$

which gives (8). □

The log criterion reflects repeated play. Equation (8) is derived from a single interval, but each renewal is a repeated gamble with wealth after n rounds $\prod R_i$ and growth rate controlled by $\mathbb{E}[\ln R]$. The multi-period extension assumes conditional independence of A_{t+1} across non-overlapping intervals—a standard Kelly-type assumption, strained here because success events cluster and one interval's outcome can shift the next's conditions. The one-period threshold is exact; the compounding interpretation inherits this idealisation. Large κ depletes the sleeve after losing rounds, making future play unaffordable; under repeated play, burn rate matters. Under a one-shot arithmetic-mean criterion, expected return is $(1-\pi)(1-\kappa) + \pi(1-\kappa+\kappa L) = 1 - \kappa + \pi\kappa L$, giving $\pi \geq 1/L$ (the burn rate κ cancels).[10] The time-average boundary (8) breaks this symmetry: under log returns, losing fraction κ requires recovering $\kappa/(1-\kappa)$, growing with κ. The entire κ-dependence of π^*—the upward curvature in Figure 1—is the price of repeated play: it depletes the sleeve faster after losses, leaving fewer rounds in which the participant can afford to continue.

Remark 1 (Relation to the Kelly criterion)**.** Proposition 1 uses the same log-growth criterion as Kelly sizing [33, 34, 35], but solves a different problem: instead of maximising $\mathbb{E}[\ln R]$ over bet size, it finds the minimum success probability at which $\mathbb{E}[\ln R] \geq 0$ for a fixed κ. Mapping $f = \kappa$ and net odds $b = L - 1$ into the standard Kelly growth rate $g_K(f) = p\,\ln(1+bf) + (1-p)\,\ln(1-f)$, the survival threshold is the zero-growth contour of the Kelly surface.

The Kelly criterion solves an optimisation problem: given a fixed win probability p, find the fraction f that maximises $\mathbb{E}[\ln R]$. The survival threshold solves the inverse problem at a different boundary: given a fixed fraction κ (determined by strike, tenor, and IV once the participant has chosen a contract), find the minimum probability π^* at which $\mathbb{E}[\ln R] \geq 0$. Kelly asks "how much should I bet to maximise growth?"; the threshold asks "how likely must the event be for renewal to survive repeated play?" Below $\pi^*(\kappa, L)$ but above $1/L$, the gamble is still viable at smaller sizing: the Kelly-optimal fraction $f^* = p - (1-p)/(L-1)$ is positive whenever $p > 1/L$, and $\pi^* > 1/L$ strictly (the gap is the Jensen penalty). Below $1/L$, no sizing works. The growth-rate function is the same; the question it answers is different. The contribution is therefore not a new growth criterion, but an adaptation of the Kelly/ergodicity break-even boundary to repeated option renewal when implied volatility jointly determines burn, payoff leverage, and feasibility, producing the IV-dependent threshold landscape of Figure 1. Peters [2] develops the connection between ergodicity and Kelly leverage in continuous time; the survival threshold extends this to discrete binary settings with option-market constraints. Section 6 derives the position-sizing consequences, including the Kelly-optimal fraction and how it varies with tenor and IV.

π_t^{succ} is not directly observed. Sections 4 and 6 construct model-based proxies and evaluate the threshold against them. Figure 1 maps the threshold across (κ, L).

Calibration and OTM convexity. Figure 1 anchors the (κ, L) plane to Black–Scholes prices for 21 DTE ($T = 21/252$; approximately 30 calendar days) calls at GME's two IV regimes ($\sigma = 120\%$ baseline, $\sigma = 300\%$ burst). The calibration sets $\kappa = C_{\text{BS}}/S_0$, the cost of one call per unit of spot wealth; this is the full-commitment case ($f = \kappa$ in the notation of Section 6.3). Partial commitment ($f < \kappa$) lowers the effective burn per interval and is treated in Remark 2 and Section 6.3. ATM burn runs $\kappa \approx 14\%$ per interval at baseline, rising to $\sim$34% during bursts; OTM strikes cut burn to $\kappa \approx 2.6\%$, and the cheaper premium implies a higher payoff multiple L per dollar spent for the same target move (Appendix B.1).

OTM strikes sit in the low-κ, high-L corner where π^* is smallest. Part is ordinary leverage: at fixed total spend $\kappa = 14\%$, one ATM contract gives $L \approx 14$ but the same outlay buys ≈ 5.4 OTM contracts at $L \approx 59$ each. The geometric framework adds what arithmetic misses: a single OTM contract costs $\kappa \approx 2.6\%$, and under time-averages reducing κ independently lowers π^*. The upward curvature in Figure 1 is real purchasing power for deploying less capital per round. Under arithmetic logic ($\pi \geq 1/L$), burn rate vanishes, so smaller sizing buys nothing.

In practice, far-OTM calls carry wider bid-ask spreads that erode the effective κ advantage.

The geometric lens exposes the sizing advantage. Aggregate options data show substantial OTM activity during burst episodes (Section 4), though without chain-level strike distributions the split between OTM and near-the-money flow is not identifiable from public data.

Volatility as the common driver. The implicit cost (ergodicity wedge, $\hat{\Delta} \approx \frac{1}{2}\hat{\sigma}^2$) and explicit cost (premium burn κ) share

[10] This is the core ergodicity distinction. Under an arithmetic-mean criterion, bet size is irrelevant. Under time-average logic, bet size determines survival long enough to collect.

volatility as common driver. High volatility widens the Jensen gap and raises premium burn κ, imposing a double penalty during burst regimes: the implicit compounding cost and the explicit renewal cost both spike together. The co-movement is partly endogenous: Section 4 quantifies the feedback channel and its lead-lag structure; Appendix B.2 decomposes the cost by channel.

Remark 2 (Mixed shares-plus-calls portfolio)**.** In share-equivalent units, holding shares over one renewal interval has gross factor 1 (the baseline). Let $\alpha_c \in (0, 1]$ denote the call weight (the fraction of portfolio value allocated to the convex sleeve; the remaining $1 - \alpha_c$ stays in shares). The mixed-account gross factor is

$$R_{t+1}^{\text{mix}} = (1-\alpha_c)\cdot 1 + \alpha_c\big(1-\kappa+\kappa L\, A_{t+1}\big) = 1-\tilde{\kappa}+\tilde{\kappa}\, L\, A_{t+1}, \quad (10)$$

where $\tilde{\kappa} := \alpha_c\, \kappa$ is the effective burn rate for the combined portfolio. This is the same algebraic form as equation (5), so the exact survival threshold for the mixed account is

$$\pi^*_{\text{mix}}(\alpha_c, \kappa, L) = \pi^*(\tilde{\kappa},\, L) = \frac{-\ln(1-\tilde{\kappa})}{\ln(1-\tilde{\kappa}+\tilde{\kappa}L) - \ln(1-\tilde{\kappa})}. \quad (11)$$

Since $\tilde{\kappa} < \kappa$ for any $\alpha_c < 1$, and since $\pi^*(\kappa, L)$ is increasing in κ for $L > 1$, the mixed-account threshold is strictly lower than the pure call-sleeve threshold: shares dilute the effective burn per interval, making renewal easier to sustain. In the limit $\alpha_c \to 0$ (nearly all shares, vanishingly small call sleeve), L'Hôpital's rule gives

$$\lim_{\alpha_c \to 0} \pi^*_{\text{mix}} = \frac{1}{L}. \quad (12)$$

The threshold cannot be pushed below this floor by reducing the call allocation; it is set by the payoff multiple alone. The winning-round gross factor $1 - \tilde{\kappa} + \tilde{\kappa}L = 1 + \tilde{\kappa}(L-1) > 1$ for $L > 1$, so $\pi^*_{\text{mix}} < 1$ always; no portfolio composition produces a threshold exceeding certainty. Figures 3–4 show π^*_{mix} at two call weights ($\alpha_c \in \{15\%, 50\%\}$) alongside the $1/L$ floor.

This derivation measures wealth in share-equivalent units, where the share sleeve's gross factor is 1 by construction. In dollar terms, the share sleeve has gross factor G_{t+1} (the stock's return over the interval), and the exact mixed-account condition becomes $\mathbb{E}[\ln((1-\alpha_c)G_{t+1} + \alpha_c R^{\text{cx}}_{t+1})] \geq 0$, which does not reduce to a shifted version of Proposition 1 because ln of a sum is not a sum of logs. Under the zero-log-drift benchmark of Section 6, the pure share sleeve has zero time-average growth in dollar terms ($g_{\text{equity}} = 0$). For mixed accounts, the dollar-wealth condition still depends on the joint law of (G_{t+1}, A_{t+1}); the share-equivalent threshold should therefore be read as an exact numéraire-relative object, not as a general dollar-wealth classification.

3.3 Intermittent participation

Renewal need not be continuous. A participant may renew only when conditions appear favourable and hold equity otherwise. At the individual level, let $Z_t \in \{0, 1\}$ indicate whether a participant renews at t; the sleeve factor becomes

$$R^{\text{cx}}_{t+1} = \begin{cases} 1, & Z_t = 0, \\ 1-\kappa+\kappa L\, A_{t+1}, & Z_t = 1. \end{cases} \quad (13)$$

Since $\ln(1) = 0$ when $Z_t = 0$, sitting out a round costs nothing in the convex sleeve. Renewing at t contributes $G(\pi_t; \kappa, L)$ from (9) to expected log-growth; when the conditional feasibility π_t falls below $\pi^*(\kappa, L)$, that contribution is negative, and sitting out weakly dominates. Selective renewal—only when the participant judges feasibility favourable—pays less total burn than continuous renewal.

At the collective level, let $\alpha_t \in [0, 1]$ denote the fraction of shareholders actively renewing at t. The premium burn paid by the active convex sleeve scales with the participation fraction α_t.

3.4 Persistence and access

The rare-regime thesis (Appendix A) is fundamentally a waiting game: a participant who exits forfeits the rare payoff regardless of whether the event eventually occurs, so lowering exit hazard raises the probability of still being present were it to occur.

Exposure as a survival process. Let $E_t \in \{0, 1\}$ indicate whether an agent remains exposed at calendar time t. Summarise exposure fragility via a one-step exit hazard

$$\Pr(E_{t+1} = 0 \mid E_t = 1, \mathcal{G}_t) = h_t, \quad (14)$$

where h_t subsumes all constraints that can end exposure along the realised path. Capital depletion under repeated renewal feeds directly into h_t: an agent whose wealth path W_t falls below a liquidity threshold is forced to exit regardless of conviction.

Let τ_{rare} denote the arrival time of the rare event and τ_{exit} the time of exit. Conditional on remaining exposed at calendar time t, let $\lambda_t(u)$ denote the instantaneous arrival intensity of the rare event and $h_t(u)$ the exit hazard at elapsed time $u \geq 0$ after t. Define the waiting-state survival function

$$W_t(u) := \Pr(\tau_{\text{rare}} > u,\ \tau_{\text{exit}} > u \mid E_t = 1, \mathcal{G}_t),$$

i.e. the probability that by elapsed time u the access question remains unresolved: the agent has neither exited nor yet reached the rare-payoff branch. Over a short interval $[u, u + du)$,

$$W_t(u + du) = W_t(u)\big(1 - [\lambda_t(u) + h_t(u)]\, du\big) + o(du),$$

so

$$W_t'(u) = -(\lambda_t(u) + h_t(u))W_t(u), \qquad W_t(0) = 1.$$

Hence

$$W_t(u) = \exp\Big(-\int_0^u \big[\lambda_t(v) + h_t(v)\big]\, dv\Big). \quad (15)$$

Hence the density that the rare event is the first resolving event and occurs at elapsed time u is $W_t(u)\lambda_t(u)$, so the probability of retaining access to the rare payoff is

$$a_t := \Pr(\tau_{\text{rare}} < \tau_{\text{exit}} \mid E_t = 1, \mathcal{G}_t) = \int_0^\infty \lambda_t(u)\, W_t(u)\, du. \quad (16)$$

In the constant-intensity special case, $\lambda_t(u) \equiv \lambda_t$ and $h_t(u) \equiv h_t$, this reduces to

$$a_t = \frac{\lambda_t}{\lambda_t + h_t}.$$

Proposition 2 (Persistence increases access (constant-intensity case))**.** *In the constant-intensity case $\lambda_t(u) \equiv \lambda_t$, $h_t(u) \equiv h_t$, the access probability $a_t = \lambda_t/(\lambda_t + h_t)$ is strictly decreasing in the exit hazard and strictly increasing in the rare-event arrival*

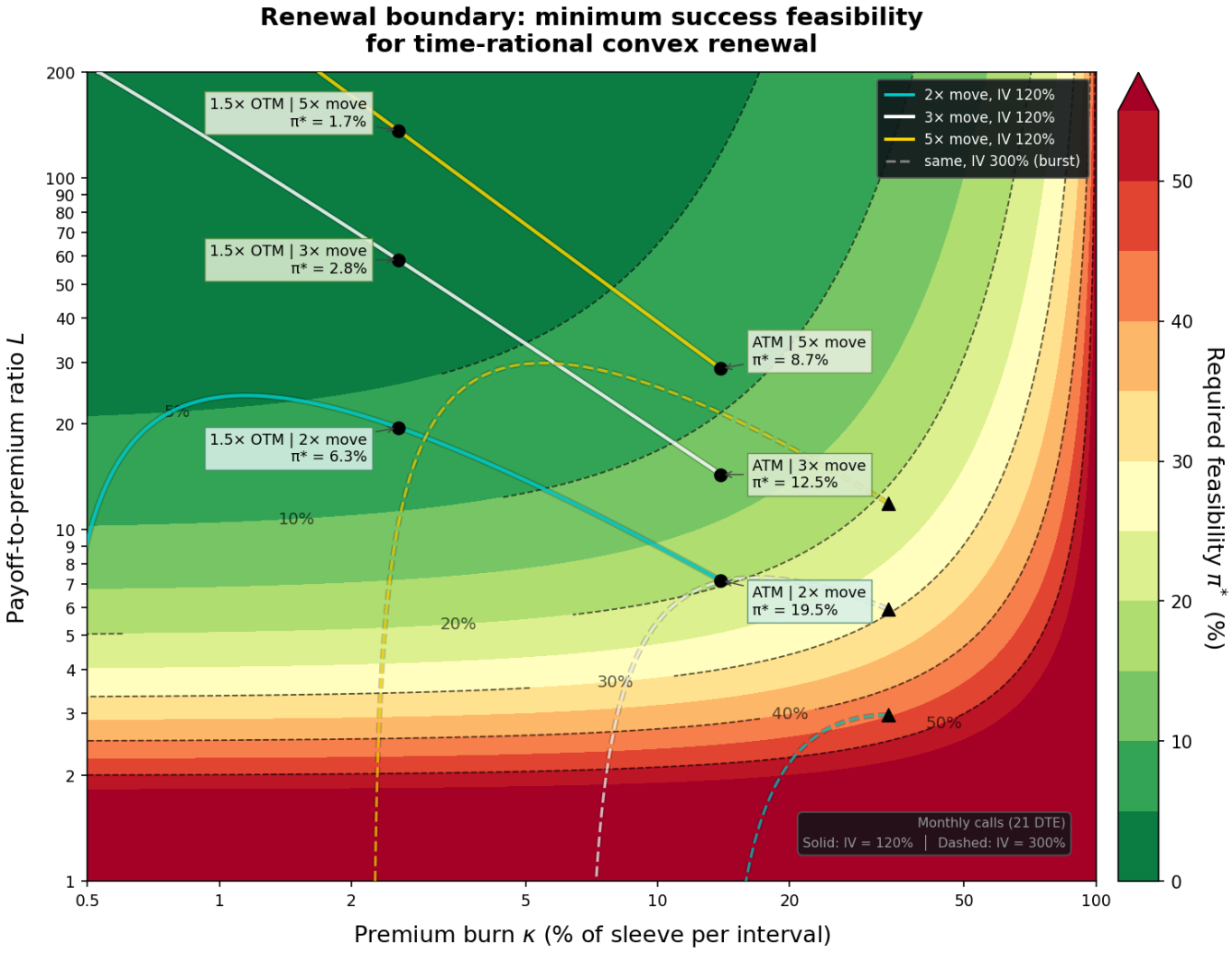

Figure 1: Survival threshold $\pi^*(\kappa, L)$ with Black–Scholes-calibrated loci (Proposition 1). Below π^* the premium burn destroys more time-average wealth than the conditional payoff contributes. Each curve traces the (κ, L) locus of monthly calls (21 DTE) at strikes from ATM through far OTM, for an assumed 2×, 3×, or 5× terminal move. Solid: $\sigma = 120\%$ (baseline IV); dashed: $\sigma = 300\%$ (burst regime). $\kappa = C_{\mathrm{BS}}/S_0$; $L = (B - K)/C_{\mathrm{BS}}$ (intrinsic value at the barrier). OTM strikes sit in the low-κ, high-L corner where π^* is smallest. Under burst-regime IV the locus shifts rightward: premiums absorb a larger share of the sleeve, compressing L and raising the threshold. The upward curvature at higher κ is the geometric compounding penalty: under an arithmetic-mean criterion the breakeven is $\pi \geq 1/L$, independent of κ, and the contours would be horizontal. At baseline IV, a 1.5× OTM call requires a rare event roughly once every 15–60 intervals; an ATM call during a burst requires it every 3–5. The rainbow crayon on the right maps colours to survival thresholds.

intensity. For any gated payoff multiple $L > 1$ conditional on the rare event preceding exit, lowering h_t strictly increases the expected log payoff.

Proof. Under constant intensities, the density that the rare event is the first resolving event at elapsed time u is $\lambda_t \exp\big(-(\lambda_t+h_t)u\big)$, so

$$a_t = \int_0^\infty \lambda_t e^{-(\lambda_t+h_t)u}\, du = \frac{\lambda_t}{\lambda_t + h_t}.$$

Hence

$$\frac{\partial a_t}{\partial h_t} = -\frac{\lambda_t}{(\lambda_t+h_t)^2} < 0, \qquad \frac{\partial a_t}{\partial \lambda_t} = \frac{h_t}{(\lambda_t+h_t)^2} > 0.$$

If the payoff is accessible only when the rare event occurs before exit, the expected log factor is $a_t \ln L$, strictly increasing in a_t for $L > 1$. □

Benchmark-relative threshold for the slow channel. Relative to a benchmark that does not access the rare payoff, the relevant coarse-grained object is whether the participant reaches the rare-payoff branch before exit. Write the benchmark-relative gross return as

$$R_{t+1}^{\mathrm{rel}} = \begin{cases} r_-, & \text{exit first,} \\ r_+, & \text{event first,} \end{cases} \qquad 0 < r_- < 1 < r_+. \tag{17}$$

The benchmark-relative zero-growth condition is

$$(1-a_t)\ln r_- + a_t \ln r_+ \geq 0. \tag{18}$$

Solving for the access probability gives the threshold

$$a_t \geq a_{\mathrm{rel}}^* := \frac{-\ln r_-}{\ln r_+ - \ln r_-}. \tag{19}$$

In the constant-intensity case this becomes an explicit threshold in the rare-event arrival intensity:

$$\frac{\lambda_t}{\lambda_t + h_t} \geq a_{\mathrm{rel}}^* \iff \lambda_t \geq \lambda_{\mathrm{rel}}^*(h_t) := \frac{a_{\mathrm{rel}}^*}{1-a_{\mathrm{rel}}^*}\, h_t = \Big(-\frac{\ln r_-}{\ln r_+}\Big) h_t. \tag{20}$$

This makes the role of persistence explicit: for the slow channel, opportunity cost and liquidity pressure matter by raising the exit hazard h_t, which in turn raises the rare-event arrival intensity required for nonnegative benchmark-relative growth.

We do not estimate this benchmark-relative threshold here. Direct shareholding and registration preserve access by lowering effective exit hazard, while continued exposure preserves the possibility of entering the rare-payoff branch at all. The empirical program below therefore continues to evaluate the access-relevant and cost-relevant objects directly observed in the data rather than introducing a second calibrated threshold family for shares.

Section 4 measures the empirical cost; Section 6 asks whether renewal can be time-rational without a temporal advantage.

3.5 Collective renewal and the relay threshold

The survival threshold π^* governs individual compounding: one participant, repeatedly risking the burn rate κ from the same wealth. But in a decentralised collective, when one participant's calls expire worthless, another may open a similar position. The collective renews even when no single member does. Here we ask whether such a relay can be viable in aggregate in regimes where renewal is time-irrational for the individual.

Divide time into T renewal intervals indexed by $t = 1, \ldots, T$. At interval t, a random cohort of size $n_t \geq 0$ enters, with $\mathbb{E}[n_t] = \lambda_t$. Each entrant commits capital $s > 0$ (measured in the same units as the call premium) to a one-period call sleeve. Let $S_{i,t} \in \{0,1\}$ denote participant i's success indicator in interval t.

In the no-feedback benchmark, conditional on n_t we assume

$$\mathbb{P}(S_{i,t} = 1 \mid n_t) = \pi_t,$$

and, within a given interval, the indicators are exchangeable with common pairwise correlation

$$\mathrm{Corr}(S_{i,t}, S_{j,t} \mid n_t) = \alpha, \qquad i \neq j.$$

Thus $\alpha = 1$ means all entrants in interval t share the same outcome, while $\alpha = 0$ means conditional independence.

The net gain to the collective in interval t is

$$\Delta W_t = \sum_{i=1}^{n_t} s\kappa\,(L S_{i,t} - 1), \tag{21}$$

so, conditional on n_t,

$$\mathbb{E}[\Delta W_t \mid n_t] = s\kappa\, n_t(\pi_t L - 1).$$

Taking expectations over n_t gives

$$\mathbb{E}[\Delta W_t] = s\kappa\, \lambda_t(\pi_t L - 1),$$

and therefore

$$\mathbb{E}[G_T] = s\kappa \sum_{t=1}^{T} \lambda_t(\pi_t L - 1). \tag{22}$$

Hence the relay has positive expected aggregate gain whenever the arrival-intensity-weighted mean success probability

$$\bar{\pi} := \frac{\sum_{t=1}^T \lambda_t \pi_t}{\sum_{t=1}^T \lambda_t}$$

exceeds $1/L$. The expected gain does not depend on α: within-interval correlation changes the dispersion of realized gains, not their arithmetic mean.

In the capacity-relevant case, let the success probability depend on cohort size through an increasing map

$$\pi_t(n) = f_t(n),$$

with $f_t'(n) > 0$ where differentiable. Then the conditional success probability faced by entrants at time t is the random variable $\pi_t(n_t)$, and

$$\mathbb{E}[\Delta W_t] = s\kappa\Big(L\,\mathbb{E}[n_t \pi_t(n_t)] - \lambda_t\Big).$$

Writing

$$\bar{\pi}_t := \mathbb{E}[\pi_t(n_t)],$$

we obtain

$$\mathbb{E}[\Delta W_t] = s\kappa\Big(\lambda_t(\bar{\pi}_t L - 1) + L\,\mathrm{Cov}(n_t, \pi_t(n_t))\Big),$$

since

$$\mathbb{E}[n_t \pi_t(n_t)] = \lambda_t \bar{\pi}_t + \mathrm{Cov}(n_t, \pi_t(n_t)).$$

Summing over t gives

$$\mathbb{E}[G_T] = s\kappa \sum_{t=1}^{T} \Big(\lambda_t(\bar{\pi}_t L - 1) + L\,\mathrm{Cov}(n_t, \pi_t(n_t))\Big).$$

Equivalently, the relay has positive expected aggregate gain iff

$$\tilde{\pi} := \frac{\sum_{t=1}^{T} \mathbb{E}[n_t \pi_t(n_t)]}{\sum_{t=1}^{T} \lambda_t} > \frac{1}{L}. \tag{23}$$

Thus the threshold remains $1/L$, but the relevant mean is now the participation-weighted success probability $\tilde{\pi}$: intervals with larger expected cohorts count more, and they count even more when large cohorts also face higher success probabilities through the feedback channel.

Define the arrival-intensity-weighted baseline mean

$$\bar{\pi} := \frac{\sum_{t=1}^{T} \lambda_t \bar{\pi}_t}{\sum_{t=1}^{T} \lambda_t}.$$

If cohort sizes are non-degenerate and each f_t is increasing, then

$$\tilde{\pi} > \bar{\pi},$$

because $\mathrm{Cov}(n_t, f_t(n_t)) > 0$ for every t with nonzero variance (given that each f_t is strictly increasing on the support of n_t with nonzero variance). For linear feedback of the form

$$\pi_t(n) = a_t + b_t n, \qquad a_t + b_t n \in [0,1] \text{ on the support of } n_t,$$

we have

$$\mathbb{E}[n_t \pi_t(n_t)] = \lambda_t \bar{\pi}_t + b_t\,\mathrm{Var}(n_t).$$

If $b_t \equiv b$ is constant across t, this simplifies to

$$\tilde{\pi} = \bar{\pi} + \frac{b \sum_{t=1}^{T} \mathrm{Var}(n_t)}{\sum_{t=1}^{T} \lambda_t}.$$

The gain from feedback is proportional to b and to the variance of cohort sizes. Bursty participation—large cohorts concentrated around hype dates, separated by quieter intervals—amplifies the feedback channel and raises $\tilde{\pi}$ further above the breakeven, because the intervals with the most participants are also the intervals where hedging pressure is strongest. This works against variance reduction: the same burstiness that raises $\tilde{\pi}$ also raises $\mathrm{Var}(G_T)$. The relay faces a tradeoff between feedback amplification (which favours concentration) and dispersion of cumulative gain (which favours equal-sized cohorts).

In the no-feedback benchmark, if $\bar{\pi} \in (1/L, \pi^*)$, the gamble is time-irrational for any individual who compounds, but the relay can still be arithmetically viable in aggregate. In the feedback case, the same statement applies with $\tilde{\pi}$ in place of $\bar{\pi}$. By Proposition 3, the gap between π^* and $1/L$ is the binary Jensen tax at arithmetic breakeven, scaled by the log-return spread between success and failure. It is therefore the difference between the geometric breakeven governing individual compounding and the arithmetic breakeven governing aggregate value across cohorts. Higher κ widens the gap because repeated-play losses steepen the Jensen tax.

Correlation does not affect the arithmetic breakeven condition; it affects how concentrated the gains are. In a single interval with n participants, the expected gain is $ns\kappa(\pi L - 1)$ regardless of α. At $\alpha = 1$, the realised gain is either $ns\kappa(L-1)$ (all win) or $-ns\kappa$ (all lose). At $\alpha = 0$, it concentrates near its expectation as n grows. In this collective, α is high: hype dates, corporate events, and shared information lead participants to concentrate in the same strikes and expiries [9]. When participants converge on the same trade, a losing round tends to be a losing round for most of them.[11]

The relay does not solve the ergodicity problem; it bypasses the compounding constraint at the aggregate level by replacing repeated play from one bankroll with sequential single-round participation. The gains are concentrated in whichever cohorts happen to coincide with the event; the losing cohorts bear the cost.

Remark 3 (Survivor concentration)**.** Let

$$R_u \in \{1-\kappa,\ 1-\kappa+\kappa L\}$$

be i.i.d. one-period gross factors with

$$\mathbb{E}[\ln R_u] = g_{\text{time}} < 0, \qquad \mathbb{E}[R_u] > 1,$$

equivalently $\pi \in (1/L, \pi^*)$. For N independent participants, each starting with wealth $W_0 = s$ and compounding for T rounds,

$$W_i(T) = s \prod_{u=1}^{T} R_{i,u}.$$

Then

$$\mathbb{E}\left[\sum_{i=1}^{N} W_i(T)\right] = Ns\,\mathbb{E}[R]^T,$$

whereas one-shot participation yields expected aggregate wealth $Ns\,\mathbb{E}[R]$. Thus repeated compounding produces much larger aggregate expectation.

At the same time, for each participant,

$$\frac{1}{T}\ln\frac{W_i(T)}{s} = \frac{1}{T}\sum_{u=1}^{T} \ln R_{i,u} \to g_{\text{time}} < 0 \qquad \text{a.s.}$$

Hence

$$\mathbb{P}(W_i(T) > s) \to 0 \qquad \text{as } T \to \infty.$$

For any fixed large T, the cross-sectional fraction of participants with $W_i(T) > s$ therefore converges in probability to a number close to zero as $N \to \infty$. The growing aggregate expectation is carried by an increasingly thin upper tail of favorable paths rather than by typical participants.

[11] Under exchangeable Bernoulli outcomes within each interval, constant success probability π, pairwise within-interval correlation α, and independence across intervals conditional on realized cohort sizes, the cumulative gain variance is $\mathrm{Var}(G_T) = s^2\kappa^2 L^2 \pi(1-\pi) \sum_{t=1}^{T} \Big[n_t + n_t(n_t-1)\alpha\Big]$. For fixed total participation and $\alpha < 1$, this is minimized when cohorts are equal-sized and maximized when all participants concentrate in a single interval.

This comparison concerns repeated play from fixed bankrolls. The relay model above differs: it replaces repeated compounding by sequential one-shot participation from new entrants.

3.6 Multi-period survival

Proposition 1 answers a single-round question: is renewal growth-positive this interval? In practice, convex exposure is maintained across many renewal cycles. The question facing any individual participant is not whether a single renewal clears π^*, but whether the bankroll survives long enough to see at least one touch across the full sequence. This subsection separates the per-round viability question (π^*) from the finite-horizon survival question, shows that the two can give opposite answers, and derives the scale dependence that correlations introduce.

A participant with initial sleeve wealth W_0 who renews k times without a touch holds wealth $W_0(1-\kappa)^k$, and the bankroll imposes a ceiling

$$k_{\max} = \left\lfloor \frac{\ln(\varepsilon/W_0)}{\ln(1-\kappa)} \right\rfloor \tag{24}$$

on the number of affordable rounds, where ε is the minimum viable position.

Let $p := \pi_t^{\text{succ}}$ denote the per-renewal touch probability. Under independent outcomes across renewal intervals, the probability of at least one touch within k rounds is

$$P_{\text{cum}}(k) = 1 - (1-p)^k. \tag{25}$$

The threshold π^* determines whether each round is growth-positive; $P_{\text{cum}}(k_{\max})$ determines whether the participant is likely to see a touch before the bankroll runs out. The two questions are distinct. A strategy can be growth-positive per round yet have a low cumulative probability of realising a touch within the available rounds.

Option markets price cumulative event probabilities at various horizons. Given an option-implied probability $P(T)$ of a payoff-relevant move within T periods, the implied per-period frequency under independence is

$$p(T) := 1 - \big(1 - P(T)\big)^{1/T}, \tag{26}$$

a rearrangement of (25) that requires no price-process assumption.

The one-period threshold π^* has a natural cumulative counterpart under independence: $P^*(T) := 1-(1-\pi^*)^T$, the minimum cumulative touch probability required over T periods for the sequence to remain growth-positive. Under independence, $p(T)$ is constant across T: the per-period frequency is a fixed point of the scale transformation $T \mapsto p(T)$. When successive outcomes are correlated, $p(T)$ flows with T and this fixed-point condition fails.[12]

Under positive dependence across renewal intervals, the survival constraint tightens beyond what the independent calculation suggests: touches cluster, the no-touch probability at every finite horizon exceeds the independent baseline, and a bankroll with finite $k_{\max}$ is less likely to survive long enough to observe a touch (Appendix B.5, Proposition 6). Under positive dependence of the kind formalised in Appendix B.5 (exchangeable beta-binomial), $P(K=0 \mid N) > (1-\mu)^N$ for $N > 1$; the qualitative direction extends to broader positive-dependence classes, though the precise bound is model-dependent. The exchangeability assumption underlying the formal result is most defensible during calm periods, which constitute the bulk of the sample and where the bankroll constraint binds; at regime boundaries the marginals shift, but the finite-horizon survival question is predominantly a calm-regime problem.

Collective persistence operates in this space. If $k_{\max}$ is small (high κ, ATM sizing), the bankroll exhausts before cumulative probability accumulates, and no amount of collective morale extends the sequence. If $k_{\max}$ is large (low κ, OTM sizing or mixed portfolios with small call allocations per Remark 2), the persistence channel has room to operate: collective infrastructure keeps participants exposed through the long stretches during which P_{cum} slowly builds.

Proposition 6 sharpens this: feedback-driven correlations ($\rho > 0$) tighten the survival constraint beyond what the independent model predicts, so the collective needs to sustain more persistence than a naive application of π^* would suggest.

Figure 2 illustrates both the bankroll ceiling and the dependence cost. Appendix B.5 develops the formal beta-binomial model and derives two falsification tests whose empirical execution requires multi-tenor touch probabilities not computed in this paper.

3.7 Jensen decomposition of the survival problem

The ergodicity wedge of Section 2 and the survival threshold of Proposition 1 are linked by the same Jensen geometry. For any positive one-period gross return factor X, define the *Jensen tax*

$$\mathcal{J}(X) := \ln \mathbb{E}[X] - \mathbb{E}[\ln X] \geq 0. \tag{27}$$

Then

$$\mathbb{E}[\ln X] = \ln \mathbb{E}[X] - \mathcal{J}(X). \tag{28}$$

Equation (28) separates multiplicative growth into an arithmetic edge, $\ln \mathbb{E}[X]$, and a time cost, $\mathcal{J}(X)$.

For the equity sleeve, let $R^{\text{eq}} := S_{t+1}/S_t$ denote the one-period gross return. The realised wedge $\hat{\Delta}(t;T)$ from Section 2 is the rolling sample analogue of

$$\mathcal{J}_{\text{eq}} := \ln \mathbb{E}[R^{\text{eq}}] - \mathbb{E}[\ln R^{\text{eq}}]. \tag{29}$$

For the convex renewal gamble,

$$R^{\text{cx}} = 1 - \kappa + \kappa L\, A, \qquad A \sim \text{Bernoulli}(\pi), \tag{30}$$

the corresponding Jensen tax is

$$\mathcal{J}_{\text{cx}}(\pi;\kappa,L) := \ln\big[1-\kappa+\pi\kappa L\big] - G(\pi;\kappa,L), \tag{31}$$

where $G(\pi;\kappa,L)$ is given by equation (9). Hence

$$G(\pi;\kappa,L) = \ln\big[1-\kappa+\pi\kappa L\big] - \mathcal{J}_{\text{cx}}(\pi;\kappa,L). \tag{32}$$

The survival condition $G(\pi;\kappa,L) \geq 0$ therefore says that the renewal gamble's arithmetic edge must exceed its Jensen tax.

At the arithmetic breakeven $\pi = 1/L$, one has $1-\kappa+\pi\kappa L = 1$, so

$$\mathcal{J}_{\text{cx}}(1/L;\kappa,L) = -\,G(1/L;\kappa,L) > 0. \tag{33}$$

Thus the arithmetic breakeven fails in time-average terms by the binary Jensen tax.

[12] Readers familiar with renormalisation-group methods will recognise the scale transformation $T \mapsto p(T)$ as analogous to a coupling flow under coarse-graining; independence is the trivial fixed point, and correlation introduces anomalous scaling that runs the coupling toward zero.

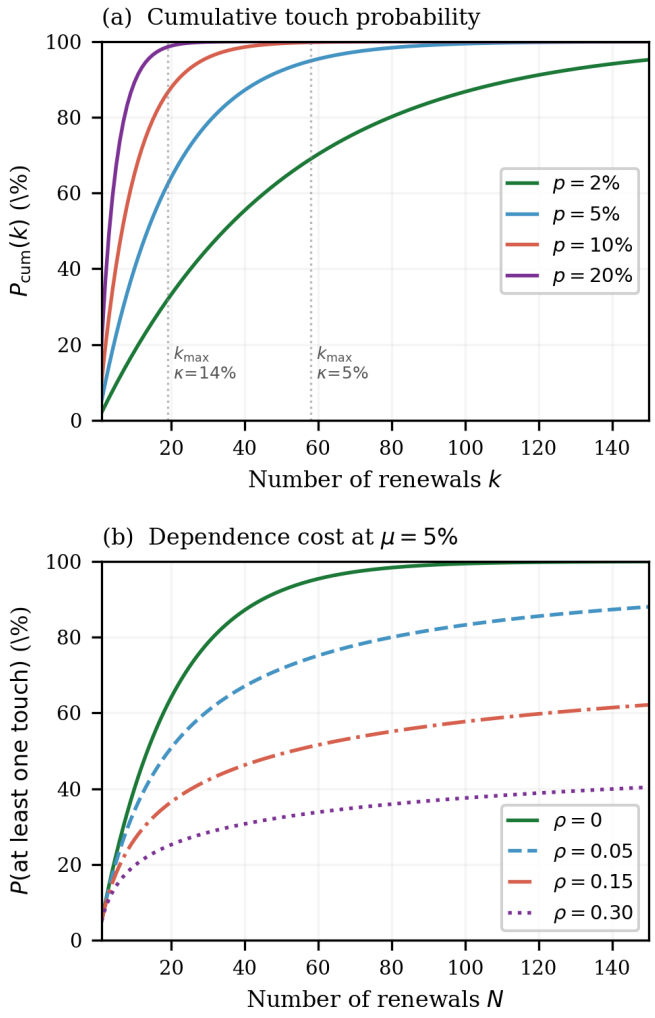

Figure 2: Multi-period survival. **(a)** Cumulative probability of at least one touch for four per-renewal touch probabilities. Vertical dotted lines mark $k_{\max}$ at two sizing assumptions ($\kappa = 14\%$, $\kappa = 5\%$; $\varepsilon/W_0 = 5\%$). **(b)** Dependence cost at $\mu = 5\%$ per period. Under independence ($\rho = 0$), the cumulative probability follows (25). At $\rho > 0$ (beta-binomial, equation 63), clustering reduces the effective number of independent trials and the cumulative probability at every horizon.

Proposition 3 (Threshold shift as a Jensen tax)**.** *Let $\pi^*(\kappa, L)$ be the survival threshold from Proposition 1. Then*

$$\pi^*(\kappa, L) - \frac{1}{L} = \frac{\mathcal{J}_{\text{cx}}(1/L; \kappa, L)}{\ln(1-\kappa+\kappa L) - \ln(1-\kappa)}. \tag{34}$$

In particular, the excess success probability required by repeated play is the binary Jensen tax at arithmetic breakeven divided by the log-return spread between success and failure.

Proof. Since $G(\pi; \kappa, L)$ is affine in π,

$$G(\pi; \kappa, L) = G(1/L; \kappa, L) + \left(\pi - \frac{1}{L}\right)\left[\ln(1-\kappa+\kappa L) - \ln(1-\kappa)\right]. \tag{35}$$

Set $\pi = \pi^*$ and use $G(\pi^*; \kappa, L) = 0$ together with equation (33). □

Remark 4 (Path-conditioned payoff and nested Jensen taxes)**.** For actual call contracts, the renewal payoff is generated by the same underlying price path as the equity sleeve. Let ω denote the stock path over one renewal interval, let $A(\omega) \in \{0, 1\}$ denote the payoff-relevant success event, and let $L(\omega)$ be the realised payoff multiple conditional on success, measurable with respect to the same path. The exact convex-sleeve gross factor is

$$R^{\text{cx}}(\omega) = 1 - \kappa + \kappa L(\omega) A(\omega). \tag{36}$$

Write $\pi := \Pr(A = 1)$ and $\bar{L} := \mathbb{E}[L \mid A = 1]$. The exact option-sleeve growth rate is

$$g_{\text{cx}}^{\text{exact}} = (1-\pi)\ln(1-\kappa) + \pi\,\mathbb{E}[\ln(1-\kappa+\kappa L) \mid A = 1]. \tag{37}$$

Proposition 1 is exact for the binary renewal model, in which the conditional-success payoff multiple is represented by a fixed scenario parameter L. Actual call contracts generally induce a finer pathwise object, with realised success-state payoff multiple $L(\omega)$ varying across success paths. The coarse-grained approximation considered here is obtained by replacing $L(\omega)$ with its conditional mean $\bar{L} := \mathbb{E}[L \mid A = 1]$, giving

$$g_{\text{cx}}^{\text{bin}} = (1-\pi)\ln(1-\kappa) + \pi\ln(1-\kappa+\kappa\bar{L}). \tag{38}$$

By Jensen's inequality,

$$g_{\text{cx}}^{\text{exact}} \le g_{\text{cx}}^{\text{bin}}, \tag{39}$$

with gap

$$g_{\text{cx}}^{\text{bin}} - g_{\text{cx}}^{\text{exact}} = \pi\big[\ln(1-\kappa+\kappa\bar{L}) - \mathbb{E}[\ln(1-\kappa+\kappa L) \mid A = 1]\big] \ge 0. \tag{40}$$

The exact threshold under random $L(\omega)$ is

$$\pi^{*,\text{exact}} = \frac{-\ln(1-\kappa)}{m_L - \ln(1-\kappa)}, \qquad m_L := \mathbb{E}[\ln(1-\kappa+\kappa L) \mid A = 1].$$

Jensen's inequality gives $m_L \le \ln(1-\kappa+\kappa\bar{L})$, hence $\pi^{*,\text{exact}} \ge \pi^*(\kappa, \bar{L})$: Proposition 1 captures the Jensen tax associated with the success/failure split itself, while actual call contracts carry an additional conditional Jensen tax from dispersion of realised payoff multiples within the success branch. The gap grows in the dispersion of $L(\omega)$ conditional on success.

The mixed dollar-wealth object. Remark 2 gives the mixed-account threshold in *share-equivalent* units, i.e. with the stock taken as numéraire. In that accounting convention, the share sleeve is the baseline asset and therefore has gross factor $G_{t+1} \equiv 1$ by construction. The mixed-account threshold π^*_{mix} is exact for that share-numéraire representation.

In dollar terms, however, the equity sleeve has stochastic gross factor $G_{t+1} = S_{t+1}/S_t$, so the one-period mixed-account gross return is

$$R_{t+1}^{\text{mix}} = (1-\alpha_c)G_{t+1} + \alpha_c\big(1-\kappa+\kappa L\, A_{t+1}\big), \tag{41}$$

and the exact growth condition becomes

$$g_{\text{mix}} := \mathbb{E}[\ln R_{t+1}^{\text{mix}}] = \ln \mathbb{E}[R_{t+1}^{\text{mix}}] - \mathcal{J}_{\text{mix}}, \tag{42}$$
$$\mathcal{J}_{\text{mix}} := \ln \mathbb{E}[R_{t+1}^{\text{mix}}] - \mathbb{E}[\ln R_{t+1}^{\text{mix}}].$$

Thus the share-equivalent threshold of Remark 2 should be read as a change of numéraire, not as an approximation: it is exact when wealth is measured in shares, whereas the dollar-wealth object depends on the joint law of the equity return and the renewal outcome.

Section 4 therefore continues with the pure-call and share-equivalent mixed threshold objects, including π^*_{mix} at fixed call weights, rather than with the exact mixed dollar-wealth condition, since π_t^{succ} is not directly observed and the latter requires the joint law of (G_{t+1}, A_{t+1}).

4 Empirical backbone

We use daily GME data from January 2021 through December 2025 (2020 is included only to initialise rolling windows, as the pre-2021 market structure differs substantially). The section measures the ergodicity wedge, shows that expensive time concentrates sharply in two burst episodes, calibrates the survival threshold against realistic option-market scenarios, and checks whether the options footprint during those windows was large enough, relative to the tradeable float, for dealer hedging to generate material price feedback. A repricing state summary compresses the options configuration into a single diagnostic; an intensity–persistence surface shows where in state space the costs of repeated play accumulate. The empirical program is descriptive (Tier 2: measured from publicly available daily data): it maps where and when time was expensive, not whether the system was above or below the threshold at any given moment—the success probability π_t^{succ} is never directly observed.

Episode markers. The two burst episodes introduced in Section 1—January–March 2021 (61 trading days) and May–June 2024 (41 trading days)—serve as descriptive anchor windows throughout. The wedge is computed independently of window selection, and the concentration result is stable across measurement horizons (Appendix C).

Data and proxies. We use daily GME OHLCV data and daily options aggregates (call/put volume, open interest, implied volatility); sourcing details are in Appendix C. The ergodicity wedge is computed from close-to-close returns on a rolling $T = 20$ trading-day window; robustness across $T \in \{5, 10, 20, 40\}$ is in Appendix C. Options intensity $\gamma_t := \ln V_t^{\text{opt}}$ is log total options volume, split-adjusted;[13] equity persistence is proxied by the normalised slope of on-balance volume (OBV) over 20-day windows.

OBV is partially entangled with returns because the sign of each volume contribution depends on return direction; we use it as a descriptive organising coordinate, not a causal persistence measure. The formal results do not depend on it; they require only options-market observables and daily returns. The slow persistence channel is independently grounded by issuer-reported DRS counts (Section 5). Cleaner daily persistence measures (account-level holding durations or transfer-agent flow data) are unavailable at daily frequency. Full proxy construction, flow-ratio diagnostic, and split-adjustment details are in Appendix C. Table 2 summarises the correspondence between theoretical variables and observables.

4.1 Two channels in the state space

The participation ecology (Section 5) suggests feasibility depends on two observable dimensions: *options intensity* and *equity persistence*. The wedge concentrates in the joint high-intensity/high-persistence region, with the threshold tightening differently across states.

Success feasibility π_t^{succ} is a conditional probability shaped by positioning but is not directly observed. Crowd belief affects the state through order flow; π_t^{succ} is structural conditional on that state. We approximate it with two independent lenses: a

[13] GME executed a 4:1 stock split dividend on July 22, 2022. Pre-split options volumes are multiplied by 4 before computing γ_t; the equity data source adjusts pre-split volumes automatically.

Variable	Meaning	Observable proxy
κ	premium burn	option premium / spot (BS calibration)
L	payoff-to-premium	strike payoff / premium (BS calibration)
π_t^{succ}	success probability	repricing diagnostic $\hat{p}_t^{\text{ign}}$ (imperfect); risk-neutral P_t^{touch} (model-dependent)
$\tilde{\kappa}$	effective burn (mixed portfolio)	$\alpha_c\,\kappa$ (Remark 2)
h_t	exit hazard	DRS counts (quarterly); OBV slope (daily)
B_t	capacity relevance	call OI / free float
γ_t	options intensity	$\ln V_t^{\text{opt}}$, log total options volume (split-adjusted; Appendix C)
q_t	equity persistence	normalised OBV slope (20-day)

Table 2: Mapping from theoretical variables (Section 3) to observable proxies (this section and Appendix C).

repricing state summary from options aggregates and risk-neutral touch probabilities from option prices (Appendix C.9).

Evidence hierarchy for persistence. Persistence enters the framework through its effect on access (Proposition 2): lower hazard raises the probability of being present were the rare event to occur, but the survival threshold itself is evaluated from options-market data alone. Further discussion is in Section 7.

4.2 Expensive time concentrates in two windows

The ergodicity wedge $\widehat{\Delta}(t;20)$ spikes sharply during two episode windows and is near-zero for most of the sample (Figure 3). The January–March 2021 window (61 trading days, 4.8% of sample) accounts for 44.8% of total wedge mass; the May–June 2024 window (41 days, 3.2%) accounts for 14.4%. Together, 8% of the full January 2020 to December 2025 sample—used here as baseline context plus the main 2021–2025 analysis period—carries approximately 59% of cumulative repeated-play cost. The remaining 41% is the irreducible variance floor: the Jensen gap is strictly positive whenever returns are dispersed, so even calm periods contribute small daily wedge (∼0.001) accumulating across ∼1,200 non-burst days. Per-day wedge intensity during bursts is roughly 85× the calm baseline.[14] Measured as excess wedge (each day's gap minus calm-period mean, clipped at zero), the two burst episodes account for ≈79% of incremental cost. The raw 59% includes background variance floor; the excess figure isolates episode-specific volatility cost.

The peak 20-day rolling wedge in 2021 reaches 0.085 (daily variance ≈17%, daily volatility above 40%); in 2024 it reaches 0.034 (≈7%, ≈26%). The median over the full sample is 0.0012. The wedge is an additional variance drag on the equity position, small relative to the option-premium burn κ that drives the survival threshold, but it compounds across the holding period and concentrates in the same episodes where κ is also highest.

This concentration is statistically selective: a circular-block permutation null places the combined 59.2% share at the 98.8th percentile (Table 5 in Appendix C). A variance placebo confirms the mechanism: realised variance is *more* concentrated than the wedge in the same windows (Λ^{rv}(combined) = 0.643 vs. 0.592; Table 5), so the wedge is driven by the variance channel rather than by a distinct source. The wedge reformulates volatility clustering in ergodicity-economics terms; its value here is as a cost-accounting device that maps dispersion to compounding drag.

[14] At $T = 20$, peak daily wedge during 2021 is ∼0.085 against calm-period mean of ∼0.001. Shorter windows amplify the spike; longer windows smooth it.

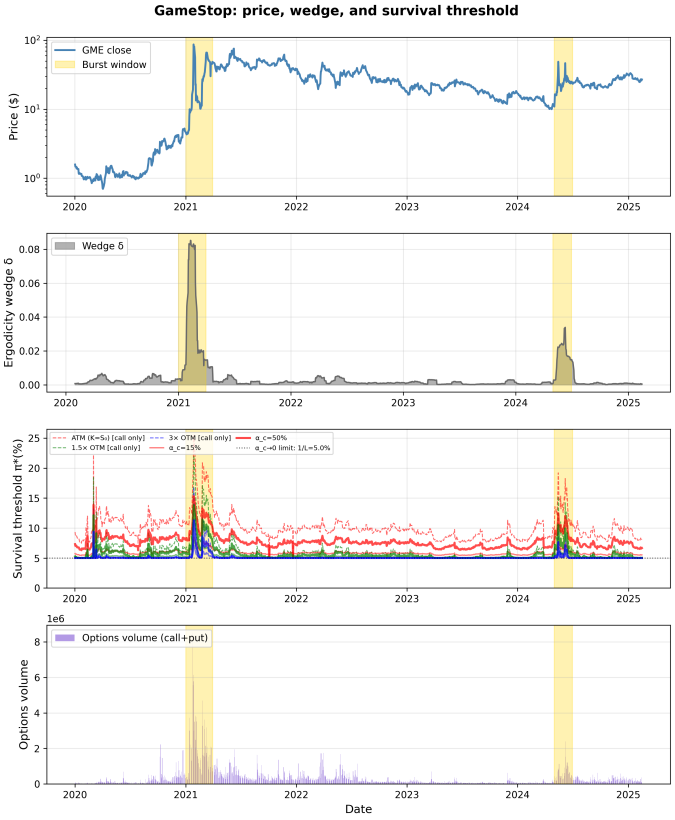

Figure 3: Top to bottom: GME price (log scale); ergodicity wedge $\widehat{\Delta}(t;20)$; survival threshold π^* (panel 3); total options volume V_t^{opt} (call + put, split-adjusted). A lower threshold is easier to clear, so lower is better for a participant who wants call renewal to be growth-positive. Panel 3 plots three strike choices at fixed conditional multiple $L = 20$, priced daily from Black–Scholes at observed IV with 21 DTE: *ATM* ($K = S_0$; at baseline IV $\kappa \approx 14\%$), *1.5× OTM* ($K = 1.5\,S_0$; baseline $\kappa \approx 2.6\%$), and *3× OTM* ($K = 3\,S_0$; near-zero κ at baseline, active only during burst IV). Fixing L isolates the moneyness channel: deeper OTM means cheaper entry (lower κ) and a lower threshold, but burst IV raises κ for every strike. Dashed lines show the pure call sleeve; solid lines at two thicknesses show the mixed-portfolio threshold π^*_{mix} at call weights $\alpha_c \in \{15\%, 50\%\}$ (Remark 2), where $\tilde{\kappa} = \alpha_c\,\kappa$. The dotted horizontal line marks the small-call limit $\lim_{\alpha_c \to 0} \pi^*_{\text{mix}} = 1/L = 5.0\%$: no portfolio with $L = 20$ can push the threshold below this floor. Yellow shading marks the January–March 2021 and May–June 2024 episode windows.

4.3 The threshold varies with implied volatility

Figures 3–4 fix $L = 20$ and compute $\kappa(t) = C_{\text{BS}}(K, \sigma_t, T)/S_0$ at each day's observed IV ($T = 21$ DTE). Because Black–Scholes maps higher IV to a more expensive call at the same strike, the BS-calibrated threshold $\pi^*(\kappa(t), 20)$ is higher whenever IV is higher. Figure 3 tracks this daily, including the mixed-portfolio threshold at two call weights (Remark 2). During quiet periods the mixed-portfolio lines sit close to the call-only baselines; during 2021 and 2024, IV spikes widen the gap between strikes.

The mixed-portfolio threshold at several call weights is shown in Figure 3; Appendix C (§C.13) gives the calibration details.

At higher IV the BS-calibrated threshold is higher, so the same

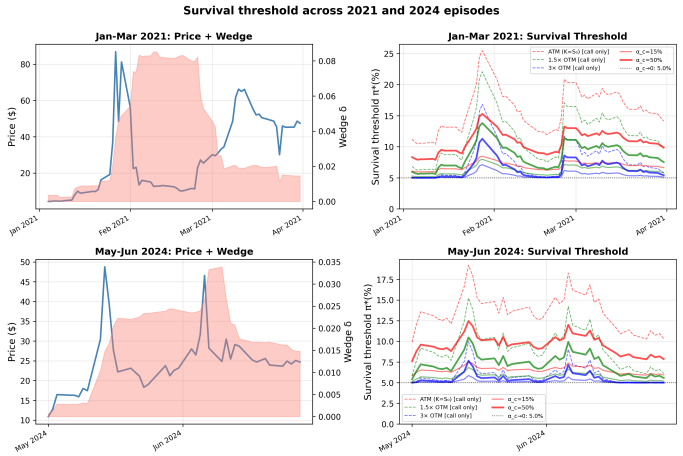

Figure 4: Episode comparison: January–March 2021 (top) and May–June 2024 (bottom). Left panels show price and wedge; right panels show the BS-calibrated survival threshold at fixed $L = 20$ for the same three strikes and call weights as Figure 3, zoomed into each burst window. The 2021 episode produces threshold spikes roughly 2.5× those of 2024, reflecting higher IV (which raises κ through the BS formula). The dotted line is the small-call floor $1/L$. The wedge appears elevated beyond the burst peaks in part because the $T = 20$ rolling window absorbs the burst's variance over the subsequent trading days; shorter windows resolve the decay more sharply (Appendix C).

unobserved π^{succ} sits further from clearing it.

The wedge tracks options intensity. At matched measurement horizons, the ergodicity wedge and smoothed options intensity are strongly correlated (Pearson $r = 0.84$, $r^2 = 0.71$ at $T = 20$ rolling windows; Spearman $\rho = 0.96$ within the 2021 burst episode; Pearson $r = 0.65$ during calm periods). The gamma-ramp channel provides a plausible link: accumulated call open interest across strikes creates positioning where dealer hedging obligations increase with price. Near expiry, when gamma peaks and share-equivalent OI represents substantial float fraction, hedging flow can amplify price moves and raise realised variance, captured with delay by the rolling wedge.

Cross-correlation of daily options volume against the wedge peaks at a +9 trading day lead ($r = 0.73$), consistent with the $T = 20$ rolling estimator lag absorbing a volatility regime shift. Options volume has significant incremental predictive power for realised volatility at horizons of one to four days, and the relationship is bidirectional: elevated volatility also attracts further activity (Appendix C, §C.14). The feedback is consistent with Barbon and Buraschi [50], who document that net gamma exposure of market makers predicts next-day returns and realised volatility, with the effect strongest when dealer inventories are concentrated.

The fast channel's time cost is partially endogenous: volatility enters both the Jensen gap and the Black–Scholes premium, so loading call exposure coincides with higher costs (Section 3; Figure 18; Appendix B.3 sketches a reduced-form model of this feedback loop and derives the resulting cycle-time scaling under simplifying assumptions). A natural concern is that the strong intensity–wedge correlation reflects self-excitation rather than two distinct channels. An auxiliary specification (Appendix D.2) is consistent with the two-channel separation: high options intensity γ_t predicts *lower* subsequent boundary relevance B_t ($\hat{\beta}_1 < 0$, significant at the 5% level), suggesting that the fast channel tests structural tightness without replicating it. The test is supportive, not dispositive; a single predictive regression cannot rule out all self-excitation channels.

The empirical framework specifies seven diagnostic checks—conditions whose absence would weaken the time-cost concentration story (Appendix C, §C.6). The data are consistent with all seven: expensive time concentrates in the predicted windows, localises in the predicted states, and persists across the predicted option-expiry cycles.

4.4 A repricing state summary

The wedge and survival threshold tell participants what persistence costs. A complementary question is whether options pricing implies feasibility above that cost. We compress a five-dimensional options state—total volume, realised variance, call tilt, call OI ratio, and absolute return—into a single scalar via an expanding-window logistic (Appendix C gives the full specification):

$$\hat{p}_t^{\text{ign}} \;=\; \text{logit}^{-1}\big(\hat{\beta}_{1:t}^{\top}\mathbf{x}_t\big), \tag{43}$$

where only data available at t enters the estimate. Despite the notation, $\hat{p}_t^{\text{ign}}$ is a repricing-state classifier score, not an estimate of π_t^{succ}. The label is an IV-repricing shock:

$$I_t \;=\; \mathbf{1}\big[\,\Delta\sigma_t \;\geq\; P_{95}\big(\{\Delta\sigma_s\}_{s<t}\big)\,\big], \tag{44}$$

i.e. a day whose IV change exceeds the expanding 95th percentile of all prior changes—a repricing criterion, not a return criterion. The positioning features (volume, call tilt, OI ratio) carry virtually all of the discriminatory power (restricted AUC = 0.816 vs. 0.825 full), so any association between $\hat{p}_t^{\text{ign}}$ and the return-based wedge is driven by positioning structure rather than mechanical correlation through shared volatility inputs. The diagnostic is a summary of options-state clustering—a quantitative fingerprint of concentrated call activity around focal dates—not a predictor of individual ignition events.

Figure 5 shows the time series; highest peaks coincide with burst episodes.

Viewed through the social-organisation lens of Section 5 (an interpretive reading; Tier 3), $\hat{p}_t^{\text{ign}}$ is collective positioning made visible in the options market.[15] Focal events that synchronise community attention coincide with the call-tilt, open-interest, and IV clustering that the logistic captures. The framework gives this activity a cost: the wedge against which elevated repricing-state readings can be descriptively compared. Because the two-gate decomposition (equation 6) factors success as $S = C \times I$, and the diagnostic captures only the ignition gate, $\hat{p}_t^{\text{ign}}$ is an imperfect diagnostic aligned with the ignition gate of the two-gate decomposition (equation 6). The factorisation guarantees $\pi_t^{\text{succ}} \leq \Pr(I_{t+1} = 1 \mid C_{t+1} = 1)$, and $\hat{p}_t^{\text{ign}}$ targets this conditional gate; but the "ignition" label used for training (an IV-repricing shock, equation 44) differs from the payoff-trigger sense of Section 3, and the logistic model introduces its own estimation error, so $\hat{p}_t^{\text{ign}}$ should be read as a diagnostic signal for ignition-like states rather than a literal bound on π_t^{succ}. The full diagnostic panel (Figure 16, Appendix C) overlays $\hat{p}_t^{\text{ign}}$ on the survival-threshold grid: elevated readings cluster in burst episodes and overlap most with low-burn / high-L regions. At the 6.0% base rate, positive predictive value is low; the diagnostic identifies elevated-

[15] This activity leaves a structured, measurable footprint in positioning data that can be evaluated against the survival threshold.

state regimes, not individual events. The feasibility sandwich (Appendix D.4) provides the formal plausibility bracket using P^{touch}. Era-stratified AUCs, the calibration curve, and the flip heatmap are in Appendix C.

4.5 Wedge concentration in the activity–persistence surface

The activity–persistence surface (Figure 6; formal concentration share in Appendix C, equation 66) shows mean wedge across decile bins of options intensity γ_t and equity persistence q_t (normalised OBV slope over 20-day windows). Expensive time concentrates in the high-activity region. The implied boundary shifts for the ATM baseline scenario are shown in the time-series panel of Figure 3.

The surface gradient runs predominantly along the activity axis; γ_t correlates strongly with the smoothed wedge (Pearson $r = 0.84$ during the 2021 burst; $r = 0.51$ full-sample). Within the top activity decile, the persistence proxy stratifies the wedge ($F = 4.79$, $p = 0.003$ across persistence quartiles; the top quartile carries higher mean wedge than the bottom). The F-test cannot discriminate between two-channel persistence and attention-driven volume asymmetry (the OBV entanglement noted above). The activity-axis gradient is the robust finding; the persistence-axis gradient is suggestive.

Episode trajectories in state space. A PCA embedding of twelve daily features compresses the state into two dimensions. PC1 loads on IV, log equity volume, and intraday range; PC2 loads on log OI overhang, options-to-stock volume ratio, and call share. Figure 20 (Appendix C) traces each burst episode's day-by-day path through this plane, with arrow opacity scaled by the local wedge. The 2021 episode reaches far along PC1 (peak activity roughly 3× the 2024 reach) and traverses a wide arc along PC2; the 2024 episode occupies the same region at lower intensity and with a tighter loop. Both trajectories fade as the wedge subsides, consistent with the concentration results above.

4.6 Capacity relevance

A *gamma ramp* (Appendix A) requires that call open interest is large enough relative to float to generate material hedging flow. We define boundary relevance $B_t := OI_t^{\text{call}}/F$ (call open interest in share-equivalents scaled by the effective float proxy F; construction in Appendix C). When B_t is small, call positioning cannot plausibly drive hedging flow at float-level scale regardless of other signals. Gross B_t counts all call OI at face value in share-equivalents (notional value), regardless of current delta: a far OTM call at $\delta = 0.05$ today becomes a $\delta = 0.50$ call if price moves up through its strike, so delta-weighting at a snapshot understates the exposure that a gamma-ramp event would cause. We retain gross B_t as the primary measure. Far-OTM calls contribute less immediate hedging demand per contract, so the effective exposure at any snapshot is lower than gross B_t; without chain-level strike distributions the magnitude of this correction cannot be pinned down.

During the January–March 2021 burst episode, B_t peaked at 0.93: call open interest covered over 90% of estimated free float in gross share-equivalents. Call OI persisted across successive OPEX dates, consistent with rolling rather than one-shot speculation. Risk-neutral pricing implied 47% median probability of a 50% move within 20 trading days. At peak IV the BS-calibrated ATM call-sleeve survival threshold is ∼20%, compared to ∼12.5% at baseline IV. The feasibility sandwich (Appendix D.4) places this threshold inside a plausibility range implied by risk-neutral option prices, with the lower risk-neutral move-probability curve lying above π^* on 87% of burst-window days. These are risk-neutral probabilities, which overstate physical-measure move probabilities under typical risk premia; the comparison establishes plausibility, not identification. The 2024 episode shows the same pattern at lower intensity (B_t peaked at 0.49, median 0.34); capacity relevance in 2024 is substantially lower than in 2021. Appendix D.4 shows all four diagnostic gauges simultaneously elevated during January–March 2021.

The interpretation rests on a material fraction of call open interest generating hedging flow—a condition that weakens if dealers internalise risk or hold offsetting long-gamma positions that reduce their net short-gamma exposure. Full hedging is not required: even at a 50% hedging fraction, $B_t = 0.93$ translates into share-equivalent hedging demand covering roughly 46% of the free float. The qualitative pattern—B_t elevated during burst episodes, negligible otherwise—holds regardless of what share of OI actually generates hedging flow; only the magnitude of implied flow changes. The float proxy F omits ETF-embedded GME shares (Appendix C); this is deliberate, since accounting for the synthetic supply that authorised-participant creation and redemption can generate requires modelling short dynamics that fall outside our scope. More broadly, circulating share-equivalents can exceed the official float because each short sale creates a synthetic long that can itself be re-lent; GME's reported short interest reached 149% of tradeable float in October 2020 [9, 10].[16] A dealer reflexivity estimate (Appendix D.1) confirms the flow side: during burst episodes, median implied hedge flow per 1% price move reached 0.5% of average daily volume (ADV) during the 2021 burst and 0.9% during 2024, and options-driven notional routinely exceeded equity notional, with daily ratios reaching 3–5× at peak.

The next section describes the collective infrastructure that sustained exposure long enough for these costs to become binding.

[16] The buyer of a shorted share receives stock indistinguishable from an original issue, and that share can be re-lent and re-sold [10]. Under normal conditions this inflated supply loosens the constraint, and B_t measured against F may overstate scarcity relative to actual circulating supply. Under stress the direction can reverse: synthetic supply exists only as long as the underlying borrows remain open, and forced settlement would contract circulating supply back toward the official float, tightening the constraint at the moment hedging demand is elevated.

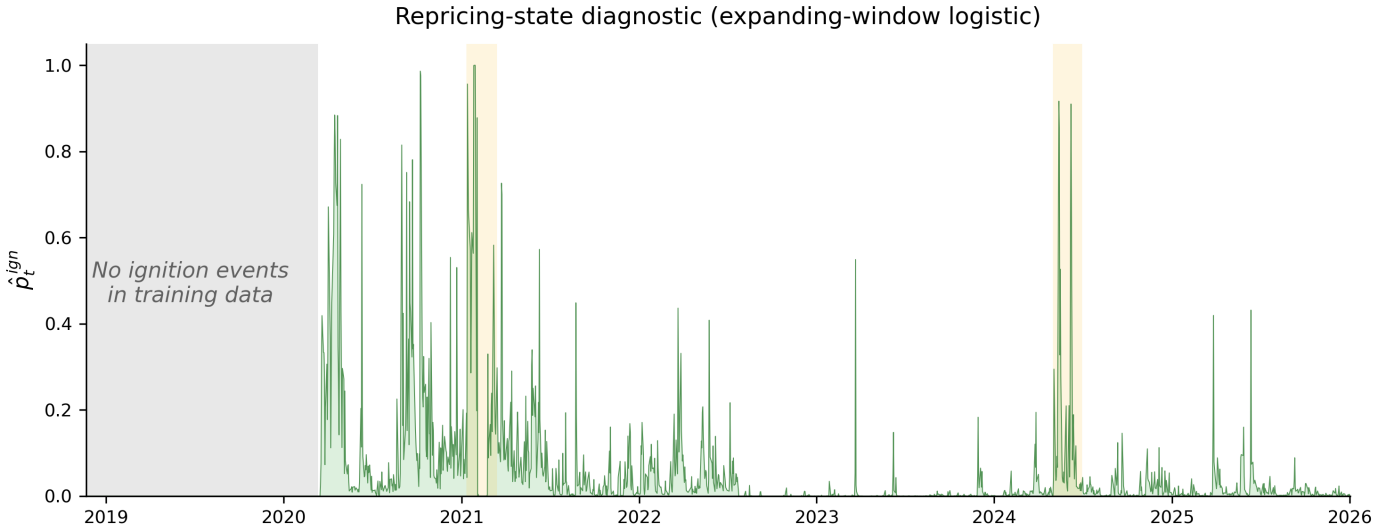

Figure 5: Repricing-state diagnostic p_t^{ign}: diagnostic score for next-day IV-repricing state, from an expanding-window logistic on options-state features (out-of-sample AUC = 0.825; positive predictive value is low at the 6% base rate). The score summarises the options configuration into a single scalar indicating how closely the current state resembles historical IV-repricing episodes. Grey region marks the period before the first ignition event (March 2020), during which no positives exist in the expanding training window. Yellow shading marks the two burst episodes. The trace is elevated throughout 2020–2021, with the sharpest spikes inside the burst episodes; it declines through 2022, settles near zero during 2023, resurges during the 2024 burst, and quiets again afterward. Full diagnostic panel in Figure 16.

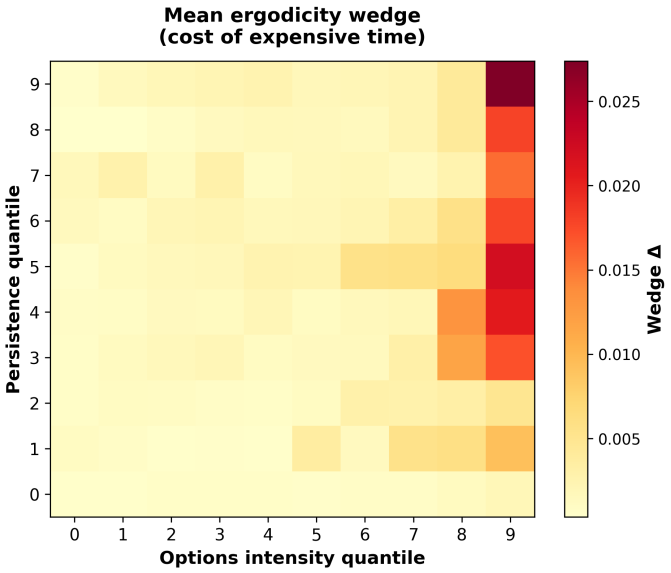

Figure 6: Mean ergodicity wedge across decile bins of options intensity ($\gamma_t = \ln V_t^{\text{opt}}$; bin 0 = lowest) and OBV-slope proxy (q_t, normalised OBV slope; same ordering). Proxy construction in Appendix C. Expensive time concentrates in the joint high-activity / high-OBV-slope region of state space. At the calibrated scenario ($\kappa \approx 14\%$, $L \approx 14$), the peak cell's wedge of $\approx$0.027 translates to a boundary shift of roughly 8 pp at $\alpha_c = 15\%$ (Remark 2). The OBV-slope axis is partially entangled with returns (OBV sign depends on return direction); the persistence-axis gradient cannot be distinguished from attention-driven volume asymmetry and should be read as suggestive. The activity-axis gradient carries the dominant signal. Replacing total options volume with log call open interest yields a qualitatively similar concentration pattern.

5 Community infrastructure

The preceding sections define the cost of repeated play and measure where that cost concentrated. This section describes the collective mechanisms that sustained exposure long enough for the cost to become binding. In most single-equity market episodes, household conviction decays and positions dissolve within months. The available evidence is consistent with a core group of shareholders that has held for years, sustained by collective infrastructure that plausibly lowers exit hazard and keeps conviction alive faster than time erodes it. The mechanisms described below are interpretive: we identify them from sustained observation, not from identified causal estimates. The measurable cost structure has already been established; what this section adds is the social account of why participants were still present to pay it.

Five mechanisms are documented below, each plausibly lowering exit hazard or sustaining renewal conditions: epistemic infrastructure that circulates analytical conclusions in compressed form across years; social norms and identity costs that raise the price of exiting; hype-date synchronisation that concentrates renewal timing around focal calendar events; direct registration as a financial commitment device that alters float composition; and platform resilience that ensures the social layer survives disruptions. The account is interpretive (Tier 3); the formal results of the preceding sections are invariant to it.

Everything here is downstream of the belief that MOASS is still possible. That belief functions as a lived strategic framework, held higher than any single price target. The community reasons that if obligation constraints can bind against a depleted effective float, then the degree of float depletion and exposure matters. Participants observe that direct registration removes shares from the intermediary chain. Memes and in-group language reinforce cohesion and functionally, sometimes, may filter outsiders. Due

diligence researches paths to the rare regime (e.g. corporate actions, rule changes, obligation exposure) and speculates on which are most plausible. Each mechanism below is a facet of that ecology.

History in a nutshell. GameStop was not the only stock to attract sustained retail attention; AMC Entertainment was the most prominent companion trade,[17] but GME had the highest short interest relative to shares outstanding and the visibility of Keith Gill's publicly shared analysis and position, which made it the structural centre of the thesis. In 2021, speculation was at its peak: MOASS could be any day, and the community treated every price spike as a potential trigger. By late 2021, a direct-registration campaign was under way, shifting emphasis from price action to float reduction. In 2022, GameStop launched an NFT marketplace and issued a 4:1 stock split as a stock dividend, which many participants hoped would force obligation settlement and catalyse MOASS; the split did not. In 2023, the bankruptcy of Bed Bath & Beyond[18] widened speculative scope in some subgroups, but the core MOASS expectation remained. In 2024, Roaring Kitty's return to social media after three years of silence coincided with the second burst episode. Throughout, the community's self-understanding is perhaps best captured by one of Roaring Kitty's most circulated memes: the emoji timeline, a sequence of pictographic symbols narrating the arc from crisis through patience to resolution.[19]

Methods note. The account draws on five years of continuous participant observation (January 2021 through early 2026) across the community's primary platforms (Reddit—r/wallstreetbets, r/GME, r/SuperStonk; X/Twitter; YouTube), following the extended-case method [36]. Artefact selection follows theoretical sampling [37]: recurring practices were identified through saturation across platforms and years, not through random sampling of posts. The discourse is heavily mediated by memes, irony, and layered symbolism, making automated sentiment classification unreliable; each interpretive claim is triangulated against at least one of: SEC filings, issuer-reported DRS counts, equity and options data, or documented platform histories. Appendix E documents representative publicly observable artefacts and timeline anchors for the recurring practices described below; the claims here describe patterns that showed up repeatedly over years, not a count of every post. The author is a participant-observer and holds GME equity. The resulting claims are interpretive, not causal.

Relation to existing community studies. A growing literature examines the r/wallstreetbets community during the January 2021 squeeze [30, 31, 32, 15, 14]. These studies overwhelmingly treat the January 2021 event as the unit of analysis and model retail participants as sentiment-driven and momentum-responsive. The community described here is distinct on two counts. First, the institutional setting changed: r/wallstreetbets banned sustained GameStop discussion in early 2021; the persistence ecology migrated to r/SuperStonk (the primary hub to date) and smaller spinoff subreddits, which operate under restrictive moderation rules designed to filter adversarial engagement and sustain epistemic infrastructure. Second, the actor type differs: existing work models momentum-responsive retail traders; we examine participants who assign positive probability to rare constraint-driven regimes and maintain exposure through collective infrastructure consistent with that belief. None of the existing studies, to our knowledge, examines the post-2021 ecology or the collective mechanisms sustaining multi-year participation.

Burry [12] provides an independent account of the pre-2021 short-interest conditions; he held approximately 3 million shares (pre-split) through 2019–2020 and pushed the board toward share buybacks that reduced the float. His retrospective describes the January 2021 episode as a gamma squeeze (Appendix A)—the only "legal market corner" he has witnessed—in which retail call buying forced dealers into hedging flow that overwhelmed available supply. In a later assessment [13], Burry characterises the post-2021 capital raises as "clever accretive dilution" and frames a long-term value case around tangible book value and CEO capital allocation, explicitly separating his thesis from the rare-regime hypothesis the community maintains.

5.1 Epistemic infrastructure

The community produces and maintains a body of research—referred to internally as "due diligence" or DD—that functions as shared justification for the position. DD posts range from detailed analysis of SEC filings, options data, and market-structure rules to highly speculative inference chains about institutional behaviour, hidden obligations, and market-maker positioning—often built on incomplete or circumstantial evidence and acknowledged as such by their authors. Some posts achieve canonical status and are repeatedly cited across platforms and years; a community-curated DD library[20] compiles the major contributions. The style is distinctive and hyped—the memes, the tone, the sourcing habits—and new contributors pick it up fast. The canon evolves in response to firm-specific fundamentals but also to idiosyncratic connections that shareholders draw between the stock and the wider world: macroeconomic shifts, political developments, fraud scandals, dealer positioning. The interpretive net extends far beyond capital markets; *even the liftoff of a rocket that goes to the* moon *could be read as an omen within a greater memetic constellation of signs*, each *potentially decision-relevant* to the rare-regime thesis. The bulk of foundational DD was produced in 2021, when content volume and community intensity were at their peak; subsequent years show lower volume but continued periodic activity. The belief object—the rare-regime thesis—is continuously maintained without centralised direction. The same person might produce detailed analysis one month, create memes compressing that analysis the next, and go quiet for months before re-engaging when a new event captures attention. Functional contributions to the epistemic infrastructure overlap and shift; there is no stable division of labour. The research effort is also geographically decentralised: participants span time zones and jurisdictions, so when someone surfaces a lead in another country, there is often someone local willing to follow up on it. The result is a kind of decentralised open-source research ecology.

[17] According to community lore, AMC (aka. *sticky floors*; *popcorn*) may squeeze before GME.

[18] *Posthumous Proof* that the original meme-stock bet carried terminal risk.

[19] Arguably, it is also accepted by Occam's Razor by some within the community that Roaring Kitty is a bona fide time traveller. The prophecy of the emoji timeline has it that in the end there will be beer.

[20] SuperStonk Library of DD, Art Books and Periodicals, https://GME.fyi.

In the two-channel ecology, epistemic infrastructure sustains the belief object that motivates both channels: it is how participants arrived at the thesis, learned about direct registration, and developed the analytical framework that informs individual decisions.

5.2 Memes as collective infrastructure

Memes are a primary medium through which conviction is produced, compressed, and transmitted. A complex DD argument about, say, options settlement mechanics or short-interest reporting methodology gets condensed into a joke that circulates for months, carrying the conclusion in a form that travels further and sticks longer than the original post. "MOASS is tomorrow" has been posted daily for years (cf. Section 3.4); purple-circle DRS screenshots make aggregate persistence visible to the shareholders themselves. The humour is load-bearing—it keeps spirits up through the long stretches of not-yet time. Dips are celebrated as buying opportunities; rips are just celebrated.[21] The social experience of holding is collective rather than isolating. The label "memestock" in public discourse is typically dismissive, but it inadvertently identifies the mechanism: memes function as a compression medium, performing epistemic compression, identity reinforcement, and morale maintenance simultaneously. In functional terms, memes compress the epistemic infrastructure into transmissible form: they carry conclusions across platforms and years, sustaining the belief object that motivates both the slow persistence channel (shareholding) and the fast renewal channel (options activity).

5.3 Norms, identity, and exit costs

To have "diamond hands" functions as a social norm, persistent in community language since at least 2021.[22] Within the community, selling is often framed as defection (in the game-theoretic sense: exiting a repeated game) and holding as conviction. As in any community built around shared conviction, leaving carries costs beyond the financial: identity exit (repudiating a publicly held position), social exit (losing standing in a community that has become part of daily life), and epistemic concession (accepting that the belief was mistaken). All of these plausibly raise the cost of leaving, lowering exit hazard—the quantity h_t in the access model of Section 3.4—and thereby supporting the slow persistence channel.

The harder test is holding through a rip: the temptation to exit for profit when the stock surges, not the drawdown. The community has developed customs built around this constraint.

An adversarial stance toward mainstream financial media and regulators coexists with a culture of independent verification.[23] External signals that would ordinarily push toward exit—negative price action, unfavourable analyst coverage, contradictory data—get interpreted through the community's own analytical frame. The community is self-aware about this: "confirmation bias" is itself a running joke, acknowledged openly and worn as a badge.

5.4 Hype dates and renewal cycles

Community discourse treats every day as a hype date. Anticipation is continuous, but unevenly distributed across the calendar. OPEX dates carry the most structural weight, because they are directly linked to open call interest and therefore to the potential for a gamma-driven move (Appendix A). Beyond OPEX, much of the anticipation is driven by idiosyncratic speculation about what the company will do and when a large move will come. Corporate actions, rule changes, and—most notably—the public reappearances of Roaring Kitty concentrate that speculation further, generating new DD and short-dated options activity.

The synchronisation requires no explicit coordination. The relevant dates are public[24], their timing often predictable (OPEX cycles, corporate actions), and the community's shared epistemic infrastructure ensures rapid interpretation through the lens of the rare-regime thesis. The fast channel—options-intensive call renewal—therefore operates at a continuous low-level baseline, with high-intensity bursts around the most salient dates. Hype dates concentrate renewal activity in narrow calendar windows, producing the wedge spikes measured in Section 4.

5.5 Direct registration as a social-financial commitment device

Direct registration of shares (DRS) operates simultaneously as a financial action and a social signal. The DRS campaign gained momentum in September–October 2021 and peaked in mid-2023 at approximately 76.6 million split-adjusted shares (∼25% of outstanding at the time), based on issuer-reported account counts in quarterly filings [16, 17].

Financially, direct registration removes shares from intermediated ("street name") circulation, reducing broker discretion over lending and liquidation pathways. A directly registered share cannot be lent, cannot be used as collateral, and is not subject to broker-level liquidation risk in the same way as a street-name share. Participants cite intermediary-level risks—including broker insolvency, lending without consent, and DTCC[25] obligation failures—as reasons for registering shares. DRS shares sit on the company's transfer-agent books rather than as entitlements within the depository system, which participants interpret as reducing exposure to those risks. The degree of protection in extreme broker, clearing, or depository stress scenarios is a legal and operational question beyond the scope of this paper, but it is not unbounded.

Socially, DRS counts are publicly trackable: the community aggregated individual DRS posts before GameStop began disclosing official counts in quarterly filings [16, 17]. The campaign functions as a commitment device (hard to reverse, deliberate), a publicly observable indicator of aggregate persistence, and a systemic insulation measure: if the rare regime stresses the intermediary chain, directly registered shares are recorded on the company's transfer-agent books independently of the depository system.

Direct registration maps to the formal framework in two ways. First, systemic insulation: directly registered shares are held on

[21] Paraphrasing Nietzsche's Zarathustra: *the shareholder is a rope stretched between the ape and MOASS—a rope over an abyss. A dangerous crossing, a dangerous looking-back, a dangerous trembling and halting. What is lovable in the shareholder is that they are an overgoing and an undergoing.*

[22] The community's commitment rituals extend well beyond the phrase itself: crayon-eating jokes, banana bets, and purple-circle DRS confirmations each reinforce collective identity and make individual commitment publicly legible.

[23] The SEC's June 2022 *Investomania* campaign satirised meme-stock investors in a game-show format; the community treated it as confirmation that the regulator was dismissing rather than engaging with substantive concerns about short-selling transparency and market-structure risks.

[24] At least as far as I'm aware of. Check with your calendar provider.

[25] Depository Trust and Clearing Corporation.

the transfer agent's books outside the depository system, which participants interpret as reducing exposure to broker insolvency or intermediary-chain failure (Section 3.4). The operational friction of transfer-agent interaction and multi-day settlement also plausibly lowers accessibility to selling and lowers gamble attrition for committed shareholders. Second, float tightness: direct registration mechanically removes shares from intermediated circulation, altering the effective float denominator in the constraint boundary of Appendix A. Subsequent equity issuance diluted the DRS fraction, and the absolute count, after holding near 75M through early 2024, has declined to approximately 66M by early 2026—still a large base, and difficult to reconcile with a fully transient shareholder base, but no longer stable. Because DRS counts are stepwise between quarterly reporting dates and sensitive to float definition, we do not treat them as a daily persistence signal.

5.6 Platform resilience

The community has survived multiple platform disruptions: the migration from r/wallstreetbets to r/GME, then to r/SuperStonk[26], along with further subreddit splits, moderator conflicts, migrations to alternative platforms, and evolving content-moderation policies. The social infrastructure that supports the position does not depend on any single platform or leadership structure. When a platform has become inhospitable, the community has reconstituted elsewhere, carrying its epistemic infrastructure and customs with it. Community posts have explicitly discussed contingency scenarios—including total platform outages and externally driven mass disinformation campaigns—that most online communities never consider. The community practically treats communication-infrastructure failure as a when, not an if. The adversarial environment extends beyond platform mechanics: r/gme_meltdown, a dedicated counter-community, has tracked and ridiculed GME shareholders throughout, providing a sustained external source of scepticism and hostility. Platform resilience ensures that the social infrastructure supporting both channels survives disruptions that would dissolve less robust communities.

5.7 Aggregate exposure and attrition

Appendix E documents representative artefacts for the persistence rituals, DRS campaign, and platform migrations referenced above. A large portion of participants likely engage only through the slow channel (holding shares), where these social mechanisms operate without any options cost at all. Individual participants read the same public research, watch the same public dates, and discuss conclusions in open forums; convergent reasoning from shared inputs can produce correlated positioning without centralised direction. The survival threshold (Section 3) applies at both the individual and the aggregate level.

At the aggregate level, exposure is sustained by the balance between attrition and replenishment (formalised in Section 3.5). Exit was front-loaded: the 2021 shakeout and 2024 short-horizon entrants plausibly selected out high-hazard participants early; the core shareholders entering in 2021 and remaining through both episodes exhibited relatively low attrition by 2024, as inferred from the aggregate DRS trajectory and sustained community activity (participant-level holding data are unavailable). A pure cost-basis selection story—survivors held low cost bases and therefore faced low opportunity cost—would produce similar aggregate patterns without requiring any of the five mechanisms above; the social account and cost-basis selection are observationally equivalent at the aggregate level. One discriminating observation: during the May–June 2024 burst, the stock rose from roughly $12 to $65, putting many holders deeply in profit; cost-basis selection predicts substantial exit under those conditions. Issuer-reported DRS counts declined by only ∼0.7 million shares (0.9%) across the quarter spanning the burst (75.3M to 74.6M), consistent with the social-infrastructure account and difficult to reconcile with pure cost-basis attrition driving the pattern. Group norms and the social cost of exiting discourage attrition; epistemic infrastructure sustains re-entry. Participants who close profitable call positions frequently reinvest gains into shares, adding to aggregate exposure without appearing as new entrants. Episodes of high options intensity can therefore leave persistent residue in the slow channel even after the burst subsides. Section 3.4 formalises the individual access logic; Appendix B.2 supplies the compositional-turnover algebra.

[26] Known internally as the *great ape migrations*.

6 Just up: escape velocity

Sections 3–4 established that repeated renewal is expensive and that the cost concentrates in brief windows. A participant who bought at low IV faces a more favourable model-implied margin: the survival threshold was locked at a low premium burn, while the touch probability rises with the subsequent volatility burst. When the gambles are successful, each renewal resets the entry IV upward and thins (or flips) that advantage. This section asks whether there is a volatility regime where renewal pays for itself at the prevailing IV, so that entry timing is irrelevant. The margin formula and asymptotic ordering are Tier 1 (exact within stated assumptions); the positive-Φ window and its overlap with historical IV are Tier 4 (theoretical, drift-conditional, untested against historical data).

The section begins with the general renewal margin, where entry and current IV can differ, then focuses on the static case ($\sigma_0 = \sigma_t$) where the margin reduces to a single-parameter cross-section in IV. Constant IV corresponds to geometric Brownian motion, in which the price path is exponential; the static benchmark asks whether convex renewal can sustain itself under those dynamics.

Under the zero-log-drift benchmark used throughout, such a region exists in the calibrations tested[27] (Table 7): inside a narrow IV band, the model implies nonnegative time-average growth at every renewal regardless of when the participant entered. Since this benchmark imposes no directional tailwind on the underlying, the window cannot be attributed to assumed appreciation; it arises from the interaction between renewal geometry, Black–Scholes option cost, and the zero-log-drift touch-probability convention. The region appears at every option tenor in the calibration grid, each time where option cost and touch probability are balanced. Nonzero drift is a comparative static around this baseline: favourable drift broadens the window, adverse drift shrinks or eliminates it (Table 4). The compositional exhaustion that normally erodes a burst is structurally absent inside this region, because the gamble does not require a timing gap to break even. The static assumption requires IV stability across each renewal interval; during bursts, IV moves sharply within days, so the benchmark is most strained where it is most relevant.

At baseline IV, even a correct thesis does not make high-burn renewal growth-positive; that region unlocks only past a critical volatility σ_c (Definition 1), whose location varies across the calibration grid (Table 4).[28]

6.1 The renewal margin

Whether a given renewal clears the threshold depends on two quantities that move on different timescales: the threshold π^*, which is locked at purchase because it depends on the entry IV σ_0 (through κ and L), and the touch probability $P^{\text{touch}}(\sigma_t)$—the probability that the stock reaches the target price before expiry, at which point we assume the position is closed and L is realised (derivation in Appendix C.9). P^{touch} is a function of the current IV σ_t through the diffusion model specified below (equation 46). Their difference defines the *renewal margin*

$$\Phi(\sigma_0, \sigma_t) \;=\; P^{\text{touch}}\big(\sigma_t\big) \;-\; \pi^*\big(\kappa(\sigma_0),\, L(\sigma_0)\big). \tag{45}$$

When $\Phi > 0$, the implied touch probability clears the survival threshold; when $\Phi < 0$, it does not. Both quantities are evaluated at the start of each renewal interval: π^* is locked at entry because κ and L depend on the IV at purchase, while $P^{\text{touch}}(\sigma_t)$ is the barrier-contact probability for a fresh call bought at current spot and current IV. The margin does not track the existing position intra-interval; it governs the economics of the next renewal.

Rising IV and the temporal (dis)advantage. The renewal margin $\Phi(\sigma_0, \sigma_t)$ compares the threshold locked at entry (through κ and L at σ_0) against the touch probability at current IV (σ_t). Outside the static positive-Φ window (Section 6), Φ can only be positive when $\sigma_t > \sigma_0$: higher current IV raises P^{touch} while the threshold remains locked at the lower entry cost. A participant's existing call can go ITM from price movement alone at any IV level; the renewal margin governs whether buying the next call at current conditions is growth-positive.

For the benchmark contract (1.5× OTM, 3× target, 21 DTE), suppose the call is purchased when $\sigma_0 = 80\%$. This locks in a low threshold through $\kappa(\sigma_0)$ and $L(\sigma_0)$. Holding that threshold fixed, the renewal margin becomes positive once current IV rises to $\sigma_t \approx 135\%$. If instead the initial purchase occurred at $\sigma_0 = 120\%$, the locked-in threshold would be higher, and current IV would need to reach ∼170%; at $\sigma_0 = 300\%$, roughly 310% (Figure 7, panel b). The gap between curves at any given σ_t is the temporal advantage of buying early: the cheaper position clears the threshold at IV levels where later entries do not. This advantage is conditional on the IV rise occurring within the option's remaining life; if it does not, the position expires in the $\sigma_0 = \sigma_t$ regime where the margin is negative. Other strike/target combinations shift the curves but preserve the ordering.

Under any sustained IV rise, this asymmetry is self-limiting: each exit-and-rebuy resets σ_0 upward and thins (or flips) the margin. As early-cycle contracts expire and are replaced by entries at elevated premiums, the share of renewals whose next round clears the threshold shrinks: the burst contains the seed of its own exhaustion through compositional turnover.[29] Appendix B.2 gives the full algebra; Appendix B.3 derives the conditions under which each renewal cycle degrades future headroom.

Static IV: renewal under stable volatility. When IV does not change between purchase and evaluation ($\sigma_0 = \sigma_t$), the IV-based temporal advantage vanishes: the renewal threshold is no longer improved by having purchased at a lower volatility, and the margin depends only on the prevailing IV. Across the calm regime the margin is negative, peaking deficit near $\sigma \approx 185\%$ at monthly tenor (dark curve, Figure 7, panel b). A fairly-priced call approximately satisfies arithmetic-mean breakeven $\pi \geq 1/L$, but the survival threshold adds a compounding penalty $-\ln(1-\kappa)$ that fair pricing does not compensate. The next subsection formalises this case and identifies the critical volatility at which

[27] "So you're telling me there's a chance." —Lloyd Christmas, *Dumb and Dumber* (1994).

[28] Below σ_c, the static margin is negative: a participant whose next call is priced at the same IV as the one that expired cannot break even, because κ, L, and P^{touch} are all functions of the same σ. Renewal can still be growth-positive if the participant entered at lower IV, because the threshold is locked at the cheaper entry while P^{touch} reflects the higher current IV. Past σ_c, renewal can sustain itself at the prevailing IV. Each combination of strike, tenor, and sizing defines its own σ_c, and its location shifts with the assumed drift.

[29] This is the popular intuition that early buyers win and late buyers get crushed.

the deficit reverses.

6.2 Static benchmark

Everything from this point forward is theoretical, and assumes static IV: entry and current IV coincide ($\sigma_0 = \sigma_t \equiv \sigma$), collapsing the two-parameter renewal margin to a single-parameter cross-section. Under this assumption, a call's cost is set by the market; Black–Scholes gives κ and L from observed prices. Whether the stock can reach the target price within the option's life depends on the physical dynamics, which requires a drift assumption. The barrier-contact probability is not observable: it depends on what the stock actually does, which requires a physical-measure assumption about drift. We use zero log-drift ($g = 0$, the median-neutral case where the median price path is flat) as the baseline because it builds no directional appreciation or depreciation into the median price path. Any positive-Φ region that appears under this assumption cannot be attributed to an assumed trend.

The gap between the pricing measure and the physical measure drives the result. Option costs are priced under the risk-neutral measure; in the zero-rate, zero-dividend benchmark used here, the corresponding log-drift is $g_{\mathbb{Q}} = -\sigma^2/2$. P^{touch} is evaluated under zero physical log-drift ($g = 0$). The two differ by $\sigma^2/2$; at $\sigma = 500\%$ this is 12.5 in annualised log-drift units. In the parameter grid of Table 4 (first row), risk-neutral drift eliminates the positive-Φ region at every tenor and strike tested. The window exists because the physical measure assigns higher probability to reaching the barrier than the pricing measure builds into the cost. Using risk-neutral P^{touch} for the survival calculation would be circular: risk-neutral pricing embeds $P^{\text{touch}}_{\mathbb{Q}} \approx 1/L$ into the call price, and since $\pi^* > 1/L$ by the Jensen penalty, no risk-neutral touch probability can clear the threshold. Throughout this benchmark, IV serves as the diffusion volatility in both the pricing and physical first-passage calculations; this abstracts from volatility risk premia and isolates the role of drift and renewal timing. The benchmark is deliberately hybrid: option costs are taken from risk-neutral Black–Scholes prices, while renewal feasibility is evaluated using a physical first-passage probability. This reflects the economic distinction between the market price paid for the option and the participant's belief about reaching the barrier. Φ_{static} should therefore be read as a conditional benchmark comparing a market-observed cost to a model-based feasibility object.

Concretely, with $r = 0$[30], the risk-neutral process has zero *level* drift ($\mathrm{d}S/S = \sigma\,\mathrm{d}W^{\mathbb{Q}}$), giving a log drift of $-\sigma^2/2$; the physical assumption has zero *log* drift ($\mathrm{d}\ln S = \sigma\,\mathrm{d}W$), giving a level drift of $+\sigma^2/2$. Zero log-drift is median-neutral (the median path is flat), but it implies positive level drift, which at burst-level IV is large.

The drift assumption in P^{touch} has a direct physical reading. Under static IV and constant physical log-drift g, the time-t median of the price distribution is $S_0 e^{gt}$. Each row of Table 4 corresponds to a different median trajectory: the risk-neutral log-drift benchmark uses $g = -\sigma^2/2$ (in the zero-rate, zero-dividend case); the zero-log-drift benchmark uses $g = 0$, giving a median-flat path; and volatility-proportional positive drifts impose progressively more aggressive directional assumptions. We treat g as a scenario parameter rather than a calibrated estimate, in the same spirit as the survival threshold's treatment of π^{succ} and L. Appendix B.4 develops this geometry and maps the positive-Φ region in (σ, g) space.

Under GBM with physical log-drift g and barrier-to-spot ratio $b := B/S_0$, the first-passage probability is

$$P^{\text{touch}} \;=\; N\!\left(\frac{-\ln b + gT}{\sigma\sqrt{T}}\right) + e^{2g\ln b/\sigma^2}\, N\!\left(\frac{-\ln b - gT}{\sigma\sqrt{T}}\right). \quad (46)$$

At zero log-drift ($g = 0$) this reduces to $P^{\text{touch}} = 2\,N\!\big(-\ln b/\sigma\sqrt{T}\big)$.

The static renewal margin. In the general renewal problem (Section 3), the threshold $\pi^*_t := \pi^*(\kappa(\sigma_0),\, L(\sigma_0))$ is locked at entry while the feasibility measure $P^{\text{touch}}(\sigma_t)$ reprices with current IV, so the margin is path-dependent. Setting $\sigma_0 = \sigma_t \equiv \sigma$ collapses this to a single-parameter cross-section: option cost, payoff leverage, touch probability, and threshold are all functions of the same σ, and the selective-renewal condition of Section 3.3 ($\pi_t \geq \pi^*_t$, where π_t is the conditional feasibility at time t) reduces to $P^{\text{touch}}(\sigma) \geq \pi^*(\sigma)$. The static margin is then

$$\Phi_{\text{static}}(\sigma) \;=\; P^{\text{touch}}\big(\sigma\big) \;-\; \pi^*\big(\kappa(\sigma),\; L(\sigma)\big), \quad (47)$$

where $\kappa(\sigma) = C(\sigma)/S_0$ is the fraction of wealth committed to the call and $L(\sigma) = (\text{target} - K)/C(\sigma)$ is the payoff leverage. Both depend on strike K and target: a far-OTM call has lower κ but needs a larger move to pay off. Different strikes produce different growth-positive windows; Table 7 reports the full calibration grid. Where $\Phi_{\text{static}} > 0$, the model no longer implies bankroll depletion per renewal round, so the capital-depletion channel that feeds into the exit hazard h_t (Section 3.4) shuts off: the static margin is positive rather than erosive, and the participant can in principle maintain convex exposure without the wealth trajectory pushing toward forced exit. Outside the window, each renewal round drains the bankroll and persistence is costly.

Whether Φ_{static} is ever positive depends entirely on the assumed drift.[31] Under risk-neutral log-drift ($g = -\sigma^2/2$) the window collapses entirely; under zero log-drift ($g = 0$, the baseline used here) a positive region opens at high IV; positive drift only widens it (Table 4). Risk-neutral drift is a pricing convention, not a forecast: at 547% IV it implies roughly −1,500% annualised log drift. Zero drift is conservative within the non-negative-drift family and during burst episodes, where realized daily log returns averaged +3.9% (2021, 60 days) and +2.0% (2024, 41 days), though these are noisy path statistics at 28% daily volatility. All numerical results below are conditional on zero drift; "full commitment" means $f = \kappa$ (one call per unit of sleeve wealth).

Mathematical structure.

Proposition 4 (Asymptotic ordering of the static margin terms)**.** *As $\sigma \to \infty$, the barrier-contact probability satisfies*

[30] During January 2021 the effective federal funds rate was 0.09%, making $r = 0$ a good approximation. By May 2024 the rate had risen to roughly 5.33%. The risk-neutral log drift is $r - \sigma^2/2$; at $\sigma = 300\%$ this is −4.50 when $r = 0$ and −4.45 when $r = 5.33\%$, a relative change of order 10^{-2}. Setting $r = 0$ therefore has negligible effect on BS option prices at the IV levels relevant here.

[31] We use "growth-positive" rather than "time-rational" (Section 3) because time-rationality conditions on the unobserved π^{succ}, while growth-positivity conditions on the shape of $\Phi_{\text{static}}(\sigma)$: the window boundaries σ_c, σ_u, and their drift sensitivity are determined by option prices and the diffusion model alone.

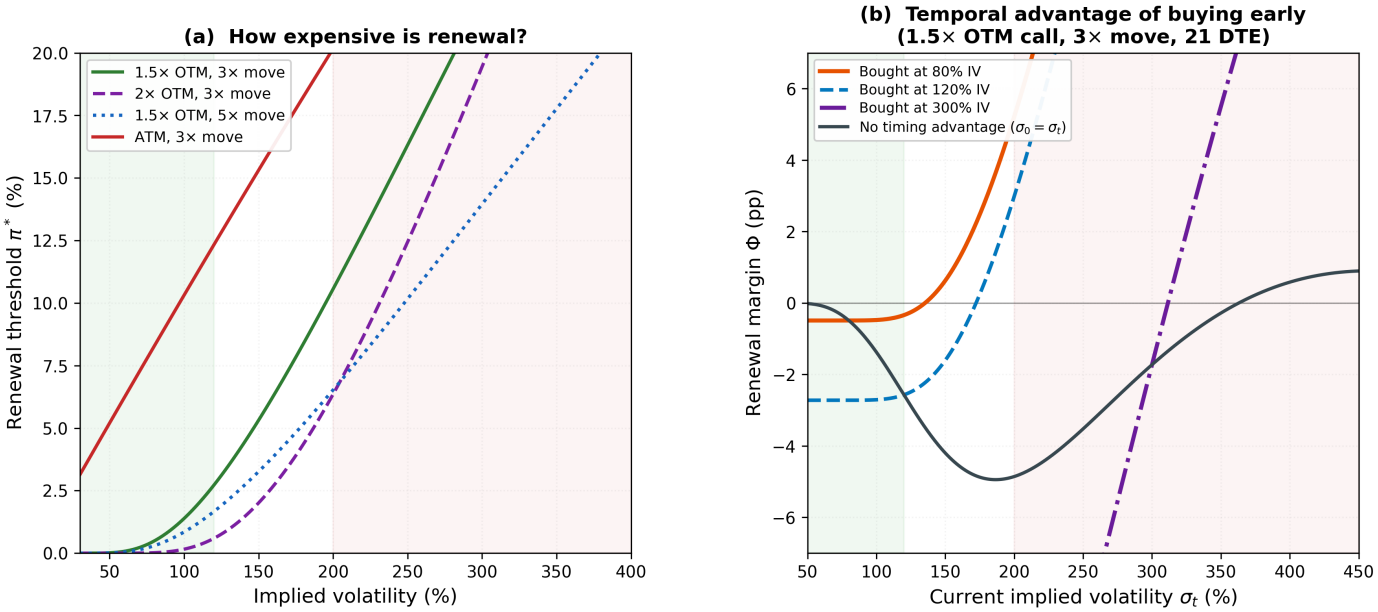

Figure 7: Conditional zero-drift benchmark: implied volatility, renewal cost, and the temporal advantage of buying early. P^{touch} evaluated under zero log-drift; κ and L from Black–Scholes. Green shading: $\sigma \approx 80$–120%; red shading: $\sigma \gtrsim 200\%$. **(a)** Survival threshold π^* as a function of implied volatility for four call positions, all 21 DTE. **(b)** Renewal margin $\Phi(\sigma_0, \sigma_t) = P^{\text{touch}}(\sigma_t) - \pi^*(\kappa, L(\sigma_0))$ for a 1.5× OTM call targeting a 3× move, 21 DTE. Each curve corresponds to a different entry IV. Where $\Phi > 0$ the implied touch probability clears the survival threshold; where $\Phi < 0$ it does not. Participants who entered at low IV cross into positive territory at moderate current IV; late entrants remain negative until dispersion rises well above their entry level. The dark curve is the static-IV case ($\sigma_0 = \sigma_t$, where the next call is priced at the same IV as the one that expired); it is negative across the observed range and crosses zero only near $\sigma \approx 363\%$.

$1 - P^{\text{touch}}(\sigma) = \mathcal{O}(1/\sigma)$, *while the survival threshold satisfies* $1 - \pi^*\big(\kappa(\sigma), L(\sigma)\big) = \mathcal{O}(1/\sigma^2)$.

Proof. Touch probability. Under zero-drift log-diffusion,[32] $P^{\text{touch}} = 2\,N(-\ln b/\sigma\sqrt{T})$ with $b := B/S_0$. As $\sigma \to \infty$, the argument $x := \ln b/(\sigma\sqrt{T}) \to 0^+$. The expansion $N(-x) = \frac{1}{2} - x/\sqrt{2\pi} + \mathcal{O}(x^3)$ for small x gives $1 - P^{\text{touch}} = 2\ln b/(\sigma\sqrt{2\pi T}) + \mathcal{O}(\sigma^{-3})$, decaying as $\mathcal{O}(1/\sigma)$.

Survival threshold. Write $\epsilon := 1 - \kappa(\sigma)$. At $r = 0$ the Black–Scholes call price satisfies $\kappa = N(d_1) - (K/S_0)\,N(d_2)$ with $d_1 = [\ln(S_0/K) + \sigma^2 T/2]/(\sigma\sqrt{T})$, $d_2 = d_1 - \sigma\sqrt{T}$. As $\sigma \to \infty$, $d_1 \sim \sigma\sqrt{T}/2$ for any fixed strike, so $\epsilon = 1 - \kappa \sim 2N(-\sigma\sqrt{T}/2) \sim 4/(\sigma\sqrt{2\pi T})\, e^{-\sigma^2 T/8}$ by Mills: ϵ vanishes exponentially in σ^2. With $L_\infty := \lim_{\sigma\to\infty} L(\sigma) = (\text{target} - K)/S_0 > 1$ (which requires target $> K + S_0$), the threshold from Proposition 1 satisfies

$$1 - \pi^* = \frac{\ln L_\infty + o(1)}{\ln(1/\epsilon)} \sim \frac{8 \ln L_\infty}{\sigma^2 T},$$

because $\ln(1/\epsilon) \sim \sigma^2 T/8$. Hence $1 - \pi^* = \mathcal{O}(1/\sigma^2)$. □

Calibration result. In the Black–Scholes calibrations of Table 7, $\Phi_{\text{static}}(\sigma)$ is numerically single-humped: it achieves a positive value at intermediate σ, and the asymptotic ordering of Proposition 4 implies that π^* must eventually overtake P^{touch} at sufficiently high σ; in the calibrations tested, this bounds the positive region to a single finite interval $[\sigma_{\text{lower}}, \sigma_{\text{upper}}]$. This interval structure is a calibration-dependent numerical finding, not a general consequence of the asymptotic rates alone.[33]

At monthly tenor and baseline calibration, the static curve peaks at $\sigma \approx 458\%$, where $\mathrm{d}\Phi_{\text{static}}/\mathrm{d}\sigma = 0$—by definition, the point at which a marginal increase in volatility raises the touch probability at the same rate as it raises the cost of the gamble (through higher κ and lower L). Below the peak, additional volatility is net fuel: P^{touch} responds more strongly than π^* because the barrier is still far away and wider diffusion opens new paths. Above the peak, additional volatility is net friction: the call price is approaching S_0, so κ absorbs the marginal IV faster than the touch probability improves. The peak is the volatility level at which the model-implied static margin is widest.

The positive-Φ window is bounded by two zeros of Φ_{static}. Both sides of equation (47) are known functions under Black–Scholes, so the crossing condition is an implicit equation in σ alone. In market terms, the lower zero is the implied-volatility level at which the benchmark physical touch probability, evaluated at market IV, compensates for the compounding cost of repeated play. Below it, the benchmark says the barrier is too far away relative to what each round costs. Above it, the gamble pays for itself at a single IV level, with no timing gap needed.

Definition 1 (Critical volatility)**.** *The* critical volatility σ_c *is*

[32] Reflection principle for driftless Brownian motion in log-price space.

[33] Both P^{touch} and π^* converge to 100% as volatility grows without bound, but the threshold gets there faster. If P^{touch} overtakes π^* at some intermediate σ, the rate mismatch eventually forces π^* back above, creating a bounded window. Whether that intermediate crossing occurs at all depends on the calibration; the asymptotics establish the tail ordering but not the crossing.

the smallest solution to

$$P^{\text{touch}}(\sigma) \;=\; \pi^{*}\big(\kappa(\sigma),\, L(\sigma)\big) \tag{48}$$

satisfying $\mathrm{d}\Phi_{\text{static}}/\mathrm{d}\sigma\big|_{\sigma_c} > 0$. *For the calibration used throughout* ($K = 1.5$, *target* $= 3.0$, $T = 21/252$), $\sigma_c \approx 363\%$. *The* upper critical volatility σ_u *is the largest solution to the same equation with* $\mathrm{d}\Phi_{\text{static}}/\mathrm{d}\sigma\big|_{\sigma_u} < 0$; *at the baseline calibration,* $\sigma_u \approx 575\%$.

In the calibrated drift rows of Table 4, changing the drift shifts the boundaries but preserves the single-hump geometry. The asymptotic argument applies directly to the zero-log-drift case; other drift scalings require checking the corresponding high-volatility limit of P^{touch} (Table 4).

6.3 Position sizing

Under the static benchmark, P^{touch} is a known function of σ through the diffusion model, so the calculations below are independent of unobserved probabilities and Kelly optimization becomes possible.

Throughout, "full commitment" denotes the benchmark rule $f = \kappa$: the participant commits the option premium required for one unit of exposure each interval. It does not mean investing 100% of wealth in options. The static margin Φ_{static} assumes full commitment. At smaller commitment the gamble can become growth-positive at lower IV. The Kelly criterion makes this precise.

For the binary payoff structure of Section 3—risk fraction f of wealth, win $f \times L$ with probability p, lose f with probability $1 - p$—the time-average growth rate is

$$G(f) \;=\; p\,\ln\big(1 - f + f\,L\big) \;+\; (1-p)\,\ln(1-f)\,, \tag{49}$$

Setting $\partial g/\partial f = 0$ and solving gives the Kelly-optimal fraction

$$f^{*} \;=\; p \;-\; \frac{1-p}{L-1}\,, \tag{50}$$

which is positive whenever $p > 1/L$.

In the general renewal framework (Section 3), κ is a free parameter. Once a strike, target, and tenor are fixed, Black–Scholes maps the prevailing IV to a specific (κ, L) pair on the threshold surface; the participant cannot vary κ independently of L at a given σ. What the participant can choose is how many contracts to buy per unit of wealth, deploying f per interval (where $f = \kappa$ corresponds to one call per unit of wealth). At any σ where $f^{*} > 0$, the gamble has positive growth at optimal sizing; full commitment ($f = \kappa$) may over- or under-bet relative to f^{*}. At the baseline calibration, $f^{*}/\kappa \approx 0.46$–$0.51$ across the monthly full-commitment positive-Φ window, meaning full commitment exceeds the Kelly-optimal fraction by roughly a factor of two. The ratio varies substantially with tenor and IV level (Figure 8): at shorter tenors the ratio drops sharply (e.g. $f^{*}/\kappa \approx 0.26$ for weekly calls at $\sigma = 547\%$), and weekly calls at $\sigma = 363\%$ are not growth-positive at all.

Over-betting matters quantitatively: Kelly-optimal growth turns positive at a much lower IV than full commitment (see "Tenor dependence" below), and at the monthly static peak ($\sigma = 458\%$) delivers 4.6× higher growth per interval (+0.051 vs +0.011). Sizing at f^{*} preserves the barrier-reach probability while widening survival margins per losing round. An OTM call and an ATM call are different gambles with different (κ, L, p) triples, so their Kelly fractions and growth-rate landscapes differ.

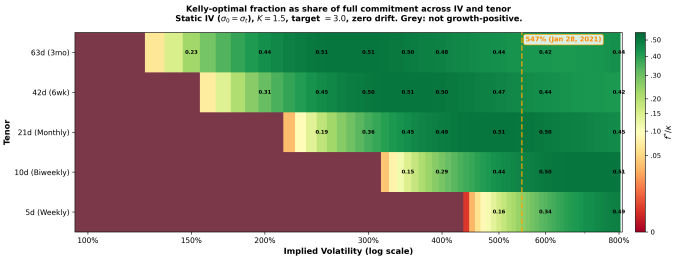

Figure 8: Kelly-optimal fraction as a share of full commitment (f^{*}/κ) across implied volatility and tenor, under the static assumption ($\sigma_0 = \sigma_t$; IV constant across each renewal interval). Baseline calibration: $K = 1.5\times$ spot, target $= 3.0\times$, zero drift. Grey cells: gamble is not growth-positive ($f^{*} = 0$). At monthly tenor within the full-commitment window (363–575%), the ratio sits in the range 0.46–0.51; at shorter tenors and lower IV the ratio drops sharply, indicating severe overbetting under full commitment. Dashed orange line marks the 30-day IV peak on January 28, 2021.

6.4 The growth-positive window

Figure 9 plots the per-interval growth rate $G(f)$ across three tenors (weekly, biweekly, monthly) under both Kelly-optimal sizing and full commitment; the description below follows the monthly curves (tenor dependence is discussed separately below). Under full commitment ($f = \kappa$), the growth rate turns positive at $\sigma \approx 363\%$, peaks near +1.1 pp at $\sigma \approx 464\%$, and falls back through zero at $\sigma \approx 575\%$, diverging negatively as overbetting at extreme IV destroys the bankroll. Under Kelly-optimal sizing ($f = f^{*}$), the positive region opens much earlier ($\sigma \approx 214\%$) and the growth rate rises monotonically through the burst-IV range, peaking at +6.1 pp near $\sigma \approx 631\%$. The Kelly curve is more robust at every IV level within the positive region.

Friction sensitivity. The full-commitment window is fragile: a 5% proportional bid-ask spread on the option premium (applied as a cost increase to κ at entry) eliminates the full-commitment peak entirely, because the monthly full-commitment peak margin (+1.1 pp) is small relative to realistic round-trip costs for far-OTM weeklies (15–30% of mid-market premium) and monthlies (5–15%). Under Kelly-optimal sizing the positive region is considerably wider and its onset lower ($\sigma \approx 214\%$ vs. 363% at monthly tenor), so the Kelly curve survives moderate friction at IV levels where the full-commitment window has already vanished. During burst episodes, bid-ask spreads on GME options narrowed as volume surged [55], so the zero-friction benchmark is most defensible during the episode where the window was binding. Friction also operates at exit: bid-ask spreads on the option at the moment of sale reduce the effective payoff multiple L, raising the threshold through the same channel as higher κ. For far-OTM calls during bursts, exit spreads of 20–50% of option value are plausible, compressing L substantially. The frictionless results in the remainder of this section should be read in light of both entry and exit friction.

At monthly tenor, the trough around $\sigma \approx 200\%$ is the region of maximum drag: volatility raises the cost of the gamble faster than it opens new paths to the barrier, so the margin deepens to its most negative point. Reaching the positive region from the trough requires IV to traverse the entire increasing-drag zone.[34]

[34] An analogy: a rocket must push through the densest atmosphere before reaching orbit. The trough at $\sigma \approx 200\%$ is that dense atmosphere; the

In the dynamic (non-static) case, a locally negative static margin at the trough does not condemn a strategy: if IV rises, a participant positioned at low IV benefits from the temporal advantage. Whether any particular episode's IV trajectory reaches the growth-positive region depends on conditions the framework does not predict.

Inside the positive static region, the time-average and arithmetic-mean criteria agree on sign. The reason is Jensen's inequality: at the arithmetic-mean breakeven $\pi = 1/L$ (where $\mathbb{E}[R] = 1$), the time-average growth rate is $G(1/L) = \mathbb{E}[\ln R] < \ln(\mathbb{E}[R]) = 0$, strictly negative because ln is concave and R is non-degenerate. The survival threshold π^* (where $G = 0$) therefore sits above $1/L$. Whenever $\Phi_{\text{static}} > 0$, i.e. $P^{\text{touch}} > \pi^* > 1/L$, the gamble clears both criteria—but the time-average criterion remains the binding one because it governs repeated survival under multiplicative wealth.

6.5 Tenor, sensitivity, and historical overlap

Tenor dependence. Under continuous renewal, shorter-dated options burn faster per interval, shifting the growth-positive onset upward (Table 3). Monthly options open the positive region at the lowest IV and dominate at moderate volatility; biweekly options require higher IV but produce the highest annualised growth at the January 2021 burst level ($\sigma \approx 547\%$); weekly options become growth-positive only at extreme IV but dominate the annualised column above $\sigma \approx 800\%$, because the shorter interval compounds more frequently. During a volatility event the term structure inverts, so shorter-tenor contracts face higher effective IV than the 30-day measure suggests. Tenor also governs how restrictive the static assumption is: the growth-rate results assume IV is constant across each renewal interval, so for weekly calls the approximation requires IV stability over each five-day interval, while for monthly calls it requires stability over each twenty-one-day interval. The static assumption requires IV stability only across each renewal interval, so shorter tenors impose a weaker requirement in calendar time; but IV can move sharply within a single week during a burst, so the advantage is suggestive rather than decisive.

The structure extends to longer tenors. At quarterly and yearly horizons the full-commitment window descends into the 100–300% IV range, where Black–Scholes pricing is well-calibrated and the underlying behaves more like a continuous diffusion. A 3× target move is also more plausible over a year than over a week, so the calibration sits in more natural territory at longer tenors. The margins are modest compared to the short-tenor burst-IV figures, but they sit in terrain where the model's assumptions are least controversial. Figure 10 shows how the threshold landscape compresses at short tenor and extreme IV.

The annualised figures in Table 3 are mechanical extrapolations of fixed-IV per-interval growth rates; they are not forecasts and should not be read as historically attainable returns, because IV, bid-ask spreads, liquidity, and position availability all vary within bursts.

Historical overlap: January 2021 (Tier 4). At the baseline calibration ($K = 1.5$, target $= 3.0$), the static benchmark's full-commitment positive region was entered once in five years of data: during three trading days in January 2021 (January 26–29, $\sigma_{30\text{d}} \in [393\%, 547\%]$), before broker purchase restrictions ended the episode. The 30-day IV on January 28 reached 547%, inside the monthly full-commitment window (363–575%) and above the weekly Kelly-optimal onset (≈440%). Near-term weekly contracts traded at IVs well above the 30-day measure—industry sources reported contract-level IVs exceeding 1,000%—entering the weekly full-commitment window (744–1,179%). At the IV levels prevailing over the rest of the five-year period, the static benchmark is negative at every tenor. This identifies overlap with the benchmark's parameter region, not evidence that the benchmark conditions were historically satisfied.[35] The window's location is set by calibration parameters (strike, target, tenor, drift), not by any GameStop data; the overlap is an observation, not an input to the derivation.[36] Table 7 (Appendix D) reports the full calibration grid.

Table 3: Kelly-optimal growth rate $G(f^*)$ per renewal interval and annualised, across three tenors. Baseline calibration: $K = 1.5$, target $= 3.0$, zero drift. Blank cells indicate the gamble is not growth-positive at that tenor and IV. Annualised figures are computed as $\exp(G(f^*) \cdot 252/T) - 1$ and assume continuous renewal at the stated tenor with IV held fixed.

	Weekly (5 d)		Biweekly (10 d)		Monthly (21 d)	
σ	$G(f^*)$	Ann.	$G(f^*)$	Ann.	$G(f^*)$	Ann.
225%	—	—	—	—	+0.0003	0.4%
300%	—	—	—	—	+0.015	20%
363%	—	—	+0.004	9%	+0.033	48%
400%	—	—	+0.009	26%	+0.041	64%
458%	+0.0002	1%	+0.020	65%	+0.051	85%
500%	+0.002	13%	+0.028	102%	+0.056	95%
547%	+0.007	41%	+0.036	149%	+0.059	103%
600%	+0.013	97%	+0.044	203%	+0.061	107%
700%	+0.027	290%	+0.054	291%	+0.060	105%
800%	+0.039	618%	+0.059	345%	+0.057	99%
900%	+0.048	1044%	+0.061	362%	+0.054	92%
1000%	+0.055	1471%	+0.060	356%	+0.052	87%
1200%	+0.060	1989%	+0.056	314%	+0.051	85%
1500%	+0.059	1879%	+0.052	267%	+0.059	104%

Sensitivity. The baseline calibration ($K = 1.5\times$ spot, target $= 3\times$ spot) reflects a common structure for far-OTM GME calls during the sample period: the strike sits mid-chain, and the target corresponds to the stock reaching roughly the farthest available strike. Lower targets exit closer to the strike, compressing L; higher targets require moves that the diffusion rarely delivers within one tenor. The benchmark is not unique to the baseline cell: across the calibration grid (Table 7, Appendix D), positive static regions appear whenever the target sufficiently exceeds the strike, and σ_c falls strongly with tenor. Overlap with the January 2021 IV range is common but concentrates in longer-tenor and OTM configurations; short-tenor near-ATM cells fail to reach the burst range.

Figure 11 maps Φ jointly over strike and target at monthly tenor, for four IV levels. At calm IV the margin is negative everywhere. As IV rises, a positive region opens from moderate OTM strikes toward higher targets; at extreme IV, near-ATM

positive window is orbit, where each renewal that clears the threshold funds the next cycle; past σ_u the threshold's faster convergence reasserts itself—the spacecraft escapes orbit entirely, too fast to stay in the window, too expensive to sustain.

[35] WallStreetBets folklore warns, in its own colourful terms, to never go full commit. Kelly agrees: $f^*/\kappa \approx 0.46$–0.51 across the monthly window (Figure 8), so $f = \kappa$ overbets by about 2×. That even this overbetting rule finds a growth-positive window is the surprise.

[36] Option bid-ask spreads on GME narrowed during the burst as volume surged [55], making the zero-friction assumption more plausible in practice during the episode where the window was binding.

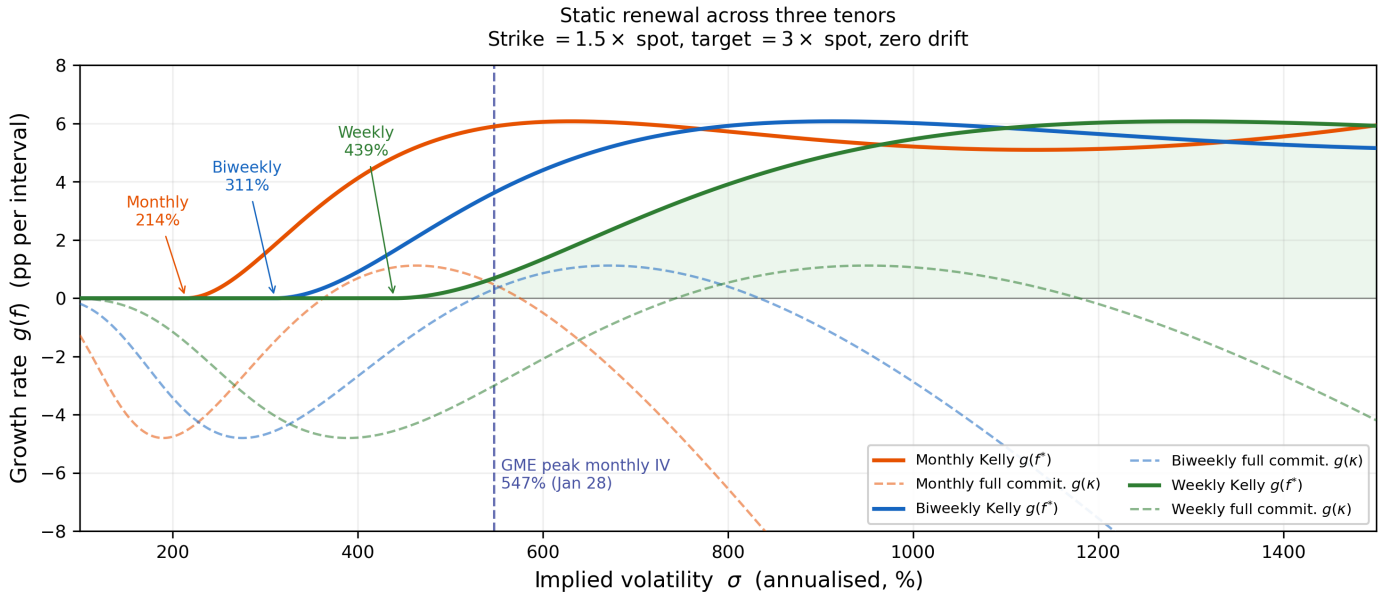

Figure 9: Conditional benchmark ($\mu = 0$): static renewal growth rate $G(f)$ when entry and evaluation IV coincide ($\sigma_0 = \sigma_t$), across three tenors. Under risk-neutral log-drift ($g = -\sigma^2/2$) no positive region exists at any tenor (Table 4). Solid curves (primary): Kelly-optimal $G(f^*)$, where $f^* = p - (1-p)/(L-1)$ is recomputed at each IV; dashed (secondary): full commitment $g(\kappa)$, which overbets and whose positive region is fragile to transaction costs. Green: **weekly** (5 trading days); blue: **biweekly** (10 trading days); amber: **monthly** (21 trading days). Kelly onset shifts with tenor: monthly at $\sigma \approx 214\%$, biweekly at $\approx 311\%$, weekly at $\approx 440\%$. The dashed vertical marks the 30-day IV peak on January 28 (547%); near-term contract IVs traded substantially higher. Green shading marks the weekly Kelly growth-positive region. Strike at 1.5× spot, target move 3× spot.

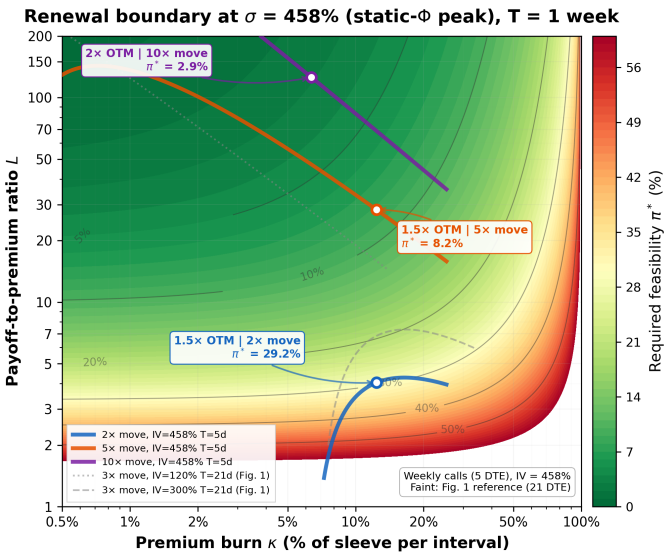

Figure 10: Survival-threshold landscape at $\sigma = 458\%$ (static-Φ peak), $T = 5$ trading days. Solid curves trace the Black–Scholes locus from ATM to far OTM for three target moves (2×, 5×, 10× spot). Faint reference curves show the IV = 120% and 300% loci from Figure 1 ($T = 21$ d). At extreme IV and short tenor, the loci compress toward higher κ and lower L relative to the monthly baseline.

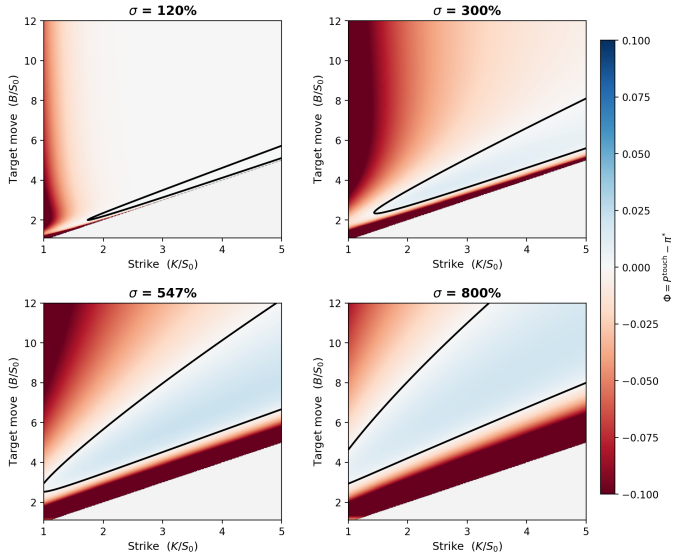

Figure 11: Renewal margin $\Phi = P^{\text{touch}} - \pi^*$ over the strike-target plane at monthly tenor (21 d), zero drift. Blue: $\Phi > 0$ (renewal is growth-positive); red: $\Phi < 0$ (renewal destroys time-average wealth). Black contour: $\Phi = 0$. Grey region below the diagonal ($B = K$): call has no intrinsic value at the target. Each panel fixes IV; both κ and P^{touch} are computed from Black–Scholes and the zero-drift diffusion respectively.

calls lose margin again as κ approaches saturation. The dark red band along the diagonal ($B \approx K$) is the low-L trap: when the target barely exceeds the strike, L is small and π^* is prohibitive. Shorter-tenor versions (Appendix D) compress the feasible zone and shift it toward higher IV.

Table 4 reports the window boundaries under varying drift. The window first opens at approximately $m \approx -0.02\,\sigma^2$, far above the risk-neutral value ($m = -0.5\,\sigma^2$); this is the existence threshold for a positive full-commitment region. Volatility-dependent positive drifts ($m = +\sigma^2/8$, $+\sigma^2/4$) eliminate the upper boundary within the computed range.

Table 4: Drift sensitivity of the positive-Φ window ($K = 1.5$, target $= 3.0$, $T = 21$ d). "—": no positive region; ">2k": upper boundary exceeds search range. Ascent rate $g = m + \sigma^2/2$ is the log-drift of the median path; at $\sigma = 300\%$, $g = +\sigma^2/4$ implies median doubling every ≈3.5 months. See Appendix B.4 for the (σ, g) phase diagram.

Drift m	Ascent g	σ_c	σ_u	Peak	Width
$-\frac{1}{2}\sigma^2$ (r.-n.)	$-\sigma^2/2$	—	—	—	—
$-\frac{1}{4}\sigma^2$	$-\sigma^2/4$	—	—	—	—
$-\frac{1}{8}\sigma^2$	$-\sigma^2/8$	—	—	—	—
0 (baseline)	0	363	575	+0.9	212
$+\frac{1}{8}\sigma^2$	$+\sigma^2/8$	279	>2k	+7.1	>1721
$+\frac{1}{4}\sigma^2$	$+\sigma^2/4$	246	>2k	+13.8	>1754
$+\frac{1}{2}\sigma^2$	$+\sigma^2/2$	100	>2k	+98.6	>1900
+5% fixed	+5%	357	581	+1.0	225
+10% fixed	+10%	351	587	+1.1	236

Convex renewal versus equity holding. Under our zero-log-drift assumption ($g = 0$, symmetric random walk in log space), a fully invested stockholder's time-average growth rate is $g_{\text{equity}} = 0$: the median trajectory is flat regardless of volatility. The Kelly-optimal call buyer at $\sigma = 547\%$ (the January 28 30-day IV peak) earns $G(f^*) \approx +0.06$ per monthly interval (≈103% annualised) or +0.007 per weekly interval (≈41% annualised). The entire edge comes from the convex payoff structure: the call buyer's downside is bounded (lose at most f per interval) while the upside scales with L. At extreme volatility, the large random fluctuations hit the barrier often enough that this asymmetry compounds into positive time-average growth, even though the underlying has zero log-drift and a flat median trajectory. The stockholder, holding linear exposure, gets none of this—*the call buyer's loss is capped at the premium each round while the win scales with L; the equity holder holds symmetric exposure to the same diffusion and converts none of that volatility into growth.*

6.6 Scope and model dependence

The positive-Φ window rests on the measure gap introduced above: π^* is model-free (set by call prices alone), while P^{touch} depends on the physical drift. Appendix B.4 makes this geometry explicit by parameterising the measure gap as a choice of exponential ascent rate for the median price path. From (46), the Itô drag $-\sigma^2/2$ dominates at high IV, making the risk-free rate irrelevant; during a burst, directional forces consistent with the patterns in Sections 4–5 may offset the geometric drag.

The static margin $\Phi_{\text{static}}(\sigma)$ collapses the path-dependent general margin to a memoryless cross-section by setting $\sigma_0 = \sigma_t$. The positive-Φ window is therefore a property of the static geometry alone; how the system moves through IV space, and whether headroom degrades irreversibly, are questions beyond the present scope.

The window requires no volatility model beyond the Black–Scholes diffusion used to calibrate option costs, but it does require a physical-measure drift scenario ($g = 0$ in the baseline). In the static benchmark, the same σ drives both $\kappa(\sigma)$ and $P^{\text{touch}}(\sigma)$, while the drift parameter determines how the physical barrier probability differs from the risk-neutral pricing measure. Under the static regime ($\sigma_{\text{physical}} = \sigma_{\text{implied}}$) and zero drift, a single parameter drives both the cost $\kappa(\sigma)$ and the barrier-hitting probability, so the existence of the window is a theorem about the pricing formula evaluated against its own dynamics. Ensemble no-arbitrage holds throughout: under the risk-neutral measure every call is fairly priced at every σ. But ensemble no-arbitrage does not constrain time-average growth rates in either direction. Over most of σ space the renewal gamble is time-average-negative ($\Phi < 0$); in the positive-Φ interval it turns growth-positive. Both facts are consistent with ensemble-fair pricing because the ensemble breakeven κ/L and the time-average threshold π^* are distinct objects (separated by the concavity of log), and nothing in the fundamental theorem of asset pricing equates them. Risk-neutral pricing rules out static arbitrage under the pricing measure; it does not rule out positive physical-measure log growth for a risky strategy when the assumed physical hitting probability differs from the risk-neutral one. The positive-Φ interval is a statement about the specified physical benchmark, not a model-free arbitrage.

7 Discussion and conclusion

This section summarises the contributions by evidentiary tier, interprets the findings through the collective-infrastructure lens, connects to ergodicity-based cooperation, and assembles a real-time constraint stress checklist from publicly observable gauges. It also states limitations and scope boundaries. The strongest results are along the intensity axis (Tiers 1–2); the persistence axis is suggestive (Tier 3); the static margin is theoretical (Tier 4).

7.1 Summary of contributions

Derived (Tier 1, within stated assumptions): The survival threshold under multiplicative renewal (Proposition 1); the Jensen decomposition linking the ergodicity wedge and the survival threshold (Proposition 3); the access probability $\pi/(\pi+h)$ showing that lower exit hazard strictly increases the chance of being present when the rare payoff arrives (Proposition 2); the relay threshold showing that collective arithmetic renewal can clear $1/L$ even when individual compounding is time-irrational (Section 3.5); the mixed dollar-wealth survival object (Section 3.7); the static renewal margin formula (Section 6); and asymptotic convergence rates (Proposition 4).

Measured (Tier 2): Wedge concentration in two descriptive anchor episodes (59% of cumulative mass in 8% of trading days, significant against permutation null); state-dependent threshold shifts; capacity relevance during bursts. A durable slow persistence channel is established at low frequency by issuer-reported DRS counts peaking at ∼25% of shares outstanding, with relative fraction declining under dilution.

Interpretive (Tier 3): The collective-infrastructure account of how decentralised practices sustained exposure (Section 5)—consistent with the measured patterns but not causally identified.

Theoretical and forward-looking (Tier 4): The Kelly-optimal growth-positive region (onset dependent on strike, target, and tenor under zero drift; Figure 11), whose location and width are sensitive to drift assumption (Table 4): under adverse drift the region shrinks or vanishes; under favourable drift it broadens. The full-commitment window (363–575% monthly, 744–1,179% weekly at the baseline calibration) is a zero-friction, zero-drift limiting case.

The framework replaces the conventional dismissal of speculative persistence with a sharper question: what does it cost to maintain convex exposure long enough for a rare-regime payoff to arrive?

7.2 Observed participation patterns

The social object is a heterogeneous group of tail-concerned shareholders whose core membership has persisted for over five years, alongside collective infrastructure consistent with lower exit hazard (Section 5). In practice, participation appears in two broad forms: long-horizon shareholding, including direct registration, which mechanically removes shares from intermediated circulation and alters the effective float denominator; and recurring short-dated call purchases around focal dates. Shared research and public discussion accompany both forms, circulating interpretations of publicly available data that inform individual positioning. This description is interpretive; the causal links are not identified. For the slow persistence channel, Section 3.4 shows that the relevant discipline is benchmark-relative access rather than contractual burn: opportunity-cost and liquidity pressure act through exit hazard, while continued exposure preserves access to the rare payoff.

Attention is not all you need. A pure attention story predicts that retail participation decays rapidly once price action reverses and that the intensity–persistence surface is one-dimensional. Three features of the data resist that prediction: call OI persists across successive monthly OPEX dates during burst episodes, consistent with systematic rolling (Section 3.3) rather than one-shot speculation; the shareholders have maintained exposure across a five-year horizon that includes dilution, adverse price action, the 2024 burst and its aftermath, and platform disruptions; and within the top activity decile the persistence proxy stratifies the wedge ($F = 4.79$, $p = 0.003$; Section 4), suggesting the surface carries information beyond a single activity dimension. The persistence pattern connects loosely to the literature on timing in speculative environments [49], though the present evidence is descriptive and does not identify a coordination mechanism. The duration itself is the fact that any alternative account has to match.

7.3 Relation to prior work

Our dynamics-first stance follows Peters and Gell-Mann: evaluate a gamble after specifying its time embedding and identifying the appropriate ergodic observable [6, 5, 4]. On market structure, we use the SEC staff report as an anchor for early-2021 conditions and for treating obligations versus elastic supply as the structural object [9]; the May–June 2024 burst, coinciding with the return of Roaring Kitty, serves as the second anchor episode; the ATM offerings and subsequent dilution were a consequence of that episode. For the options channel, we adopt a reduced-form proxy stance consistent with demand-based option pricing perspectives [8].

Nested-option recursions. The renewal model studied here is a multiplicative stochastic process: realised wealth after one round determines the capital available for the next, and repeated losses can force exit. Kremnev [54] studies a distinct object: a deterministic recursion on expected values for an iterated rectified-payoff chain, motivated by options written on the expected payout of earlier layers. In Kremnev's at-the-money expected-value recursion, the per-stage gain is $\beta = \sigma/\sqrt{2\pi}$, yielding an arithmetic critical threshold at $\sigma^* = \sqrt{2\pi} \approx 251\%$ for divergence of the infinite expected-value sum. In a separate selective-survival/ATV model—not the same nested-expectation recursion—Kremnev derives a lower conditional-growth threshold $\sigma^*_{\text{th}} = \sqrt{\pi/2} \approx 125\%$ and uses it to motivate heavy-tailed survivor outcomes. We cite Kremnev as adjacent work on recursive rectified-payoff systems, not as a derivation of the survival threshold developed here. The distinction is conceptual as well as mathematical: Kremnev's threshold concerns divergence of iterated expectations, an arithmetic-mean property, whereas Proposition 1 studies the sign of $\mathbb{E}[\ln R]$ for a participant repeatedly renewing convex exposure, a time-average growth criterion under multiplicative wealth dynamics. The connection is therefore qualitative rather than identity: both frameworks involve rectified payoffs and iterative feed-forward, but our threshold shift relative to arithmetic breakeven is given internally by the Jensen-tax decomposition of Section 3.7 and should not be read as a direct restatement of Kremnev's volatility thresholds.

Limits to arbitrage and heterogeneous beliefs. The standard limits-to-arbitrage framework [56] explains why mispricings persist when arbitrageurs face capital constraints and performance pressure: a position that is correct on fundamentals can be liquidated before convergence if interim losses trigger withdrawal. The survival threshold adds a complementary dimension: even unconstrained participants face a compounding penalty under multiplicative dynamics that the ensemble-average framework misses. The two are different layers of the same problem—capital-constraint risk operates through the fund-investor relationship, while the survival threshold operates through the wealth process itself. Scheinkman and Xiong [57] model speculative dynamics under heterogeneous beliefs with short-sale constraints; their overvaluation result—where the resale option allows prices to exceed agents' fundamental-dividend valuations—addresses price formation under disagreement, while the present framework addresses the cost of holding under a maintained belief. Their model explains why an asset can trade above fundamental valuation; ours asks what it costs a believer to stay exposed long enough for the belief to resolve. The community ecology of Section 5, where tail-concerned shareholders assign decision-relevant probability to a rare regime that most market participants dismiss, is the empirical setting where both frameworks apply simultaneously.

7.4 Survivorship bias

The obvious alternative is survivorship bias: whoever stayed just happened to have a low cost basis. The DRS trajectory does not eliminate that possibility, but it is difficult to reconcile with a pure rapid-attrition account: absolute registrations declined only modestly over nearly four years despite a 4:1 split, multiple ATM offerings, and sustained adverse price action (details in the DRS trajectory paragraph of Section 7.9). Aggregate call OI has also declined at low frequency since 2021, consistent with gradual erosion of the fast channel alongside the slow channel. The evidence favours durable persistence with gradual erosion over a fully transient-holder interpretation.

7.5 Relation to ergodicity-based cooperation

Peters and Adamou [1] show that pooling and sharing resources raises the time-average growth rate of each cooperator, so that cooperators outgrow non-cooperators even when the expected-value calculation sees no benefit. The GME case shares the multiplicative dynamics but differs in form: there is no formal wealth pooling; instead, decentralised contributions to a shared informational environment may lower exit hazard (Section 3.4) and accompany renewal conditions. The aggregate exposure can be mathematically approximated as a single participant facing a repeated rare-payoff gamble—many independent decision-makers whose convergent reasoning from shared inputs can produce correlated positioning. Whether the collective infrastructure improves the gamble's terms or only prolongs exposure is an open question the framework identifies but does not resolve.

7.6 Reading the threshold

The upward curvature of the threshold surface (Figure 1) is the central object: the ergodicity distinction applied to repeated option renewal. The threshold $\pi^*(\kappa, L)$ sets the bar that π^{succ} must clear; it does not say whether renewal is rational, because π^{succ} is unobserved. A participant who holds mostly shares and sizes the call sleeve small faces a lower portfolio-level threshold, because the shares do not burn; in the limit the floor is $1/L$ (Remark 2). The relay (Section 3.5) means the collective can sustain arithmetic pressure even where individual compounding is negative: the gap between π^* and $1/L$ is the Jensen penalty, and for any π^{succ} that falls inside it the gamble is time-irrational for a single compounder but arithmetically viable across cohorts.

The ergodicity wedge $\hat{\Delta}_t$ and the survival threshold π^* are not merely parallel objects but two instances of the same Jensen-tax functional developed in Section 3.7. For the equity sleeve, the wedge is the realised analogue of $\mathcal{J}_{\text{eq}} = \ln \mathbb{E}[G] - \mathbb{E}[\ln G]$. For the renewal sleeve, the gap $\pi^* - 1/L$ is the binary Jensen tax scaled by the log-return spread—the compounding penalty that separates time-average from arithmetic breakeven. The wedge measures this penalty on the equity sleeve; the threshold measures the success probability required to overcome it on the options sleeve. In the mixed dollar-wealth problem, the relevant object is the full portfolio Jensen tax $\mathcal{J}_{\text{mix}}$, so the share-equivalent threshold should be read as a slice of a more general mixed survival condition rather than as the final object in dollar terms. For actual call contracts, this link is stronger than a shared functional form: Remark 4 shows that the binary renewal model is a coarse-graining of a path-conditioned payoff generated by the same underlying price path as the equity sleeve, with an additional conditional Jensen tax arising from dispersion of realised payoff multiples within the success branch.

The renewal margin $\Phi(\sigma_0, \sigma_t)$ connects the threshold to frictionless options pricing. When $\Phi > 0$ the implied touch probability clears the threshold; when $\Phi < 0$ the gamble destroys time-average wealth over repeated play under the assumed physical diffusion. The margin can be negative during calm periods and can turn positive when IV rises above the entry level.

Together, these give a structural reading of the hyperrationality argument [11]. If the hedging-feedback channel of Appendix B.3 operates, aggregate call open interest during negative-Φ periods may pressure dealer hedging books, which may feed back into IV: the positioning would then be not passive waiting but an input to a price-mediated feedback loop that requires no coordination among participants. In January 2021 this is what the data show: options demand and 30-day IV moved together from baseline into a burst regime, consistent with the feedback channel [9], and at the peak levels reached the static benchmark places the IV inside the growth-positive region for weekly tenor (Figure 9).

The static-IV benchmark becomes empirically relevant when an exogenous mechanism stabilises, rather than spikes, the volatility regime. Convertible-bond issuance can be one such channel: the embedded conversion option supplies equity optionality to the market, while convertible-arbitrage holders commonly hedge by shorting the underlying at the bond's delta and rebalancing dynamically. When those hedges are maintained smoothly, the resulting flows are mechanically contra-price and can dampen realised price swings, which may feed back into lower implied volatility. More broadly, capital-structure events that credibly reduce residual uncertainty or tail optionality—a definitive acquisition, a sustained earnings trajectory, or financing that resolves balance-sheet risk—can narrow the distribution of outcomes and make the static-IV approximation more realistic. In the present setting, however, that same compression moves IV away from the high-volatility growth-positive region.

7.7 Drift sensitivity

As established in Section 6.6, positive log-price drift widens the growth-positive window, lowering σ_c and raising σ_u, while adverse drift can collapse it. The negative-drift rows in the sensitivity table show no window because the tested adverse-drift specifications scale with σ^2, making the drift penalty enormous at burst-level volatility. Interest rates enter through this drift channel. If λ denotes the arithmetic excess price-return drift and dividends are ignored, the physical log-price drift is approximately $g \approx r + \lambda - \frac{1}{2}\sigma^2$. In burst regimes ($\sigma > 200\%$), the Itô drag $\sigma^2/2$ dominates plausible rate effects, so rates are second-order for the window location. At moderate IV, however, the rate term can matter: mechanically, higher r raises g for a fixed λ, widening the positive-Φ window. But λ is not fixed across macro regimes. Rate increases can change expected cash-flow growth, required returns, financing conditions, and risk premia, so the net effect on $g = r + \lambda - \sigma^2/2$ is ambiguous and regime-dependent. The drift channel becomes most relevant at long tenor, where the growth-positive onset occurs at moderate volatility: at yearly tenor with Kelly-optimal sizing, the onset is already near 62% IV under zero drift, and modest positive drift could push it lower, potentially into the IV range of high-volatility single-name equities. Which macro regime delivers that drift—and whether rate environments that raise r also alter λ enough to offset it—is an empirical question the present framework identifies but does not answer.

Whether realised drift over a given holding period is large enough to matter, and how margin dynamics interact with stochastic IV paths rather than static snapshots, remain open questions. Tenor matters here: the static assumption requires IV stability only over each renewal interval, so weekly renewals require a shorter local-stability window than monthly renewals, though at the cost of greater rollover frequency and potentially greater transaction-cost sensitivity. Quantifying the interaction between tenor, IV dynamics, and the static benchmark is left to future work.

7.8 What the appendices do

Three appendices supply the technical background that the discussion draws on. Appendix B calibrates the abstract (κ, L) parameters against Black–Scholes prices, supplies a simplified cohort-average algebra for the ignition-to-exhaustion arc, and sketches a reduced-form feedback loop between the renewal margin and implied volatility; under a mean-field approximation, aggregate call buying feeds back into IV (Lemma 1), cycle-time heuristics near the critical boundary suggest quadratic compression while margin vanishes linearly (Remark 5), and each completed cycle weakly degrades future headroom (Proposition 5, Corollary 1). Appendix C defines the empirical proxies—options intensity γ_t, the persistence coordinate q_t, boundary relevance B_t (call open interest relative to the float proxy), and the repricing diagnostic—and reports the concentration tests and diagnostic stress checks. Appendix D runs mechanical stress tests: the self-excited volatility test (Appendix D.2) finds that high intensity predicts *lower* subsequent B_t, consistent with the two-channel separation; the counterfactual π stress test (Appendix D.3) maps the viable parameter region and identifies a sharp threshold crossing between ruin and growth at $\pi \approx 2$–5% in the tested parameter grid.

7.9 Capacity relevance and the constraint pathway

The survival threshold tells a participant what renewal costs. The constraint pathway asks how *the* rare regime—MOASS—might arrive. "Capacity relevant" means B_t large enough that dealer hedging against outstanding call OI generates material price feedback; "constraint pathway" means a scenario in which price-inelastic obligations exceed elastic supply, generating forced buying that feeds back into price (formalised in Appendix A).

Dealer reflexivity estimates (Appendix D.1) confirm that median hedging flow during burst episodes reaches 0.5–0.9% of ADV per 1% move, consistent with capacity-relevant flow on days with large price swings. The near-binding scorecard (Appendix D.4) assembles four observable gauges—capacity relevance B_t, the expensive-time wedge $\hat{\Delta}_t$, risk-neutral touch probability P_t^{touch}, and post-OPEX OI persistence—into a *constraint stress checklist* (Appendix D.5). Gross B_t counts all call OI at face value; far-OTM calls contribute less immediate hedging demand per contract, so B_t is an upper bound on effective exposure, but without chain-level strike distributions the magnitude of the correction cannot be pinned down. During the January 2021 burst all four were simultaneously elevated ($B_t = 0.93$, peak wedge 0.085, risk-neutral move-probability bounds above the comparison benchmark on 87% of days, OI persisting across monthly OPEX). An elevated configuration does not establish that constraint binding is imminent—only that the observable preconditions are present.

Issuer supply elasticity. Between April 2021 and September 2024, GameStop conducted five ATM equity offerings, raising over $5 billion and attenuating B_t ($0.93 \to 0.49$ between 2021 and 2024). Subsequent capital-structure actions—convertible-note offerings in March 2025 (∼43M potential shares) and June 2025 (∼78M), a warrant dividend in October 2025 (∼59M shares), and a performance-based stock-option award proposed for the CEO in January 2026 (∼171.5M shares, subject to shareholder approval and market-cap milestones)—bring potential fully diluted share count to approximately 800M, or ∼80% of the one-billion authorised ceiling. Increasing the authorised share count beyond one billion requires shareholder approval—a governance constraint given the community's ownership stake. The issuer conducted ATM offerings shortly after both burst episodes (April and June 2021; May and June 2024); whether future episodes follow the same pattern depends on conditions—cash position, capital-structure strategy, board composition—that have changed materially since 2021. Whether ATM issuance would outrun a sufficiently fast catalyst is an open question the framework does not resolve. Three conditions would falsify the constraint pathway: (i) B_t fails to reach capacity-relevant levels (> 0.5) during future high-intensity windows after controlling for dilution; (ii) OI persistence across monthly OPEX cycles during burst windows drops persistently below 0.5; (iii) the conditional amplification of the wedge by persistence within fixed intensity deciles disappears (F-test $p > 0.10$). None has been crossed, but the B_t trajectory is adverse. Aggregate call OI has also declined at low frequency since 2021, partly reflecting dilution and partly the structural fact that annual-expiry OI accumulates throughout the year and rebuilds slowly after January OPEX; the burst-episode rolling claims above are confined to monthly cycles within those windows.

Premium recycling and collective dynamics. Covered-call premium recycling illustrates a different dynamic: writing calls against an existing position generates income that can offset holding costs or fund additional purchases. Under an information asymmetry about timing, this is the only strategy that turns the collective system into one with strictly growing wealth. Without that asymmetry, capping upside contradicts the St Petersburg posture—unless calls are written against only a fraction of the position, or the writer sits outside the tail-concerned cohort, in which case the written obligations add to aggregate short exposure rather than capping the cohort's own upside. The cooperation analogy noted above has a further tension here: what may be individually optimal for survival (low κ, far OTM) is not what maximises capacity relevance, since dealer hedging pressure concentrates at near-the-money gamma where active rebalancing generates the largest flow relative to available liquidity.

DRS trajectory and relative dilution. Peak DRS reached approximately 76.6 million split-adjusted shares (∼25% of outstanding at the time, mid-2023), held near 75M through early 2024, and has since declined to approximately 66M by early 2026. Subsequent ATM offerings expanded shares outstanding from ∼305 million to ∼447 million (early 2025), diluting the DRS fraction to roughly 15%. The decline in absolute count is modest relative to the dilution and adverse price action, evidencing a durable core; the direction is adverse for the constraint pathway's financial contribution (relative float tightness) even as the sociological evidence of persistent shareholders remains. Against the fully diluted authorised ceiling of one billion shares, the current DRS total represents roughly 6.6%. The formal results depend on options-market observables, not on DRS fractions.

7.10 Conditionality and epistemic limits

The survival threshold treats π as a scenario parameter: identifying it from data would impose the belief structure the framework is designed to evaluate. The feasibility sandwich brackets π between market-implied bounds; the risk-neutral touch probability clears π^* easily at large L but the comparison becomes nontrivial at moderate leverage ($L = 5$–$10\times$), where π^* rises to 12–22%. Risk-neutral touch probabilities and the feasibility sandwich (Appendix D.4) provide bounds, not point estimates. The threshold does not require identifying the obligation variable D_t: the community's maintained hypothesis about unreported obligations is noted as epistemic infrastructure (Section 5), not asserted as fact. The threshold is derived from (κ, L, π) alone and is agnostic to the source of the payoff event.

The threshold is computed conditional on a (κ, L) pair. Both are dimensionless ratios set at entry (Section 3): κ is the fraction of the convex sleeve spent on premium per interval, L is the gross multiple on that spend conditional on the success event firing. Neither depends on the denomination of the sleeve. Until the position is closed, L is a parameter of a scenario, not an observable; it is conditioned on the success event $S_{t+1} = 1$, not on any particular market narrative. The entire threshold surface (Figure 1) is therefore a menu of conditional statements: *if* the payoff leverage turns out to be L, then the threshold rises or falls accordingly. At high L the threshold is low; at modest L it is high. Neither can be falsified until the position resolves.

7.11 Limitations

The static renewal margin (Section 6) is a theoretical benchmark whose existence depends entirely on drift: under adverse drift the window collapses (Table 4), and the framework does not resolve which drift assumption is appropriate. January 2021 is the only episode where the 30-day IV entered the monthly full-commitment window; broker restrictions ended it. The overlap is a single observation, not a test of the growth-rate predictions. The collective-infrastructure account (Section 5) is qualitative; full identification would require exogenous variation in collective infrastructure. The OBV persistence proxy is coarse and entangled with returns; independent evidence for the slow channel comes from issuer-reported DRS counts, not from the proxy. The two anchor episodes are selected by observable activity concentration; an endogenous change-point specification would strengthen the identification. Almost every empirical proxy would be sharper with chain-level option data; three categories of unavailable data would materially improve the analysis: participant-level cost-basis records, strike-by-strike open interest and greeks, and daily transfer-agent flow data.

7.12 Portability

The binary survival-threshold formula applies directly wherever wealth is multiplicative, exit is absorbing, and exposure is maintained through repeated fixed-cost, fixed-payoff-multiple renewal rounds. In richer payoff settings, the same logic applies after replacing the binary (κ, L) representation with the corresponding pathwise gross-return law and evaluating the log-growth condition directly. The static renewal margin is narrower: it requires option-market pricing of κ and L through Black–Scholes, a barrier-contact probability from a diffusion model, and a locally stable IV assumption, so it is specific to repeated option strategies on a single underlying, or to settings that can reasonably be reduced to that structure.

No setting parallels the GME structure in full, but several share enough renewal dynamics to illustrate portability. In repeated biotech option strategies, known regulatory or clinical catalysts create binary-event exposure. Options activity and implied-volatility measures are often elevated before FDA announcements, and post-event IV compression can sharply reduce extrinsic option value even when the trader is directionally correct. A participant sizing across a sequence of catalyst dates faces the same compounding problem: each failed or insufficiently large event burns premium, while the success probability is low and event-specific. The threshold surface maps directly once the event is specified: κ is the pre-event premium as a fraction of the options sleeve, L is the conditional payoff multiple after a favourable event net of IV crush, and π^{succ} is the stage-specific success probability (Phase III success, NDA approval, PDUFA decision, etc.). In commodity squeeze dynamics, constrained physical delivery against accumulated paper obligations creates a constraint pathway similar in spirit to the obligation-dominance mechanism formalised in Appendix A. The 2022 LME nickel episode is an extreme example: prices rose above $100,000 per metric tonne, the exchange suspended trading, and roughly $12 billion of trades were cancelled amid severe margin stress. For a participant maintaining long exposure through repeated futures rolls, the renewal cost is the roll spread, financing, and margin liquidity; the threshold governs how frequently squeeze-like windfalls must arrive relative to the cost of carrying the

position through contango. The LME cancellation also exposes a risk outside the formal model: the payoff event can occur, but the institution can alter settlement after the fact. Venture capital is a looser but useful analogy. Deal outcomes are highly skewed: most investments fail to return capital, while a small minority generate most fund returns. The threshold logic translates most cleanly at the level of repeated fund deployment or manager survival across vintages: κ is the capital committed per deal or per vintage as a fraction of deployable capital, L is the gross multiple on winners, and π^* is the minimum hit rate needed for positive long-run log growth. Because VC bets resolve concurrently and outcomes depend on market regime, sector, and follow-on financing, the binary formula is a coarse-grained approximation; still, a manager deciding whether to continue deploying after a barren vintage faces the same survival question.

In each setting the framework's core question applies: what does it cost to maintain exposure through time, and at what success probability does the gamble become time-irrational? GameStop supplies the test case; the threshold itself is general.

7.13 Conclusion

The standard account of GameStop usually stops at "irrational retail traders." We ask what follows once the time embedding is taken seriously. Repeated call renewal faces a survival threshold, set by premium burn and conditional payoff, below which renewal destroys time-average wealth. The threshold landscape (Figure 1) tells a participant what call renewal costs given strike, tenor, and commitment size. Tracking the threshold through time shows why timing matters: the bar rises when IV lifts premium burn κ, so renewal is most demanding when options are most expensive (Figure 4). The ergodicity wedge, computed from daily returns rather than option prices, measures the compounding drag of living through the realised stock path. In the GME sample from January 2021 through December 2025, that drag is highly concentrated: the January–March 2021 and May–June 2024 burst episodes account for roughly 59% of cumulative wedge mass while occupying roughly 8% of the sample (Figure 3).

The option channel shows the same regime dependence from the implied-volatility side. During the January 2021 burst, 30-day GME IV peaked around 547%, and near-term contracts traded at still higher IVs. Under the zero-drift static-IV benchmark, a growth-positive region for call renewal opens only in high-volatility regimes, with the onset shifting by tenor and sizing (Figure 9). At the IV levels prevailing through most of the remaining five-year period, the static benchmark is negative at every tenor. The cost of maintaining convex exposure is state-dependent and computable: most of the time renewal burns wealth, but under particular volatility, tenor, and sizing configurations the survival threshold can be crossed.

During the wait, a decentralised community persisted, with direct shareholding and registration consistent with lower exit hazard and altered float composition, alongside recurring call purchases consistent with continued convex exposure. That social account is interpretive; the formal and measured results do not depend on it. Whether the GME shareholders' thesis is correct is beyond what we can adjudicate here. What the framework establishes is the cost structure of waiting, the regimes in which that cost concentrates, and the success probability required for the wait to be time-rational.

Competing interests. This is a draft, not financial advice. The author holds a personal long position in shares of GameStop Corp. (GME) and is the participant-observer described in Section 5. This manuscript is a theoretical and empirical analysis of renewal costs, persistence, and time-average growth. It does not recommend any transaction and does not depend on the future performance of any specific asset. Large language models were used as research, writing, and editing assistants; all claims, calculations, and interpretations remain the author's responsibility.

Appendices

A The belief object: MOASS as constraint-based rare-path thesis

A.1 Constraint dominance: obligations versus elastic supply

Let $D_t \geq 0$ denote forced buy/borrow obligations over a short horizon (e.g. close-outs, buy-ins, margin-driven covering, hedging-driven purchases), and let $A_t \geq 0$ denote willing supply over the same horizon. A constraint-dominant episode is characterised by

$$D_t \gg A_t \quad \text{and} \quad A_t \text{ cannot expand quickly enough.} \tag{51}$$

The mechanism generating D_t can differ (close-outs/buy-ins, risk-driven covering, or intermediary hedging feedback). The SEC staff report emphasises that the early-2021 GME dislocation reflected substantial buying pressure interacting with intermediary constraints, motivating an obligations-versus-supply framing rather than a single canonical squeeze mechanism [9].

A.2 Market-plumbing clarification (close-outs and "gamma squeeze")

Forced buy-ins and close-outs. "Forced buying" refers to price-inelastic buy/borrow obligations that arise when settlement or risk constraints bind. Clearing participants facing settlement failures can be required to close out fails-to-deliver by purchasing or borrowing securities under Regulation SHO's close-out rule (Rule 204), and broker-dealer buy-in procedures specify notice and execution requirements [18, 19, 20]. We treat such events as contributors to D_t: obligation-like demand that arises when effective float becomes binding. This framing does not require the clearing agency itself to literally purchase shares.

"Gamma squeeze" discourse. A widely used label is "gamma squeeze," typically referring to a delta-hedging positive feedback cycle whereby intermediaries dynamically purchase the underlying as call exposure becomes more share-like with rising prices. A related term is "gamma ramp": the accumulated open-interest structure across strikes—particularly near-expiry contracts whose high gamma means large hedging adjustments per unit price move—that, when representing a substantial fraction of the tradeable float, creates the conditions for such feedback. The ramp is the *setup*, not the feedback itself. We treat both as discourse-level shorthand for hedging-driven obligation dynamics rather than as primitives of the model. Formal treatments show that option-hedging feedback can generate directional instabilities under certain positioning and liquidity conditions, while calibrations to GME in early 2021 suggest that such feedback need not be the sole driver [26]. We neither assume nor deny a dominant gamma mechanism; hedging-driven purchases are subsumed into D_t.

A.3 Practically unbounded tails and expectation-ranking collapse

The analytical role of "infinity" is that sufficiently extreme right-tail dispersion can make expectation-based ranking unstable or effectively non-discriminating—prices need not be literally infinite for this to apply.

Assumption 1 (Subjective extended-support tail)**.** *Let $X \in [0, \infty)$ denote the payoff-relevant rare-regime sleeve multiple under a participant's subjective distribution $\mathcal{F}$. Assume $\mathcal{F}$ has sufficiently extreme right-tail dispersion (relative to household balance sheets and decision horizons) that expectation-based ranking among nonzero-exposure tactics becomes unstable or effectively non-discriminating.*[37]

Under Assumption 1, evaluation is pushed toward time-embedded criteria: whether exposure can be maintained, what it costs to maintain it, and whether a typical trajectory survives long enough to access a rare regime [3, 4].

A.4 Conversion as effective-float tightness (corner boundary)

Section A.1 defines constraint dominance as obligations overwhelming willing supply ($D_t \gg A_t$). The corner definition below specifies *how* supply becomes inelastic: the effective tradable float itself shrinks to near zero. In the post-sneeze[38] belief object, conversion requires this stock-scarcity condition, not just a large price move.

Definition 2 (Corner in the economic (microstructure) sense)**.** *A state in which the effective tradable float available to satisfy short-horizon obligations becomes negligible, so that marginal price formation is dominated by obligation-driven (price-inelastic) demand rather than discretionary (elastic) supply. This definition does not imply illegality, does not require manipulation, and does not require hidden positions.*

Let F_t^{eff} denote effective tradable float and let $M_{t+1}^{\star} \in \{0, 1\}$ denote *conversion*—the event that the system enters the constraint-dominant regime (see Section 3.4 for the formal treatment). Define conversion as:

$$M_{t+1}^{\star} = 1 \quad \text{if} \quad F_t^{\text{eff}} \leq \varepsilon, \tag{52}$$

where $\varepsilon \geq 0$ is a small tolerance. This is a conceptual regime definition; the main text operates with the survival threshold rather than with direct conversion measurement.

A.5 Three-stage discipline

We outline *a* pathway from normal trading to the constraint-dominant regime (MOASS), structured in three stages, each a necessary precondition for the next.

Stage 1 (ignition). A catalyst pushes price through strikes fast enough that outstanding call OI becomes share-like before theta decay degrades the exposure. The repricing state summary $\hat{p}_t^{\text{ign}}$ (Section 4; Appendix C) provides a market-data proxy for Stage 1 feasibility.

Stage 2 (float-locking). Hedging demand exceeds effective tradeable float ($D_t > F_t^{\text{eff}}$)—in the community's language, the

[37] A convenient sufficient condition is $\mathbb{E}_{\mathcal{F}}[X] = \infty$. A limiting case is that participants assign a tiny probability to arbitrarily large outcomes. To illustrate: at a notional floor of $2,500,000 per share, the implied market capitalisation would exceed one quadrillion dollars, comparable to total estimated global household wealth. We do not require literal infinity; the time-embedded results depend on burn versus approach feasibility on realised paths.

[38] "Sneeze" is the community's term for the January–March 2021 episode, distinguishing it from the squeeze that has not yet occurred in their view.

float is being locked. A conservative boundary-relevance covariate is:

$$B_t := \frac{OI_t^{\text{call}}}{F}, \tag{53}$$

where F is a documented float proxy and OI_t^{call} is call open interest in gross share-equivalent units; elevated B_t (with > 0.5 used only as a rule-of-thumb reference level under the gross latent-capacity measure) is a necessary condition for an option-linked float-locking story to be quantitatively plausible.

Stage 3 (constraint dominance). Forced buying raises prices, triggering further obligation-driven demand against shrinking supply; the demand–supply ratio $\Omega_t = D_t/F_t^{\text{eff}}$ is increasing and convex in price, so the system accelerates into deeper constraint dominance. *Conversion* denotes the system entering Stage 3.

A.6 Exit ordering during the payoff event

If the payoff event occurs at some interval τ, participants with active positions realise the payoff multiple L in principle, but the realised payoff may depend on how and when they exit. Let s_i denote participant i's position size (in share-equivalent units) and let V_τ denote the available trading volume at time τ. When $s_i \ll V_\tau$, a participant can sell with negligible market impact and plausibly realise the full payoff. When s_i is of order V_τ, the sale itself can move the price, so the realised payoff may fall below L. Whether a large position is better liquidated gradually or all at once depends on the prevailing liquidity profile and how price responds to the selling pressure; in either case, the holder remains exposed to reversal risk on any unsold portion. To the extent that later exits face thinner residual liquidity, the collective's aggregate payoff would be front-loaded toward early, smaller exits. This ordering effect means that the nominal payoff L is an upper bound on what any given participant can extract, with the gap depending on position size relative to volume.

A.7 Precedents

Episodes consistent with effective-float tightness are empirically feasible. In the 2008 Porsche–Volkswagen episode, Porsche cornered the VW float by accumulating 74.1% of voting shares through direct ownership and undisclosed cash-settled options, leaving roughly 6% tradeable against approximately 13% sold short—a classical corner that triggered an extreme short squeeze [21]. Porsche subsequently released approximately 5% of its holdings to provide liquidity, and the price collapsed by more than half within days [22]. In a recent OTC precedent, FINRA imposed a trading-and-quotation halt in MMTLP effective December 9, 2022, citing an "extraordinary event" and potential settlement uncertainty [23, 24, 25]. Forced buy-ins of extreme magnitude were observed immediately before the halt. These cases are existence proofs of states in which effective tradable float can become binding.

B Renewal calibration and dynamics

This appendix anchors the abstract (κ, L) parameters in observable option prices, supplies a stylised cohort-average algebra for the ignition-to-exhaustion arc, and sketches a reduced-form feedback channel between the renewal margin and implied-volatility dynamics.

B.1 Black–Scholes calibration

To anchor the abstract (κ, L) plane in observable option prices, we price European calls under Black–Scholes. The call price at spot S_0, strike K, time to expiry T (in years), risk-free rate r, and annualised implied volatility σ is

$$C_{\text{BS}} \;=\; S_0\, N(d_1) \;-\; K\, e^{-rT}\, N(d_2), \tag{54}$$

where

$$d_1 = \frac{\ln(S_0/K) + (r + \tfrac{1}{2}\sigma^2)T}{\sigma\sqrt{T}}, \qquad d_2 = d_1 - \sigma\sqrt{T},$$

and $N(\cdot)$ is the standard normal CDF. The two renewal parameters follow directly:

$$\kappa \;=\; \frac{C_{\text{BS}}}{S_0}, \qquad L \;=\; \frac{B - K}{C_{\text{BS}}}, \tag{55}$$

where B is the target price level at which the participant exits (Section 3). L is therefore the intrinsic-value-at-barrier payoff per unit of premium paid; it is a benchmark convention, not a mark-to-market valuation. If the contract retains time value at exit (e.g. because the move arrives well before expiry), the realised payoff exceeds $B - K$, so this convention understates L and overstates the threshold—making the calibration conservative. Both κ and L are scale-invariant (spot cancels), so the loci in Figure 1 apply at any price level.

All calibrations use $T = 21/252$ (monthly renewal) and $r = 0$; using the contemporaneous risk-free rate changes numerical values by less than one basis point at these tenors. GME options are American-style, but Black–Scholes is used here only as a calibration benchmark for (κ, L), not as a claim about the full microstructure of GME options. The early-exercise premium on short-dated calls is small when the underlying pays no dividend (GME pays none) and rates are moderate; for the calm regime the gap is at most a few basis points, and at extreme IV it remains small relative to the bid-ask spread.[39]

Two annualised implied-volatility regimes anchor the discussion: $\sigma = 120\%$, representative of GME's pre-event baseline, and $\sigma = 300\%$, representative of burst episodes.

At the baseline IV, an ATM monthly call burns roughly $\kappa \approx 14\%$ of the convex sleeve per interval. If the assumed terminal move is $2\times$, the payoff-to-premium ratio is $L \approx 7$ and the renewal boundary sits at $\pi^* \approx 19.5\%$; for a $5\times$ move, $L \approx 29$ and π^* falls to roughly 8.7%. Moving to $1.5\times$ OTM strikes cuts burn to $\kappa \approx 2.6\%$ while raising L into the range 20–137, which pushes the threshold down to $\pi^* \approx 1.7$–6.3%. The tradeoff is intuitive: cheaper calls require the event to happen less often, but each call pays off only if the move is large enough to traverse the strike.

Under burst-regime IV the entire locus shifts rightward and downward. ATM burn jumps to $\kappa \approx 34\%$ and the payoff-to-premium ratio compresses: $L \approx 3$ for the $2\times$ move, $L \approx 12$ for $5\times$. The survival threshold rises accordingly—π^* now ranges from 21% to 45% at the money—meaning that buying calls during a volatility spike is time-rational only if the participant assigns a substantially higher probability to the ignition event. This is consistent with the observed burst-concentration pat-

[39] At extreme IV ($\sigma > 400\%$) the American premium may be somewhat larger, but the bid-ask spread on OTM contracts is the dominant friction during burst episodes (Section 6). The true (American) boundary is marginally more favourable than the plotted one.

tern (Section 5): convex renewal clusters around dates when participants perceive catalyst probability to be elevated.

B.2 Ignition and exhaustion through compositional turnover

Section 6 introduces the renewal margin $\Phi(\sigma_0, \sigma_t) = P^{\text{touch}}(\sigma_t) - \pi^*(\kappa(\sigma_0),\, L(\sigma_0))$ (equation (45)) and notes that a burst seeds its own exhaustion through compositional turnover. This subsection supplies the algebra.

Suppose a burst lifts IV from a baseline σ_b to a peak σ_p. At time t during the burst, let $\omega_t \in [0,1]$ denote the fraction of outstanding convex positions that were opened at (or near) the baseline IV σ_b; the remaining fraction $1-\omega_t$ was opened at the current elevated level σ_p. The two-cohort setup is the simplest reduction of a more general entry-IV distribution: one could write $\bar{\Phi}_t = \int \Phi(\sigma_0, \sigma_t)\, \mathrm{d}F_t(\sigma_0)$ for a time-varying entry-IV distribution F_t; equation (56) below is the two-point case. We adopt it for tractability; the qualitative conclusion (margin decays as early entrants are replaced) survives under any dispersed F_t.

The descriptive cohort-average renewal margin is

$$\bar{\Phi}_t \;=\; \omega_t\, \Phi(\sigma_b,\, \sigma_p) \;+\; (1-\omega_t)\, \Phi_{\text{static}}(\sigma_p). \tag{56}$$

$\bar{\Phi}_t$ is a weighted average of probability margins across the two cohorts, not the aggregate log-growth rate of the population or a market-clearing condition.

Early entrants carry a temporal advantage: $\kappa(\sigma_b) < \kappa(\sigma_p)$ and $L(\sigma_b) > L(\sigma_p)$, so their threshold $\pi^*(\sigma_b)$ is lower and their margin $\Phi(\sigma_b, \sigma_p)$ is large. Late entrants pay burst-level premiums, so their margin reduces to the static case $\Phi_{\text{static}}(\sigma_p)$, which is smaller or negative (Section 6).

As early holders exit—profit-taking, rolling forward, or selling shares—they are replaced by new entrants at elevated IV. Model ω_t as decaying at rate $\lambda > 0$:

$$\omega_t = \omega_0\, e^{-\lambda t}. \tag{57}$$

This is the constant-hazard special case: if each early entrant faces exit hazard $h(t) = \lambda$ (independent of calendar time), the fraction surviving to t is $e^{-\lambda t}$. Linking to the persistence formalism of Section 3.4, a richer model would replace λ with the state-dependent hazard h_t developed there; the exponential form is adopted for closed-form tractability. Substituting into (56):

$$\bar{\Phi}_t \;=\; \Phi_{\text{static}}(\sigma_p) \;+\; \omega_0\, e^{-\lambda t}\, \big[\Phi(\sigma_b, \sigma_p) - \Phi_{\text{static}}(\sigma_p)\big]. \tag{58}$$

The bracketed term is the temporal advantage of early entry, always non-negative. It decays exponentially as the population turns over. The margin converges to $\Phi_{\text{static}}(\sigma_p)$—the memoryless benchmark of Section 6—at rate λ.

The half-life of the advantage is $t_{1/2} = \ln 2/\lambda$. If turnover is fast (high λ), the burst exhausts its own margin quickly; if turnover is slow (e.g. because shareholders hold through the burst rather than rolling), the temporal advantage persists longer. The aggregate margin $\bar{\Phi}_t$ crosses zero when

$$\omega_t \;=\; \frac{-\Phi_{\text{static}}(\sigma_p)}{\Phi(\sigma_b, \sigma_p) - \Phi_{\text{static}}(\sigma_p)}, \tag{59}$$

which gives the exhaustion time $t^* = -\lambda^{-1} \ln(\omega_{t^*}/\omega_0)$. This crossing is well-defined when two conditions hold: the early-entry advantage is positive ($\Phi(\sigma_b, \sigma_p) > \Phi_{\text{static}}(\sigma_p)$, which is satisfied whenever $\sigma_b < \sigma_p$ and both lie in the positive-Φ window), and the static margin at the burst level is negative ($\Phi_{\text{static}}(\sigma_p) < 0$, which holds when σ_p exceeds the upper boundary σ_u of Section 6). After t^*, the population-weighted gamble is time-irrational even though the burst-level IV persists.

The entry IV at which a participant opens a position is itself a function of intensity and persistence conditions at that date, linking the per-decision diagnostic Φ to the aggregate state variables.

B.3 Demand-response dynamics and exhaustion

The compositional-turnover algebra of Section B.2 describes how the population-weighted margin decays, but takes the IV path as exogenous. This subsection asks what happens when the loop is closed: participants respond to the margin by adjusting call buying, and that aggregate demand in turn moves implied volatility. The resulting dynamics are stylised and rest on several simplifying assumptions; they should be read as a reduced-form sketch of the feedback channel, intended to clarify the qualitative structure rather than as a calibrated model of IV.

The results below hold under the following conditions on the static renewal margin $\Phi_{\text{static}}(\sigma) := P^{\text{touch}}(\sigma) - \pi^*(\sigma)$:

(i) $\Phi_{\text{static}} \in C^2$ on the relevant IV range;
(ii) Φ_{static} has exactly two zeros $\sigma_c < \sigma_u$, with $\Phi'(\sigma_c) > 0$ and $\Phi'(\sigma_u) < 0$;
(iii) $\Phi_{\text{static}} > 0$ on (σ_c, σ_u) and $\Phi_{\text{static}} \le 0$ outside;
(iv) $\pi^*(\sigma_0)$ is strictly increasing in σ_0.

These conditions are not general theorems; they are properties of the Black–Scholes parametrisation verified numerically under specific drift assumptions. The calibration of Section B.1 satisfies all four at monthly tenor under zero drift (Section 6), and the conditions become easier to satisfy under positive drift: Table 4 shows that the positive-Φ window broadens as drift increases (the lower boundary σ_c falls from 363% at zero drift to 279% at $m = +\sigma^2/8$, while the upper boundary σ_u moves beyond the computed range). Under negative drift, the window shrinks and eventually vanishes; the assumptions fail whenever no positive-Φ region exists. All propositions below are conditional on assumptions (i)–(iv) holding; they inherit the parametric scope of the calibration, not a general property of option markets.

We assume implied volatility mean-reverts toward a long-run level $\bar{\sigma}$ at rate $\theta > 0$ in the absence of order flow. On top of that, participants modulate call buying in response to the renewal margin. For the remainder of this subsection, Φ_t denotes the representative-agent static renewal margin $\Phi_{\text{static}}(\sigma_t)$ (not the cohort-weighted $\bar{\Phi}_t$ of Section B.2); the heterogeneity that $\bar{\Phi}_t$ captures is folded into the threshold distribution below. The question is how aggregate demand inherits a smooth dependence on Φ from a population of discrete, heterogeneous agents.

Lemma 1 (Mean-field demand response)**.** *Let there be N agents. Agent i buys one unit of convex exposure when the renewal margin exceeds an idiosyncratic threshold $\chi_i > 0$ and sells when it falls below $-\tilde{\chi}_i$ ($\tilde{\chi}_i > 0$), where the $\{\chi_i\}$ and $\{\tilde{\chi}_i\}$ are drawn from distributions with continuous densities g_+ and g_- at 0. Write $Q_N(\Phi)$ for aggregate net order flow per capita. Then*

$$Q_N(\Phi) \;=\; Q_N(0) \;+\; \rho_0\, \Phi \;+\; \mathcal{O}(\Phi^2),$$

with $\rho_0 := g_+(0) + g_-(0) > 0$. If implied volatility responds linearly to net order flow with coefficient $\kappa_{\text{imp}} > 0$ (market

impact per unit flow) and mean-reverts in the absence of flow, the IV dynamics at leading order are

$$\mathrm{d}\sigma_t \;=\; \left[-\theta\,(\sigma_t-\bar\sigma) + \lambda\,\Phi_t + \mathcal{O}(\Phi_t^2)\right]\mathrm{d}t + \xi\,\mathrm{d}W_t, \qquad \lambda := \kappa_{\mathrm{imp}}\,\rho_0, \tag{60}$$

where $\xi > 0$ is exogenous IV noise and W_t is a standard Wiener process.

Proof. For small Φ, a Taylor expansion of the fraction of agents whose thresholds are crossed gives $Q_N(\Phi) - Q_N(0) = \rho_0\,\Phi + \mathcal{O}(\Phi^2)$. Substituting into the linear-impact mean-reversion model and writing $\lambda = \kappa_{\mathrm{imp}}\,\rho_0$ gives (60). □

Several simplifications are worth flagging. The linear-impact assumption (σ responds proportionally to net flow) is a leading-order approximation; real impact is likely concave and state-dependent. The mean-reversion rate θ is taken as constant, whereas empirical IV dynamics may exhibit regime-dependent reversion speeds. The exogenous noise ξ absorbs all IV variation not attributable to margin-responsive demand; in practice this residual may itself be correlated with positioning. These are standard in reduced-form volatility models and are adopted here for tractability; the cycle-time heuristic below should accordingly be understood as qualitative structure rather than a calibrated forecast.[40]

The coupling $\lambda = \kappa_{\mathrm{imp}}\,\rho_0$ has units of IV drift per unit time per unit of probability margin: κ_{imp} converts order flow into IV change (volatility points per unit flow per unit time), and ρ_0 converts margin into flow (agents per probability point). Their product is the rate at which a marginal improvement in the renewal margin feeds back into IV. The public discourse documented in Section 5 may be what keeps ρ_0 nontrivial: participants who follow shared research, public event calendars, and openly circulated analysis arrive at similar assessments independently. If that infrastructure were absent, ρ_0 would shrink and the demand response would weaken accordingly.

Near the lower boundary σ_c of the positive-Φ window (Definition 1), the margin vanishes linearly: $\Phi \approx \Phi'(\sigma_c)\,(\sigma_t - \sigma_c)$. Write $\Delta\sigma(\sigma_0) := \sigma_0 - \sigma_c$ for the distance from entry IV to the critical point; this is the minimum IV excursion needed to complete a cycle starting at σ_0.

Remark 5 (Cycle-time heuristic near σ_c)**.** Under a reduced-form diffusion for IV, one expects shorter cycle times as entry IV approaches the lower crossing σ_c: the distance $\Delta\sigma(\sigma_0)$ that IV must traverse shrinks, and standard first-passage scaling for Brownian motion suggests cycle time of order $\Delta\sigma^2/\xi^2$, while the margin gained per cycle is of order $\Phi'(\sigma_c)\,\Delta\sigma$. These heuristics suggest that the margin-per-unit-time ratio grows as $\Delta\sigma \to 0$—cycle time collapses faster than margin vanishes. Making this precise requires a careful conditioned boundary-value derivation that pins down the local hitting-time problem (including the correct sign conventions, conditioning event, and convergence of the conditioned process to a well-characterised limit). We do not claim a proved asymptotic here; the exact exponent, prefactor, and conditions under which the unconditional ratio inherits the same scaling are left for future work. The qualitative content—faster turnover near the lower crossing—is the relevant takeaway for the renewal narrative.

Each completed renewal cycle resets entry IV to the current level, and under the monotonicity of π^* this creates a one-way degradation of future capacity. To state this precisely, define $\Pi_{\max} := \sup_\sigma P^{\mathrm{touch}}(\sigma)$, the supremum of the touch probability over the IV range (finite because $P^{\mathrm{touch}} \le 1$).

Proposition 5 (Irreversibility of the renewal reset)**.** *Let $\sigma_{0,n}$ be the entry IV at the start of the n-th renewal cycle, and define the remaining headroom*

$$\mathcal{H}_n \;:=\; \sup_{\sigma}\,\Phi(\sigma_{0,n},\,\sigma) \;=\; \Pi_{\max} - \pi^*(\sigma_{0,n}).$$

$\mathcal{H}_n$ measures the best-case renewal margin the participant could achieve after reset: if the market were to reach the IV level that maximises P^{touch}, $\mathcal{H}_n$ is the gap between that ceiling and the participant's current threshold. (The equality holds because $\Phi(\sigma_{0,n},\sigma) = P^{\mathrm{touch}}(\sigma) - \pi^*(\sigma_{0,n})$ and $\pi^*(\sigma_{0,n})$ does not depend on σ.)

Under the reset rule $\sigma_{0,n+1} = \sigma_{t_n}$ (where t_n is the time at which cycle n completes), assume (iv) and that each successful cycle terminates with $\sigma_{t_n} \ge \sigma_{0,n}$. This last assumption is the empirically relevant case—a successful burst lifts IV above its entry level—but it is an assumption: if a cycle were to complete with $\sigma_{t_n} < \sigma_{0,n}$ (e.g. because IV cooled before the position was closed), the monotonicity would not hold for that cycle. Under these conditions:

1. *$\pi^*(\sigma_{0,n})$ is monotone non-decreasing, with strict inequality whenever $\sigma_{t_n} > \sigma_{0,n}$.*
2. *$\mathcal{H}_n$ is monotone non-increasing: each cycle weakly reduces the maximum attainable margin.*

Reversibility requires $\sigma_{t_n} = \sigma_{0,n}$, the static limit of Section 6, where the reset changes nothing.

Proof. (1) π^* strictly increasing and $\sigma_{0,n+1} = \sigma_{t_n} \ge \sigma_{0,n}$ imply $\pi^*(\sigma_{0,n+1}) \ge \pi^*(\sigma_{0,n})$. (2) $\mathcal{H}_n = \Pi_{\max} - \pi^*(\sigma_{0,n})$ with π^* non-decreasing gives $\mathcal{H}_n$ non-increasing. □

Corollary 1 (Quantitative headroom decay)**.** *If $\pi^* \in C^1$ on a relevant interval I and $m := \inf_{\sigma\in I}(\pi^*)'(\sigma) > 0$, then for any successful cycle with $\sigma_{0,n},\,\sigma_{t_n} \in I$,*

$$\mathcal{H}_n - \mathcal{H}_{n+1} \;\ge\; m\,(\sigma_{t_n} - \sigma_{0,n}). \tag{61}$$

Each successful upward IV cycle consumes at least m times the IV displacement in future headroom.

Proof. By the mean value theorem, $\pi^*(\sigma_{t_n}) - \pi^*(\sigma_{0,n}) \ge m\,(\sigma_{t_n} - \sigma_{0,n})$. □

To give this bound operational content: for the 1.5× OTM call targeting a 3× move at 21 DTE, $(\pi^*)'(\sigma) \approx 0.10$–$0.12$ per volatility point across the $\sigma \in [250\%,\,500\%]$ interval, so $m \approx 0.10$. A burst that lifts IV by 100 percentage points (e.g. $\sigma_0 = 200\% \to \sigma_{t_n} = 300\%$) costs at least 10 percentage points of headroom per cycle. The bound is not merely formal at the scales that matter for GME.

This headroom loss is the per-participant cost of the ignition-to-exhaustion arc described in Section 3: each cycle raises the floor

[40] The feedback loop admits a thermodynamic reading. Implied volatility plays the role of temperature, the renewal margin Φ plays the role of free energy per cycle, and the threshold π^* plays the role of a cold-reservoir temperature. A participant who enters at low σ_0 and exits during a burst extracts margin with efficiency $\eta = 1 - \pi^*/\Pi$, formally parallel to Carnot efficiency $1 - T_C/T_H$. The irreversibility result below says that each completed cycle raises the effective reservoir temperature T_C, shrinking the margin available to subsequent cycles.

probability, and the loss is unrecoverable without an exogenous IV reset. January 2021 may have provided such a reset, insofar as broker-imposed purchase restrictions collapsed demand and allowed entry conditions to cool. The compositional turnover of equation (58) describes a parallel degradation from the population side. Under the renewal map, both forces work in the same direction: the population turns over toward less favourable entry conditions, and each individual participant's headroom shrinks with every completed cycle. Bursts are, in this sense, self-limiting; the question is how quickly the limits bind relative to the timescale of the burst itself.

B.4 Exponential skeleton and the (σ, g) phase diagram

Under static IV and constant log-drift $g := \mu_{\log}$, the median price path is $S_t^{\text{med}} = S_0 e^{gt}$. This is the unique deterministic trajectory compatible with a time-invariant log-return distribution: IV is a property of proportional returns, and exponential growth is the only path with a constant proportional rate. Each drift assumption in the main text therefore selects a specific exponential skeleton for the median trajectory.

The first-passage probability (equation 46) decomposes into a deterministic and a diffusive component. For a barrier at $B = bS_0$ and tenor T:

- If $\ln(b)/g < T$ (i.e. the median path reaches the barrier within tenor), the deterministic component dominates and $P^{\text{touch}} \to 1$ as $\sigma \to 0$.
- If $\ln(b)/g > T$ (median path falls short), the touch probability requires diffusive help: variance around the median must bridge the remaining gap.

At the baseline calibration ($b = 3.0$, $T = 21/252$), the deterministic threshold is $g^* = \ln(3)/(21/252) \approx 13.2$ annualised log-drift, meaning the median price would need to triple in 21 trading days. No plausible ascent rate approaches this. The monthly positive-Φ window therefore sits entirely in the diffusion-dominated regime: the median path does not reach the barrier, and the touch probability comes from the tails of the log-return distribution around the median. At longer tenors this changes: yearly contracts at moderate g enter the deterministic-hit regime, which is why Table 4 shows the onset σ_c falling sharply with tenor.

Figure 12 maps $\Phi_{\text{static}}(\sigma; g)$ jointly over IV and median ascent rate at monthly tenor. The positive region (blue) opens along a contour whose lower boundary $\sigma_c(g)$ decreases with g: at $g = 0$ (zero log-drift, the main-text baseline), the onset is $\sigma_c \approx 363\%$; at $g = +100\%$ annualised, it falls to $\approx 279\%$; at $g = +200\%$, to $\approx 222\%$. Under risk-neutral drift ($g = -\sigma^2/2$, the lower-left region of the diagram), no positive region exists at any σ. The diagram makes the measure gap visible as geometry: the distance between the risk-neutral contour and the $g = 0$ baseline is $\sigma^2/2$, which at burst-level IV is enormous.

The (σ, g) phase diagram treats g as a scenario parameter in the same spirit as π^{succ} and L. A participant who believes in a specific directional trajectory can read off which IV levels make renewal growth-positive under that belief; the framework does not adjudicate which g is appropriate.

B.5 Correlated multi-period survival

This subsection develops the beta-binomial model for correlated renewal intervals referenced in Section 3.6. The exchangeability assumption (identical marginal touch probabilities across periods)

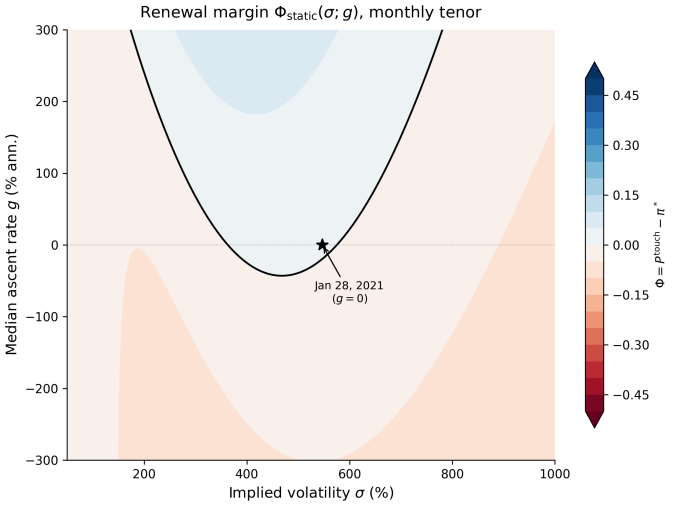

Figure 12: Renewal margin $\Phi_{\text{static}}(\sigma; g)$ over implied volatility and median ascent rate, monthly tenor ($T = 21$ d). Baseline calibration: $K = 1.5\times$ spot, target $= 3.0\times$, $r = 0$. Blue: $\Phi > 0$ (renewal is growth-positive); red: $\Phi < 0$. Black contour: $\Phi = 0$. The star marks the January 28, 2021 30-day IV peak at $g = 0$. Under risk-neutral drift ($g = -\sigma^2/2$, lower-left), no positive region exists. Each horizontal slice is a static-Φ curve at fixed g; Figure 7 is the slice at $g = 0$.

is a tractable idealisation; it is most defensible during calm periods, where κ, L, and π^{succ} are approximately stable.

Independence is a strong assumption when the underlying has feedback-driven dynamics. A natural alternative treats p as uncertain rather than fixed: draw p from a Beta(α, β) distribution, then run Bernoulli trials given the realised p. The resulting trials are exchangeable but no longer independent: they share a common but unknown success rate, and observing one outcome updates beliefs about the rest.

The Beta family is conjugate to the Bernoulli, so the posterior after observed trials remains in the same family; it gives a two-parameter exchangeable model with transparent control of the marginal mean and pairwise correlation, adding one degree of freedom without importing structural assumptions about the correlation mechanism. The marginal mean is $\mu = \alpha/(\alpha+\beta)$ and the pairwise correlation between any two trials is $\rho = 1/(\alpha+\beta+1)$ (a pairwise correlation, not a general dependence parameter), with $\rho \to 0$ recovering independence and $\rho \to 1$ collapsing all trials to a single shared outcome. Under independence the per-period rate p and the marginal mean μ refer to the same quantity; under correlation they remain identical at $T = 1$ but diverge as T grows, because μ is the marginal probability of any single trial while $p(T)$ is the rate one would infer from a horizon-T cumulative observation under the false assumption of independence. Reparametrising in (μ, ρ):

$$\alpha = \mu(1/\rho - 1), \quad \beta = (1-\mu)(1/\rho - 1). \tag{62}$$

Let K denote the number of touches in N periods. The probability of zero touches is

$$P(K{=}0 \mid N) = \frac{\Gamma(\beta + N)\,\Gamma(\alpha + \beta)}{\Gamma(\beta)\,\Gamma(\alpha + \beta + N)}, \tag{63}$$

which recovers $(1-\mu)^N$ when $\rho \to 0$ and collapses to $(1-\mu)$

when $\rho \to 1$. In product form,

$$P(K=0 \mid N) = \prod_{j=0}^{N-1} \frac{\beta + j}{\alpha + \beta + j}, \tag{64}$$

where each factor is the conditional probability of no touch on round $j+1$ given no touch on the preceding j rounds. The j-th factor equals $(\beta + j)/(\alpha + \beta + j)$, which is strictly increasing in j: each consecutive failure makes the next failure more likely.

The implied per-period frequency $p(T) = 1 - P(K=0 \mid T)^{1/T}$ extracts an effective rate from the T-period no-touch probability. Expanding, $\ln(1 - p(T)) = (1/T) \sum_{j=0}^{T-1} \ln[(\beta + j)/(\alpha + \beta + j)]$: the Cesàro mean of the log-factors. Under independence every factor equals $\ln(1 - \mu)$, so the mean is constant and $p(T) = \mu$ for all T. Under $\rho > 0$ the factors are strictly increasing (toward zero), so the Cesàro mean rises with T, and $p(T)$ falls.

Proposition 6 (Scale dependence under correlated renewals)**.** *Let outcomes follow the beta-binomial model with marginal touch probability $\mu \in (0,1)$ and pairwise correlation $\rho \in (0,1)$. Define the implied per-period frequency at horizon T as $p(T) := 1 - P(K=0 \mid T)^{1/T}$. Then:*

(i) $p(T)$ is strictly decreasing in T, with $p(1) = \mu$.
(ii) $p(T) \to 0$ as $T \to \infty$.
(iii) For any candidate threshold $\pi^* \in (0,1)$, $P(K=0 \mid T)$ under $(\mu = \pi^*, \rho)$ is strictly greater than $(1 - \pi^*)^T$ for all $T > 1$.

Proof. Write $a_j := \ln[(\beta + j)/(\alpha + \beta + j)]$ for $j = 0, 1, \ldots$ Each a_j is negative and strictly increasing in j (toward zero), because $\alpha > 0$ and the ratio $\beta + j$ over $\alpha + \beta + j$ increases with j. From (64), $\ln P(K=0 \mid T) = \sum_{j=0}^{T-1} a_j$.

The implied per-period frequency satisfies $\ln(1 - p(T)) = (1/T) \sum_{j=0}^{T-1} a_j$, the Cesàro mean of the sequence (a_j). Since (a_j) is strictly increasing, each new term a_T exceeds the running average, so the Cesàro mean is strictly increasing in T, so $\ln(1 - p(T))$ is strictly increasing and $p(T)$ is strictly decreasing. At $T = 1$: $p(1) = 1 - \beta/(\alpha + \beta) = \mu$. This gives (i).

Since $a_j \to 0$, the Cesàro mean of (a_j) converges to zero, giving $p(T) \to 0$. This gives (ii).

Under independence ($\rho = 0$), $a_j = \ln(1 - \mu)$ for all j, and the Cesàro mean is constant: $p(T) = \mu$. For $\rho > 0$ the first term $a_0 = \ln(1 - \mu)$ is identical, but $a_j > a_0$ for $j \geq 1$, so the Cesàro mean is strictly greater than $\ln(1 - \mu)$ for $T > 1$. Therefore $P(K=0 \mid T) > (1 - \mu)^T$. Setting $\mu = \pi^*$ gives (iii). □

Falsification tests. *Test 1: independence falsification.* For a candidate per-period rate p_0 under the independence null, the implied cumulative-probability curve is $P_{\text{ind}}(T) = 1 - (1 - p_0)^T$. If observed cumulative touch probabilities $P(T)$ fall below this curve at any tenor, the joint hypothesis (independence + per-period rate p_0) is rejected. Under positive dependence with marginal mean $\mu = p_0$, the cumulative probability falls below the independence benchmark (Proposition 6(iii)), so $P(T) < P_{\text{ind}}(T)$ does not falsify p_0 under correlation—only the joint independence assumption.

Test 2: dependence-adjusted estimation. Fitting the Beta-binomial to observed $P(T)$ at multiple horizons returns $(\hat{\mu}, \hat{\rho})$. $\hat{\mu}$ is the dependence-adjusted per-period rate; $\hat{\rho}$ the correlation structure across renewals. Nonzero $\hat{\rho}$ indicates that a single-tenor margin does not transfer across horizons without correction. The viability of any specific contract is then assessed by comparing $\hat{\mu}$ against that contract's $\pi^*(\kappa, L)$ from Proposition 1.

Empirical execution requires option-implied cumulative probabilities at multiple tenors and has not been computed in this paper. Appendix C.9 computes risk-neutral touch probabilities at a single tenor across multiple barriers; the multi-tenor extension required for these tests remains open.

C Measurement construction, diagnostics, and falsifiability

This appendix specifies the empirical construction: the coupled options-intensity–persistence state from market observables, the ergodicity wedge as time-cost accounting, and the repricing diagnostics used in the renewal-feasibility map.

C.1 Data scope

We use daily GME OHLCV (returns and volume) and daily options aggregates (call/put volume, open interest, implied volatility level/change, and simple tilts/ratios). We add: (i) a float proxy F with documented source/definition, (ii) boundary relevance $B_t := OI_t^{\text{call}}/F$, and (iii) a minimal open-interest persistence diagnostic across monthly expiries. We do not use social-media metrics, sentiment scores, proprietary flow, or intraday microstructure series.

Time-series integrity (no look-ahead). Standardization parameters, clustering centroids, and thresholds for labels are fit on past blocks only and applied forward. Any smoothing is backward-looking.

Pre-specified anchor windows. Two burst episodes for descriptive anchoring: January–March 2021 (the "sneeze") and May–June 2024 (the 2024 re-entry), anchored to the SEC staff report [9] and contemporaneous reporting [27, 28, 29]. These appear only as overlays; they do not enter state construction, wedge construction, or label construction.

Free-float proxy. The float proxy F is constructed as total shares outstanding minus DRS-registered shares minus insider and restricted holdings. Insider holdings are estimated at ≈56 million post-split shares, comprising Ryan Cohen / RC Ventures (≈36 million, per Schedule 13D filings) and other insiders and restricted stock (≈20 million, from proxy filings). DRS counts are interpolated from quarterly Computershare disclosures. ATM offerings are added at their documented completion dates. This proxy captures the tradeable equity supply more accurately than gross shares outstanding (≈420M), which includes locked holdings that do not participate in the secondary market. Throughout the empirical sections, F corresponds to the effective tradable float F_t^{eff} of Appendix A.

ETF-embedded GME shares (held by funds such as XRT, IWM, and sector ETFs) are not included in the B_t numerator. Options on these ETFs can generate additional hedging demand against GME shares, so B_t understates total capacity relevance to the extent that ETF-level options activity is material.

C.2 Wedge and state-variable construction

The ergodicity wedge $\widehat{\Delta}(t;T)$ is computed on a rolling window of $T = 20$ trading days from close-to-close simple returns:

$$\widehat{\Delta}(t;T) = \ln\left(\frac{1}{T}\sum_{j=0}^{T-1}(1+r_{t-j})\right) - \frac{1}{T}\sum_{j=0}^{T-1}\ln(1+r_{t-j}).$$

The baseline return stream is the underlying-only close-to-close simple return of GME.

The two state variables—options intensity $\gamma_t := \ln V_t^{\text{opt}}$ and persistence proxy q_t (normalised OBV slope, 20-day; limitations in Section 3.4)—are constructed from options aggregates and OBV respectively; neither uses returns, the wedge, or rolling variance as inputs.[41]

C.3 Repricing labels

Because conversion is not observed day-by-day, we define repricing labels that capture rare burst episodes. The primary label $M_t^U = \mathbf{1}\{U_t \geq \tau_{1-\alpha}^U(t)\}$ thresholds a held-out front-end IV repricing shock U_t at its expanding 95th percentile (same as eq. 44 in Section 4; past-only quantile, no look-ahead). A secondary state-based marker $M_t^\gamma = \mathbf{1}\{\gamma_t \geq \tau_{1-\alpha}^\gamma(t)\}$ is used for segmentation, and an auxiliary return-based label $M_t^r = \mathbf{1}\{|r_t| \geq \tau_{1-\alpha}^r(t)\}$ enters only the label-fragility falsification test.

C.4 Capacity relevance and repricing diagnostic

Boundary relevance $B_t := OI_t^{\text{call, all}}/F$ is total end-of-day call open interest (gross share-equivalent units) divided by the float proxy F; it is an inventory-style measure, not executed demand or hedging flow. OI persistence across monthly OPEX is measured as the ratio of mean call OI in the 10 trading days after expiry to the 10 days before; values above 1 indicate renewed positioning through the expiry cycle.

The repricing state summary $\hat{p}_t^{\text{ign}}$ is the expanding-window logistic defined in Section 4 (eq. 43). The renewal-feasibility (lens-flip) diagnostic compares it to the survival threshold: $\widehat{\mathcal{R}}_t(\kappa, L) := \mathbf{1}\{\hat{p}_t^{\text{ign}} \geq \pi^*(\kappa, L)\}$, reported in calendar time and as a contour in state space.

C.5 Wedge concentration and localization

The claim is selective concentration: wedge mass concentrates in (i) the two burst episodes and (ii) specific regions of the intensity–persistence manifold more than a volatility-preserving null would imply.

Window concentration. Let $\mathcal{W}_{21}$ and $\mathcal{W}_{24}$ denote the pre-specified windows. The wedge-mass share in window $\mathcal{W}$ is

$$\Lambda_{\text{time}}(\mathcal{W}) := \frac{\sum_t \Delta_t \mathbf{1}\{t \in \mathcal{W}\}}{\sum_t \Delta_t}. \tag{65}$$

Localization in state space. For a subset $\mathcal{S}$ of state space (e.g., top decile of γ_t intersected with top decile of q_t):

$$\Lambda(\mathcal{S}) := \frac{\sum_t \Delta_t \mathbf{1}\{(q_t, \gamma_t) \in \mathcal{S}\}}{\sum_t \Delta_t}. \tag{66}$$

[41] GME executed a 4:1 stock split dividend on July 22, 2022. The equity data source retroactively adjusts pre-split volume by a factor of 4; the options data source does not. Pre-split options volumes are multiplied by 4 before computing γ_t.

Nulls and placebo. (i) A volatility-preserving null breaks alignment between wedge and state realisations while preserving marginal dispersion (permutation of state labels within realised-variance bins). (ii) A circular-block permutation null (2,000 draws) respects serial dependence by shifting the entire wedge series by a random offset. As placebo, repeat (66) using rolling realised variance as "mass."

Window	Observed Λ	Null 95% CI	Percentile
Jan–Mar 2021	0.449	[0.006, 0.432]	98.2
May–Jun 2024	0.144	[0.004, 0.348]	94.5
Combined	0.592	[0.015, 0.555]	98.8

Circular-block permutation null, 2,000 draws.
Variance placebo: Λ^{rv}(combined) = 0.643.

Table 5: Wedge-mass concentration against circular-block permutation null. $\Lambda(\mathcal{W})$ is the share of total wedge mass falling in the pre-specified window (equation 65). The variance placebo ($\Lambda^{\text{rv}} = 0.643 > 0.592$) confirms the concentration is mechanically grounded in the variance channel: realised variance is *more* concentrated than the wedge in the same windows, as expected since the wedge is approximately $\frac{1}{2}\hat{\sigma}^2$.

C.6 Diagnostic stress checks

We report seven diagnostic checks whose failure would weaken the proposed interpretation. Each specifies a condition whose violation would undermine the argument; we report whether the data are consistent or inconsistent.

- **Time concentration:** wedge mass concentrates in the 2021 and 2024 windows relative to volatility-preserving null allocations. *Consistent*—see Section 4, Table 5, and Table 6.
- **Localization:** wedge localizes in high-intensity / elevated-persistence states relative to null allocations (equation 66, Section 4). *Consistent*—see Appendix D.
- **Capacity:** B_t is elevated in repricing windows. *Consistent*—see Section 4.
- **Renewal:** open-interest persistence signature is present across monthly expiries during bursts. *Consistent*—see Section 4.
- **Complementarity:** the $q_t \times \gamma_t$ interaction structure appears in fitted ignition surfaces and wedge localization. *Consistent*—see Appendix D.
- **Flip:** options-intensity does not concentrate when persistence is weakest and B_t is low. *Consistent*—the opposite pattern holds.
- **Label fragility:** conclusions hold under M_t^U as well as M_t^r. *Consistent*—see Appendix D.

Robustness checks on auxiliary choices—wedge window T, persistence proxy, alternative float definitions, and boundary relevance with alternative OI subsets—are reported in the subsections below and in Appendix D.

C.7 Clock robustness

The baseline wedge uses $T = 20$ trading days. Table 6 reports wedge-mass concentration for $T \in \{5, 10, 20, 40\}$. The combined $\Lambda(\mathcal{W}_{21} \cup \mathcal{W}_{24})$ ranges from 0.52 ($T = 40$) to 0.61 ($T = 5$); the qualitative pattern—most of the wedge mass localises in two short windows—is stable across clocks. Shorter windows resolve more of the intra-burst variation; longer windows smooth it but do not move the mass elsewhere. Figure 13 shows the wedge time series for each T.

C.8 Capacity relevance: B_t and OI persistence

Boundary relevance $B_t := OI_t^{\text{call}}/F$ (share-equivalent call open interest divided by free-float proxy) reaches a median of 0.72

T	$\Lambda(\mathcal{W}_{21})$	$\Lambda(\mathcal{W}_{24})$	Λ(combined)	Days (%)
5	0.443	0.169	0.612	7.9
10	0.443	0.163	0.606	8.0
20	0.448	0.144	0.592	8.0
40	0.416	0.105	0.521	8.2

Table 6: Wedge-mass concentration across measurement-window lengths.

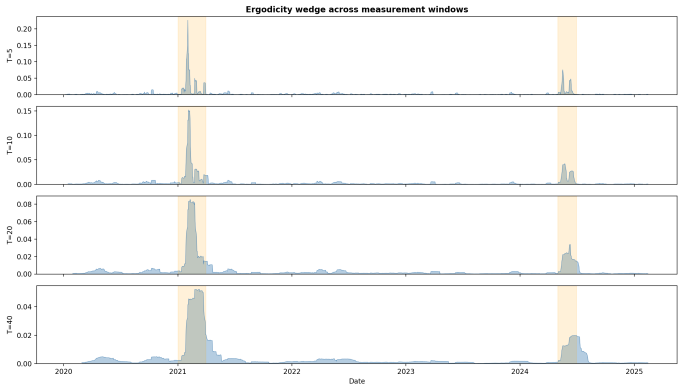

Figure 13: Ergodicity wedge $\widehat{\Delta}(t;T)$ for $T \in \{5, 10, 20, 40\}$. Orange shading marks the 2021 and 2024 burst episodes. The concentration pattern is qualitatively stable: expensive time localises in the same windows regardless of measurement clock.

during the 2021 burst episode, meaning aggregate call OI routinely exceeded two-thirds of the estimated free float. During the 2024 burst, B_t is lower (median 0.34) reflecting post-dilution float expansion. During calm periods the median is 0.10. B_t exceeds 0.50 on 17% of trading days in the full sample; high B_t establishes that call OI was large relative to float, not that it actually constrained supply.

OI persistence across monthly OPEX is measured as the ratio of mean call OI in the 10 trading days after expiry to the 10 days before (values above 1 mean OI grew through expiry; below 1 means it decayed). During burst build-up, OI persists or grows: the May 2024 OPEX ratio is 1.56, meaning call OI was 56% higher after expiry than before, consistent with renewed positioning during the Roaring Kitty return. During collapse, OI drops sharply (March 2021: 0.75; June 2024: 0.74). Calm periods exhibit median persistence of 0.99. Figure 14 shows B_t through time and OI persistence by OPEX.

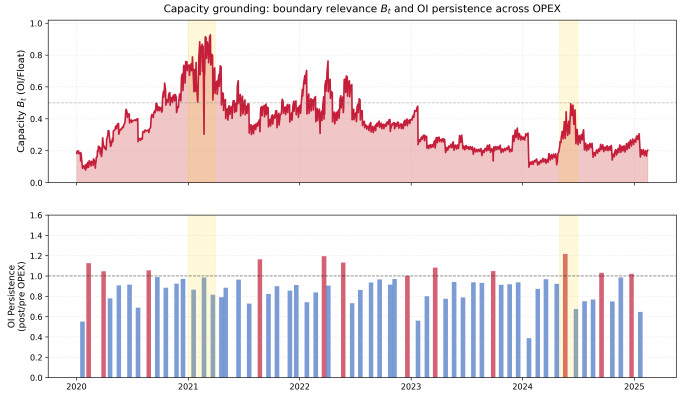

Figure 14: Top: boundary relevance B_t (call OI / float). Dashed line marks $B_t = 0.5$. Bottom: OI persistence ratio across monthly OPEX dates. Orange bars indicate burst-window expiries. The May 2024 OPEX shows the highest persistence ratio in the sample (1.56), consistent with renewed positioning rather than one-shot speculation.

C.9 Risk-neutral feasibility from option prices

The proxy-based ignition estimate $\hat{p}_t^{\text{ign}}$ is constructed from state variables; it is not directly market-implied. As a complementary lens, we read feasibility straight from option prices via the Black–Scholes *probability of touch*—the risk-neutral probability that the price path reaches a barrier level at least once within a given horizon. Let $P_t^{\text{touch}}(L)$ denote this probability for a barrier at $L \times S_t$ (i.e. an L-fold move from the current price), with annualised implied volatility σ_t and horizon $\tau = 20$ trading days. Under geometric Brownian motion,

$$P_t^{\text{touch}}(L) = N(d_1) + e^{2\mu \ln L/\sigma_t^2}\, N(d_2), \qquad \mu = -\tfrac{1}{2}\sigma_t^2,$$
$$d_1 = \frac{-\ln L + \mu\tau}{\sigma_t\sqrt{\tau}}, \qquad d_2 = \frac{-\ln L - \mu\tau}{\sigma_t\sqrt{\tau}},$$

where $N(\cdot)$ is the standard normal CDF and $\tau = 20/252$ years (matching the rolling-window length T used elsewhere, expressed in annualised units for the Black–Scholes inputs). Note the drift: $\mu = -\sigma_t^2/2$ is the risk-neutral drift, which is the pricing measure embedded in option markets. This differs from the zero-drift assumption ($\mu = 0$) used for P^{touch} in the static renewal margin of Section 6. The two serve different purposes. Section 6 asks whether the gamble can sustain itself under a physical-measure baseline where the stock has no directional tendency; the risk-neutral P^{touch} here asks what the option market itself implies about barrier-contact frequency. Under risk-neutral drift, the touch probability is lower (the $-\sigma^2/2$ drag works against reaching the barrier), so the bounds reported below are conservative relative to the zero-drift case.

A modelling caveat that applies to *all* P^{touch} calculations throughout this paper, including the renewal margin of Section 6 and the feasibility sandwich below: the formula assumes continuous sample paths (geometric Brownian motion). GME during burst episodes exhibits halt-and-gap dynamics—repeated trading halts followed by discontinuous price jumps through strikes. Jumps can raise the physical touch probability (gapping past the barrier) or lower it (halt-induced mean reversion pulling price back). During the 2021 and 2024 burst episodes, the dominant pattern was upward gapping through halts, which if anything makes the continuous-path formula a conservative estimate of actual touch probability. Outside burst episodes, price dynamics are closer to diffusive and the Black–Scholes formula is a reasonable approximation.

Figure 15 shows $P_t^{\text{touch}}(L)$ for $L \in \{1.5, 2, 3, 5, 10\}$. During the 2021 burst, the market-implied probability of a 50% move within 20 days reached a median of 47%; a doubling had median probability 25%. During calm periods these drop to 13% and 1% respectively. For the high-L multiples relevant to renewal payoffs ($L \geq 5$), P^{touch} is negligible outside burst episodes. The bottom panel shows the survival threshold $\pi^*(\kappa, L)$ for comparison: at $\kappa = 0.10$ and $L = 5$, renewal requires $\pi^* \approx 2.3\%$, which the market-implied probability exceeds only during bursts.

This confirms the proxy-based finding on a fully independent footing: the option market itself prices ignition-scale moves as feasible only during the same episodes the state variables identify as elevated.

C.10 Ignition feasibility surface and flip diagnostic

Ignition label. Label construction follows Section 4 (eq. 44): $M_t^U = \mathbf{1}\{U_t \geq \tau_{0.95}^U(t)\}$, where U_t is the expanding-window z-

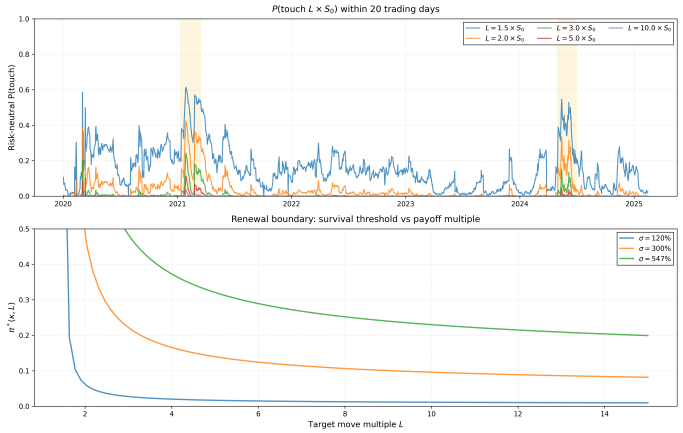

Figure 15: Top: risk-neutral probability of touching $L \times S_t$ within 20 trading days for $L \in \{1.5, 2, 3, 5, 10\}$, read directly from aggregate implied volatility. Bottom: survival threshold $\pi^*(\kappa, L)$ for three burn rates ($\kappa \in \{0.05, 0.10, 0.20\}$). The market-implied feasibility of large moves concentrates in the same burst episodes identified by the proxy-based state variables.

score of daily IV change. Over the full sample (through December 2025), this yields approximately 87 positive days. The base rate is 6.0% when computed over the evaluation period (post-2020 trading days where the expanding window contains at least one prior positive); over the full sample including the pre-2021 initialisation period the raw fraction is lower (≈4.6%).

Ignition surface (exploratory). The expanding-window logistic estimates $\hat{p}_t^{\text{ign}} = \text{logit}^{-1}(\hat{\beta}_{1:t}^\top \mathbf{x}_t)$ (eq. 43), where the feature vector is $\mathbf{x}_t = (V_t^{\text{opt}},\ \hat{\sigma}_{t,20}^2,\ \zeta_t,\ \omega_t,\ |r_t|)^\top$: total options volume, 20-day realised variance, call tilt (call share of total volume), call open-interest ratio (call OI / equity volume), and absolute daily return. Coefficients $\hat{\beta}_{1:t}$ are fitted on expanding windows $\{1, \ldots, t\}$ so that only data available at t enters the estimate. Two of the five features—realised variance and absolute return—are mechanically correlated with the IV-change label. A restricted specification using only the three positioning features (V_t^{opt}, ζ_t, ω_t) yields AUC = 0.816 versus 0.825 for the full model, a difference of less than one percentage point. The positioning features carry virtually all of the discriminatory power; the volatility-correlated features contribute almost nothing. At the 6.0% base rate, positive predictive value is roughly 15% at the median threshold; the Brier score is 0.048, close to the no-skill baseline of 0.057 (= 0.06 × 0.94), confirming that the diagnostic identifies regimes where the options state is persistently elevated, not individual ignition events. Discrimination: overall AUC = 0.825 (Brier 0.048); by era: 2021 AUC 0.807, 2022–23 AUC 0.838, 2024–25 AUC 0.850.

Flip diagnostic. The flip indicator $\hat{\mathcal{R}}_t(\kappa, L) = \mathbf{1}\{\hat{p}_t^{\text{ign}} \geq \pi^*(\kappa, L)\}$ shows when the repricing diagnostic clears the survival threshold. The $\hat{p}_t^{\text{ign}}$ time series (Figure 16 panel a) spikes during 2021 and 2024 burst episodes. The calibration curve (panel b) shows reliability AUC 0.929 (Brier 0.043), confirming well-ordered probability estimates despite moderate discrimination AUC (0.825). The flip heatmap (panel c) confirms the threshold clears only during bursts and for low-burn/high-L scenarios; the state-space contour (panel d) shows $\hat{p}^{\text{ign}}$ concentrates in the high-intensity / high-persistence corner.

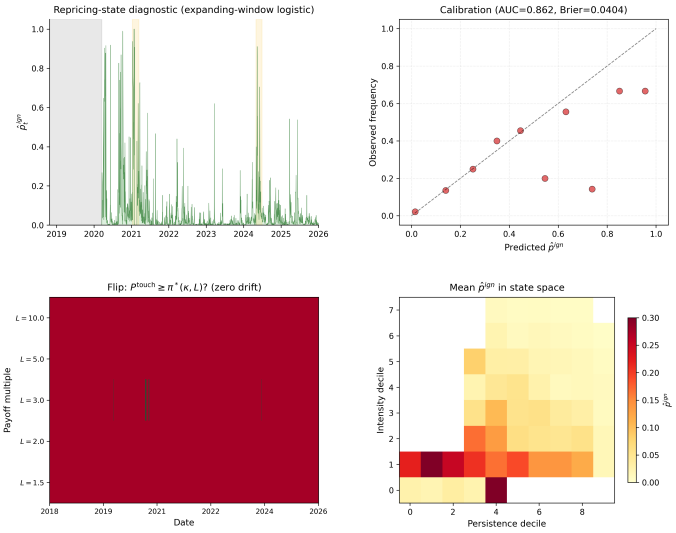

Figure 16: Ignition feasibility and flip diagnostic. (a) Expanding-window logistic estimate of $\hat{p}_t^{\text{ign}}$; grey region marks pre-2021 where no ignition events exist in the training data. (b) Reliability curve (reliability AUC= 0.929, calibration Brier= 0.043; discrimination AUC= 0.825, overall Brier= 0.048). (c) Flip diagnostic: green cells indicate $\hat{p}_t^{\text{ign}} \geq \pi^*(\kappa, L)$; the threshold clears only during burst episodes and only for low-burn / high-L tactics. (d) Mean $\hat{p}^{\text{ign}}$ across intensity–persistence quantiles, with survival thresholds overlaid.

C.11 Repricing diagnostic: discrimination and calibration

Discrimination is moderate: the expanding-window out-of-sample AUC is 0.825 overall (Brier = 0.048; evaluated on post-ignition trading days through December 2025). By era: 2021 AUC = 0.807 ($n = 252$, 21 positives); 2022–23 AUC = 0.838 ($n = 501$, 9 positives); 2024–25 AUC = 0.850 ($n = 502$, 21 positives). The calibration curve is monotonic, meaning the probability estimates are well-ordered even where binary discriminability is limited. We therefore treat the logistic output as a descriptive summary of options-state clustering rather than a reliable event predictor. At the 6.0% base rate, positive predictive value is low. Accordingly, the diagnostic identifies elevated-state regimes rather than individual ignition events. The feasibility sandwich (Appendix D.4) uses P^{touch}, not $\hat{p}^{\text{ign}}$.

C.12 State variable visualisation

Figure 17 shows the intensity and persistence time series and their joint scatter, neither collinear nor independent but consistent with the two-channel structure of Section 4.1. Burst-episode observations occupy high intensity / variable persistence regions, confirming distinct information across the two channels.

C.13 Mixed-portfolio threshold calibration

In the mixed portfolio (Remark 2), a smaller call weight dilutes the effective burn: at the ATM baseline-IV scenario ($\kappa \approx 14\%$, $L = 20$), the pure-call threshold is ≈10%; at $\alpha_c = 50\%$ it falls to ≈8%; at $\alpha_c = 15\%$ to ≈6%. In the limit $\alpha_c \to 0$ the threshold converges to $1/L = 5.0\%$, a floor set by the payoff multiple alone. The wedge remains relevant as a separate cost on the equity sleeve (panel 2 of Figure 3): it measures when holding is expensive in compounding terms, even though it does not enter the mixed-portfolio threshold formula in share-equivalent units.

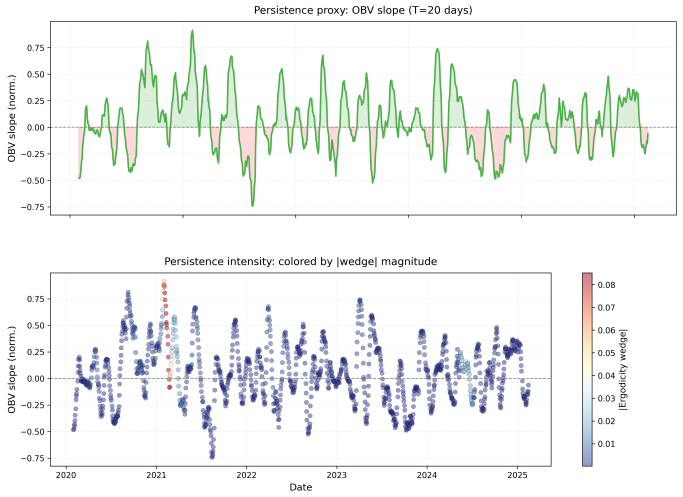

Figure 17: Left: persistence proxy q_t (OBV slope) time series. Right: scatter of intensity ($\gamma_t = \ln V_t^{\text{opt}}$) versus persistence, with burst episodes highlighted. The raw options volume time series is shown in Figure 3 (bottom panel).

C.14 IV–wedge co-movement

Predictive regression. Regressing 5-day realised volatility at $t+k$ on lagged volatility plus log options volume at t yields significant incremental predictive power at all lags ($F = 16.9$ at $k = 1$, $p < 10^{-4}$; $F = 54.9$ at $k = 4$, $p < 10^{-13}$; $N = 1{,}287$ days). The effect strengthens with horizon (ΔR^2 from 0.2% at one day to 2.7% at four days), consistent with cumulative hedging pressure translating to realised variance over multiple sessions. Reverse causality (volatility predicting next-day options intensity) is also significant ($F = 27.7$, $p < 10^{-7}$), confirming bidirectional feedback: options flow drives volatility, and elevated volatility attracts further activity.

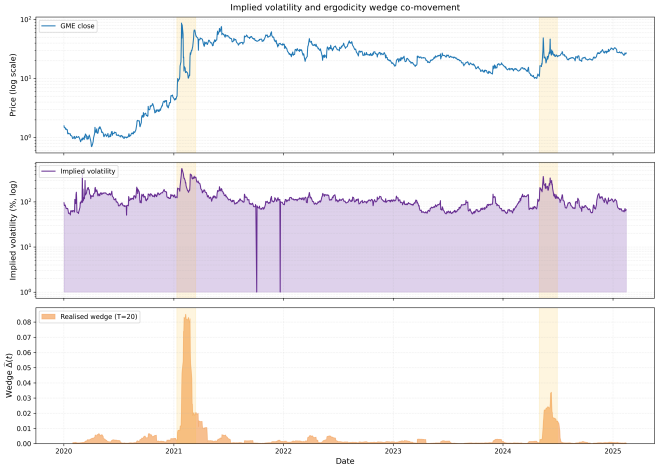

Figure 18: Co-movement of 30-day implied volatility and the realised ergodicity wedge ($T = 20$). Yellow shading marks the January–March 2021 and May–June 2024 burst episodes. Dashed lines indicate the two IV regimes used in the Black–Scholes calibration (Section 3): $\sigma = 120\%$ (baseline) and $\sigma = 300\%$ (burst). The sample correlation is $\rho \approx 0.62$: the implicit and explicit costs of convex renewal move together, as discussed in Section 3.

C.15 Lorenz concentration

Figure 19 shows the Lorenz curve of wedge mass for each T. At $T = 20$, the top 5% of days carry 52% of wedge mass; the top 10% carry 66%. The pattern is robust: shorter windows ($T = 5$) yield more extreme concentration (top 5% carry 61%); longer windows ($T = 40$) yield less extreme (top 5% carry 47%).

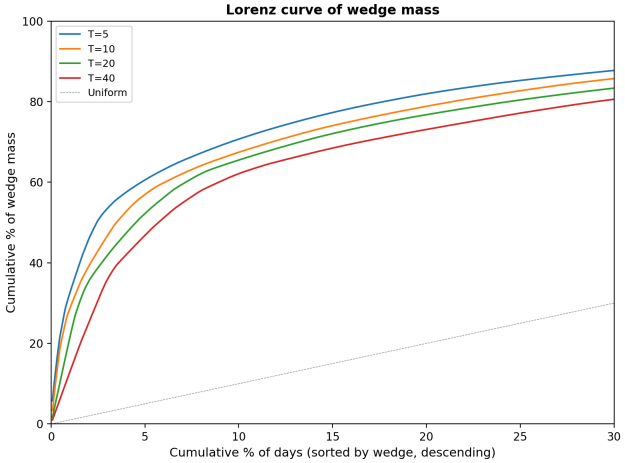

Figure 19: Lorenz curve of wedge mass. Each curve corresponds to a measurement window T. The dashed line is the uniform benchmark. All curves show extreme concentration: a small fraction of days carries the majority of the compounding penalty.

C.16 PCA episode trajectories

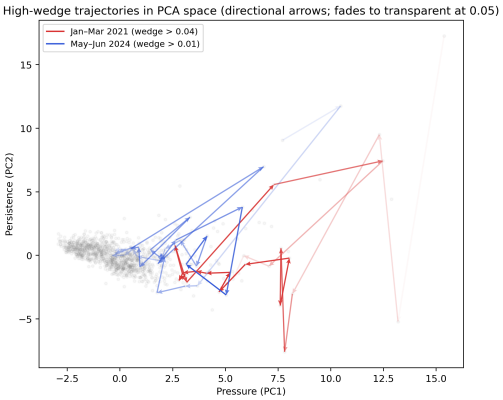

Figure 20: Burst-episode trajectories in PCA space (twelve daily features; PC1 explains 31.8% of variance, PC2 explains 13.3%). Arrows trace the day-by-day path; opacity scales with the local ergodicity wedge (fading to transparent below $\widehat{\Delta} = 0.05$). Red: January–March 2021; blue: May–June 2024. Grey scatter shows all other days. Both episodes enter the same high-activity region; the 2021 episode extends roughly three times further along PC1. The embedding is fitted once on the full sample; burst-window days are not weighted.

D Mechanical stress tests

This appendix stress-tests the renewal framework against four critiques: feasibility too low, retail convexity self-excited rather than structural, conclusions depend on unobserved π, and episodes not genuinely near-binding.

D.1 Dealer reflexivity and relative flow share

The renewal interpretation requires that options activity is *capacity-relevant*, not just volatile: dealer hedging of call OI

must generate meaningful flow relative to available liquidity. We estimate aggregate gamma from a Black–Scholes framework using aggregate implied volatility, a uniform moneyness grid (ATM to 50% OTM), and a representative 30-day expiry. We report hedge flow per 1% price move, computed as $(\Gamma_t^{\text{agg}} \times S_t) \times OI_t^{\text{call}}/100$ in share-equivalents. Using a percentage move (rather than a dollar move) ensures the metric is regime-comparable: a 1% move is the same economic event regardless of whether the stock trades at \$5 or \$60.

During the 2021 burst, median hedge flow per 1% move was approximately 0.5% of average daily volume (ADV); on peak days it reached 6.5% of ADV. Call open interest in share-equivalents reached approximately 93% of the estimated free float at peak. During the 2024 burst, median hedge flow per 1% move was 0.9% of ADV (peak 15.7%), with call OI reaching approximately 49% of the effective float at peak ($B_t = 0.49$; median 34%).

Relative flow share tells a complementary story. During burst episodes, options-driven notional (call volume × 100 × price) routinely exceeds equity notional, with daily ratios reaching 3–5× at peak; even the burst-window median exceeds unity. The options channel generates flow on the same order of magnitude as—and frequently larger than—the equity channel.

Figure 21 shows the dealer reflexivity time series; Figure 22 shows the relative flow share.

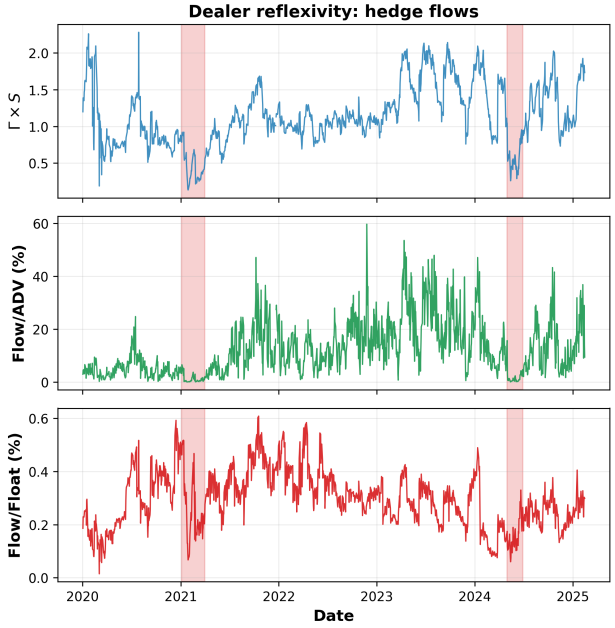

Figure 21: Dealer reflexivity. Top: price-normalised percentage gamma $\Gamma \times S$ ($\mathrm{d}\Delta/\mathrm{d}\%S$), which removes the mechanical $1/S$ scaling that makes raw per-dollar gamma appear elevated at low price levels. Middle: implied hedge flow per 1% move as % of ADV. Bottom: hedge flow per 1% move as % of float. Orange shading marks burst episodes.

The aggregate gamma estimates above assume hedging across the full moneyness grid, but in practice dealers may carry far-OTM inventory with minimal delta largely unhedged—the position costs little to warehouse when the probability of reaching those strikes is small. The hedging cascade that could reprice the stock therefore starts with near-the-money gamma, where per-contract gamma is highest and where dealers are actively rebalancing. Far-OTM positions come into play only as price runs through their strikes: each contract's delta swings from

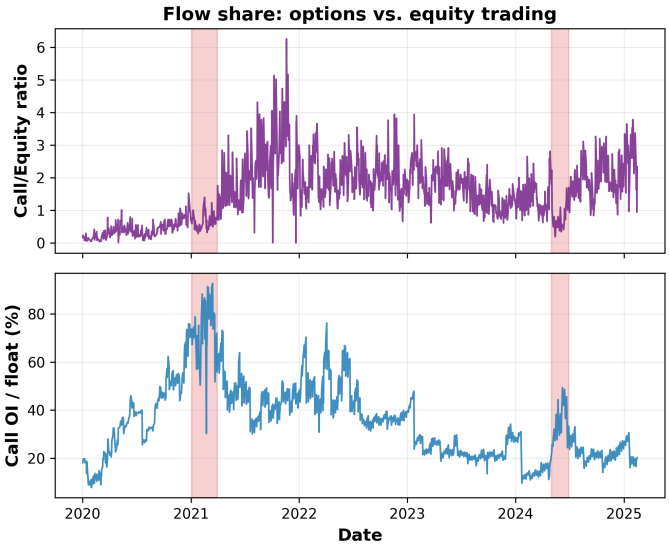

Figure 22: Relative flow share. Top: call notional / equity notional ratio. Bottom: call OI share-equivalent / float (%). Orange shading marks burst episodes.

near zero toward one, extending the cascade once it has already begun. The survival-threshold analysis (Section 6) favours OTM strikes or smaller portfolio commitments for individual renewal (lower κ, higher L, lower π^*), which means what is individually optimal for renewal discipline is not what generates the initial hedging flow. Individual survival and collective ignition pull in different directions on moneyness.

D.2 Does intensity tighten supply? The self-excited volatility test

If retail convexity is self-excited, high options intensity should predict higher volatility but *not* higher boundary relevance B_t. We proxy intensity here by $\tilde{\gamma}_t := \ln(V_t^{\text{opt}})$ (log total options volume, split-adjusted) rather than the call-tilted ratio γ_t used in the main text; this captures aggregate activity level directly, without the equity-volume denominator or call-share tilt that make γ_t a relative positioning measure. We test via regression:

$$\Delta B_{t,t+5} = \alpha + \beta_1 \tilde{\gamma}_t + \beta_2 \text{vol}_t + \varepsilon,$$

where vol_t is 5-day rolling realised volatility and both regressors are standardised.

After controlling for realised volatility, high intensity predicts *lower* subsequent B_t ($\hat{\beta}_1 = -0.004$, $t = -2.50$, $p < 0.05$), while volatility predicts higher B_t ($\hat{\beta}_2 = +0.007$, $t = 4.56$, $p < 0.001$). The highest-intensity quintile shows a mean 5-day decline of ≈8,000 call-OI contracts; the lowest-intensity quintile shows a mean 5-day gain of ≈5,000. High-intensity days consume rather than accumulate OI. The fast channel tests ignition via volatility; structural tightness builds through the slow channel (share accumulation, direct registration). The channels are complementary.

Figure 23 shows the test results.

D.3 Counterfactual π stress test

The threshold depends on unobserved feasibility π_t^{succ}. We simulate 2,000 Monte Carlo paths of cumulative log wealth under weekly Bernoulli renewal (≈380 intervals) for $\pi \in \{1\%, 2\%, 5\%, 10\%, 20\%, 50\%\}$ and five scenarios with $\kappa L = 2$

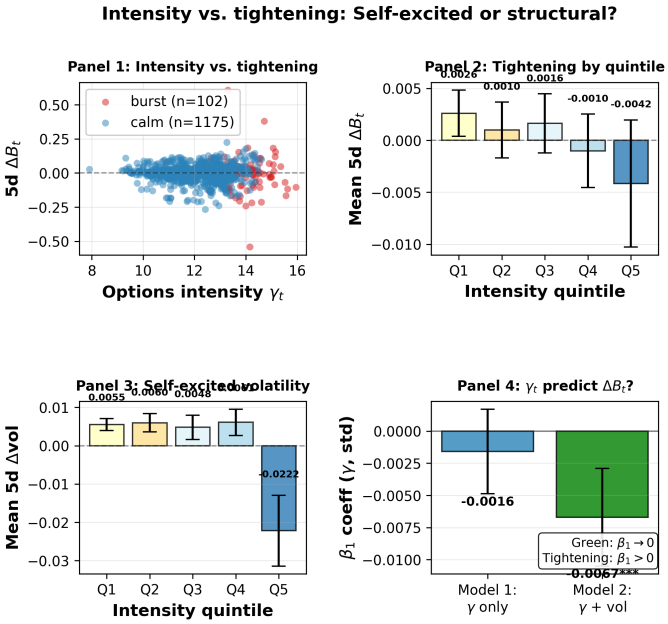

Figure 23: Self-excited volatility test. (a) Scatter of γ_t vs. 5-day-ahead ΔB_t. (b) Mean 5-day-ahead ΔB_t by γ quintile. (c) Mean 5-day-ahead Δvol by quintile. (d) Regression coefficients.

held constant (same arithmetic edge, different burn rates): $\kappa \in \{1\%, 2\%, 5\%, 10\%, 20\%\}$ with $L = 200, 100, 40, 20, 10$ respectively. Each interval draws $A_{t+1} \sim \text{Bernoulli}(\pi)$ independently; the log-wealth recursion is $\ln W_{t+1} = \ln W_t + \ln(1 - \kappa + \kappa L\, A_{t+1})$, matching the renewal model of Proposition 1.

Sharp threshold crossings emerge along the diagonal of the π–κ grid. At $\kappa = 1\%$, renewal is viable from $\pi = 2\%$ upward; at $\kappa = 5\%$, from $\pi = 5\%$; at $\kappa = 20\%$, only from $\pi = 20\%$. Higher burn rate requires proportionally higher success probability to survive, even though the arithmetic payoff ratio is identical across all five scenarios. At $\pi = 50\%$ all scenarios are strongly viable.

Whether π falls in the 2–5% range (viable for low-burn) or below 1% (unviable for all burn rates) is unobserved. Market-implied move-probability summaries from options (Appendix C.9) enter the range relevant to viability comparisons during bursts and sit below the corresponding benchmark range during calm periods. The repricing state summary $\hat{p}_t^{\text{ign}}$ (Section 4) rises into the 5–10% range during the 2021 burst and settles near zero in 2023, consistent with the burst-versus-calm separation described in the main text.

Figure 24 shows the π–scenario matrix.

D.4 Near-binding episode: January–March 2021

The preceding tests establish boundary conditions. This subsection assembles descriptive evidence that the January–March 2021 episode exhibited a configuration mechanically close to the conditions the framework treats as constraint-relevant.

1. **Boundary relevance.** B_t peaked at 0.93: call open interest in share-equivalents reached over nine-tenths of the estimated free float.
2. **Dealer hedge pressure.** Median hedge flow per 1% move was 0.5% of ADV (peak 6.5%)—not a dominant fraction at the median, but on high-move days the cumulative hedging demand scales with the move size and becomes non-trivial for a stock with concentrated float.
3. **OI persistence across expiry.** Call OI remained elevated across the January and February monthly OPEX dates, consistent with rolling or re-establishment rather than one-shot speculation.
4. **Market-implied feasibility.** The risk-neutral probability of a 50% move within 20 trading days reached a median of 47% during the burst; a doubling had median probability 25%.
5. **Wedge cost.** The peak 20-day wedge reached 0.085, indicating steep compounding penalty on the equity sleeve during burst episodes. In the mixed portfolio (Remark 2), a smaller call weight dilutes effective burn: at $L = 20$ and $\alpha_c = 50\%$ the ATM baseline-IV threshold falls from ≈10% to ≈8%. The wedge remains the dominant cost on the equity position itself.

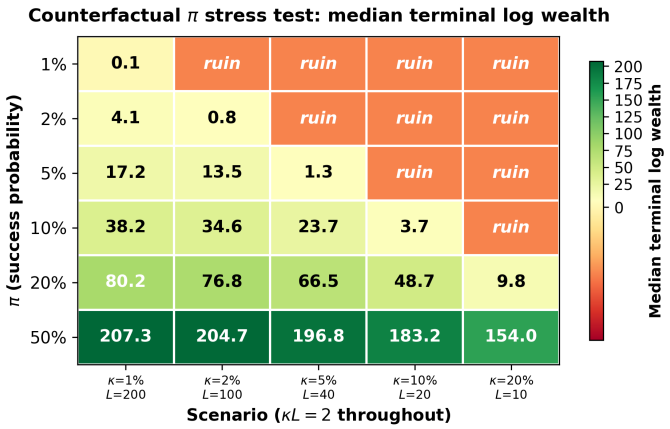

Figure 24: Counterfactual π stress test. Median terminal log wealth across π–scenario combinations, with $\kappa L = 2$ held constant (same arithmetic edge, different burn rates). Green: viable renewal; red: ruin. Higher burn rate requires proportionally higher π to survive.

The 2024 episode shows analogous mechanics at attenuated scale. Five documented ATM offerings between April 2021 and September 2024 expanded the gross share count, but direct registration (DRS) through Computershare removed up to ≈76 million post-split shares from the tradeable float by early 2023. The net effective float increased by a factor of ≈1.3× between the two burst episodes; the attenuation in B_t (0.93 → 0.49, a factor of ≈1.9×) reflects lower absolute call OI alongside the partially offset dilution.

Feasibility sandwich. The following is a plausibility bracket, not a formal probability bound. Both bounds are constructed entirely from risk-neutral touch probabilities $P_t^{\text{touch}}(L)$—read directly from aggregate implied volatility via the Black–Scholes barrier-contact formula (Appendix C.9)—and do not depend on the repricing state summary $\hat{p}_t^{\text{ign}}$ or any proxy-based diagnostic. The touch probability assumes continuous sample paths; the sandwich shows where the survival threshold sat relative to market-implied move probabilities, not relative to a fitted model. The repricing state summary is noted alongside as a confirming redundancy only and does not enter the bound construction. The sandwich shows that the survival threshold fell within a historically reachable range during burst episodes—that the cost of renewal was in the neighbourhood of market-implied feasibility. It does not establish that π^{succ} definitively exceeded π^* on any given day.

The two barriers correspond to equity moves that generate option payoffs in the range relevant to the survival threshold. A 50% equity move (1.5× spot) delivers a payoff-to-premium ratio L in the range 5–20 for typical OTM strikes; a doubling (2× spot) delivers L in the range 15–50, depending on strike and IV at entry. Lower bound: $P_t^{\text{touch}}(2)$, the risk-neutral probability of the equity doubling within 20 trading days—corresponding to the high-L payoffs where the survival threshold is most favourable. Upper bound: $P_t^{\text{touch}}(1.5)$ augmented by capacity B_t—corresponding to moderate-L payoffs where the threshold is higher but the move is more probable. Both bounds are read from aggregate implied volatility; the appendix does not identify drift.

The moderate-scenario threshold $\pi^* = 9\%$ falls below the lower bound on 87% of burst days in 2021 and 76% in 2024; only 5% of calm days clear.

See Appendix B.2 for the renewal-margin erosion across successive cycles.

Figure 25 shows the near-binding scorecard; Figure 26 shows the feasibility sandwich; Figure 27 shows the ignition-to-exhaustion cycle.

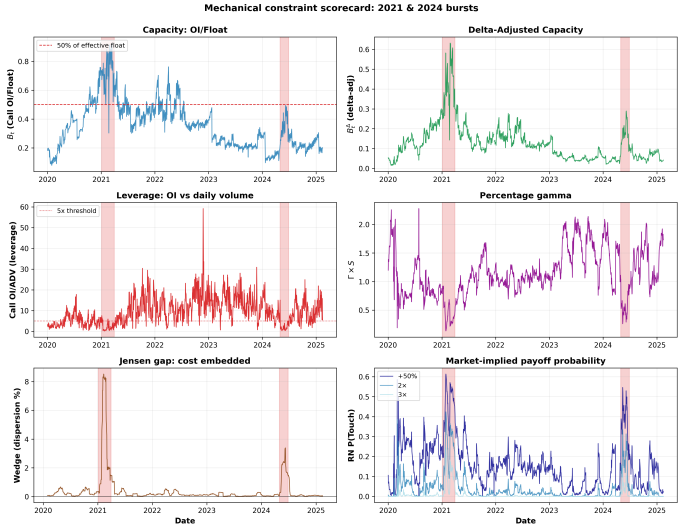

Figure 25: Near-binding scorecard: six mechanical metrics across 2021 burst, 2024 burst, and calm baseline.

D.5 Constraint stress checklist

The framework's observables reduce to four gauges that can be computed from publicly available daily data.

Gauge 1: Capacity relevance (B_t). Call OI in share-equivalents divided by free float. $B_t > 0.5$ is a rule-of-thumb reference level under the latent-capacity measure; $B_t < 0.15$ means the fast channel is quiescent. Peaked at 0.93 (Jan 2021) and 0.49 (May 2024). Gross B_t counts all call OI at face value; far-OTM calls contribute less immediate hedging demand per contract, so the effective exposure at any snapshot is lower than gross B_t suggests. Without chain-level strike distributions the magnitude of this correction cannot be pinned down.

Gauge 2: Expensive-time wedge ($\hat{\Delta}_t$). Rolling 20-day Jensen gap $\approx \frac{1}{2}\hat{\sigma}_t^2$. Negligible ($< 10^{-4}$) in quiet regimes; concentrates sharply during bursts, when IV elevation also raises call premiums.

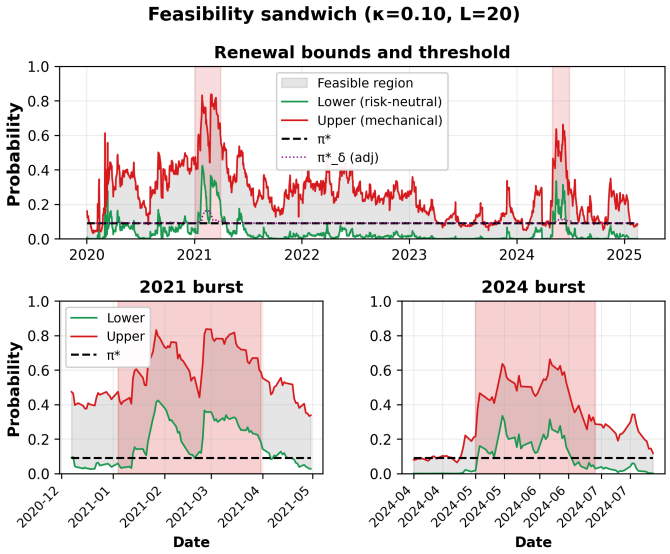

Figure 26: Feasibility sandwich. Lower bound: risk-neutral $P_t^{\text{touch}}(2)$ (probability of an equity doubling within 20 trading days; corresponds to option payoff $L \approx 15$–50 depending on strike). Upper bound: $P_t^{\text{touch}}(1.5)$ (50% equity move; $L \approx 5$–20) plus capacity adjustment. Dashed line: survival threshold π^* (moderate scenario, $\kappa = 10\%$, $L = 20\times$). During bursts, π^* falls below the lower bound on most days; during calm, the lower bound typically falls below π^*.

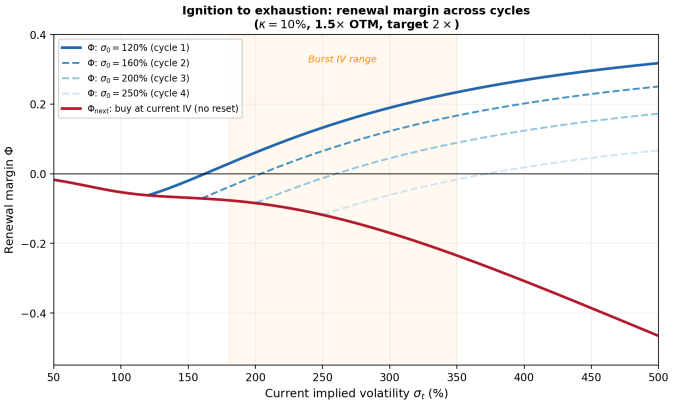

Figure 27: Ignition to exhaustion: renewal margin Φ across successive cycles (Appendix B.2). Blue curves: $\Phi(\sigma_0, \sigma_t)$ for positions purchased at increasing σ_0 (120%, 160%, 200%, 250%; $\kappa = 10\%$, 1.5× OTM, target 2×). Each cycle ratchets σ_0 upward, thinning the margin. Red: $\Phi_{\text{next}}(\sigma)$ for a participant buying at current IV (no reset between cycles). Positive Φ means renewal is time-rational. By cycle 3 ($\sigma_0 = 200\%$) the margin no longer clears even at burst peak; the process exhausts itself through compositional turnover. Orange shading marks the observed burst IV range.

Gauge 3: Market-implied move probability (P_t^{touch}). Risk-neutral probability of touching a given barrier within 20 trading days, read directly from aggregate implied volatility (Appendix C.9). During 2021, median $P_t^{\text{touch}}(1.5) = 0.47$; during calm, ≈0.13. Higher values indicate the options market prices larger moves as more probable.

Gauge 4: OI persistence. Post-OPEX call OI divided by pre-OPEX OI. Values ≥ 1 indicate rolling; values well below 1 indicate speculative washout.

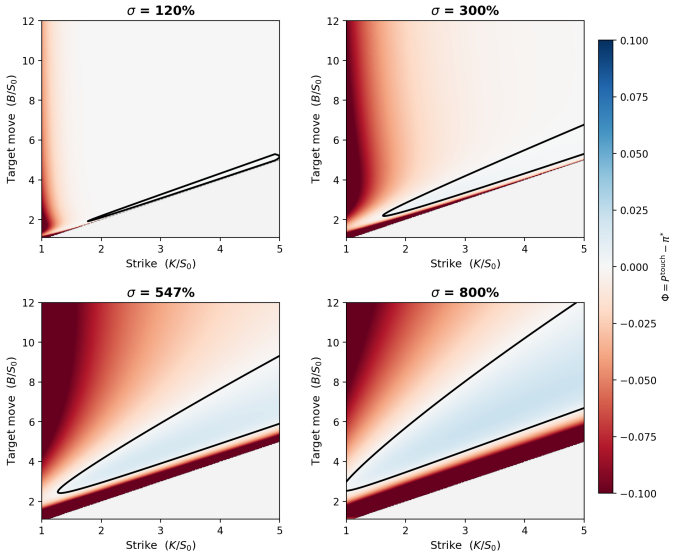

Figure 28: Renewal margin $\Phi = P^{\text{touch}} - \pi^*$ over the strike-target plane at biweekly tenor (10 d), zero drift. Same layout as Figure 11. The feasible zone is narrower than at monthly tenor and requires higher IV to open.

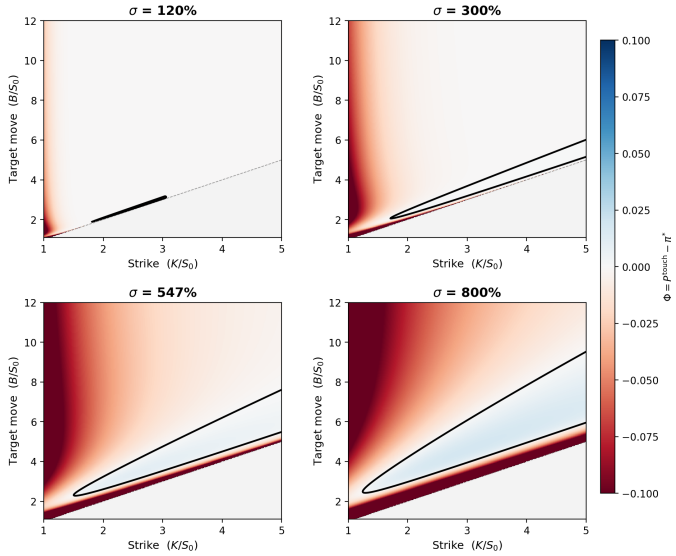

Figure 29: Renewal margin $\Phi = P^{\text{touch}} - \pi^*$ over the strike-target plane at weekly tenor (5 d), zero drift. Same layout as Figure 11. At $\sigma = 120\%$ and 300% no positive region exists; at 547% a narrow feasible zone appears for moderate OTM strikes.

D.6 Calibration sensitivity grid

Table 7: Sensitivity of the positive-Φ window to calibration parameters. Each cell reports the IV window σ_c–σ_u (annualised %) where the static renewal margin is positive. *Strike* is the call's strike price as a multiple of spot (e.g. 1.5× means 50% out of the money). *Move required* is the price move the option must reach to deliver the conditional payoff (e.g. 3× means the stock triples). Baseline calibration (1.5× strike, 3× move, 21-day tenor) shown in bold. "—" means no positive-Φ interval was found in $\sigma \in [50\%, 2000\%]$. "?" after σ_u means the upper boundary exceeds the search range; the window is open-ended within the computed domain. Under the assumptions of Proposition 4, the interval is bounded; the upper boundary in these cases lies above 2000% annualised, a level with no historical precedent for equity options.

Strike (×spot)	Tenor (days)	2× move	3× move	5× move	10× move
1.20	5	—	957–1470	—	—
1.20	10	—	676–1039	1079–?	—
1.20	21	—	467–717	744–1318	—
1.20	42	—	330–507	526–932	—
1.50	5	—	744–1179	1272–?	—
1.50	10	—	526–834	899–?	—
1.50	21	—	**363–575**	621–1225	—
1.50	42	—	257–407	439–866	—
1.75	5	232–252	600–984	1112–?	—
1.75	10	164–178	424–696	786–?	—
1.75	21	113–123	293–480	543–1129	—
1.75	42	—	207–340	384–799	—
2.00	5	—	477–815	979–?	—
2.00	10	—	337–576	693–1492	—
2.00	21	—	233–398	478–1029	—
2.00	42	—	165–281	338–728	—

D.7 Strike-target heatmaps at shorter tenors

Figures 28 and 29 extend the strike-target heatmap of Figure 11 to biweekly (10 d) and weekly (5 d) tenor. At shorter tenors the feasible region (green) shrinks and shifts toward higher IV, consistent with the tenor dependence reported in Table 3: shorter intervals burn premium faster and require larger volatility to generate sufficient touch probability.

E Community persistence infrastructure

This appendix documents observable collective features of the persistence ecology described in Section 5. The infrastructure recorded here sustained participation across years of adverse price action and public ridicule. All dates are sourced from public subreddit records, SEC filings, and contemporaneous reporting.

E.1 Platform migration timeline

Table 8 documents the community's trajectory from January 2021 through early 2026. The community survived platform disruptions—moderator conflicts, subreddit splits, content-policy changes—by reconstituting on successor platforms. The primary platform (r/Superstonk) grew from zero to approximately 900,000 subscribers between March 2021 and mid-2024, sustaining research production, hype-date engagement, and the DRS campaign throughout.

E.2 Moderation architecture as norm infrastructure

Table 9 documents the moderation rules structuring the community's information environment. These rules are the institutional architecture through which the persistence mechanisms of Section 5 operate. *Access barriers* (240-day account age, 4,800 karma to post) filter transient accounts and ensure contributors have a stake in the broader Reddit ecosystem. *No gains/losses* rule removes exited-position screenshots, reducing social salience of exits. *No brigading* rule, adopted under Reddit sitewide pressure disproportionately applied to GME shareholders, prevents community shutdown.

Most rules emerged through iterative community discussion; the no-brigading rule was adopted under external pressure. The community acknowledges that moderation narrows content range and treats this as a necessary cost of maintaining epistemic infrastructure.

Date	Event
Jan 2021	GameStop squeeze begins; r/wallstreetbets (r/WSB) is the primary venue. WSB briefly goes private on Jan 27 amid media attention; Discord server banned for content-policy violations.
Feb–Mar 2021	r/WSB moderators restrict sustained GME discussion. Dedicated GME community migrates first to r/GME, then to r/Superstonk (founded ≈Mar 2021) after moderator disputes on r/GME.
Apr 16, 2021	r/WSB ends the daily GME Megathread; moderators direct remaining GME discussion to r/GME and r/Superstonk.
Apr–Jun 2021	r/Superstonk grows rapidly (>500,000 members by mid-2021). Karma and account-age requirements are introduced to limit bot/shill infiltration.
Jul 2021	Moderator conflict on r/Superstonk (the "runic glory" episode): head moderator removed; ≈30,000 users migrate to r/GMEJungle. r/DDintoGME emerges as a research-focused splinter. r/Superstonk survives and retains the majority of the community.
Oct 2021	GameStop first discloses DRS share count in 10-Q filing (5.2M shares as of Oct 30, 2021). Community begins systematic DRS tracking via bot-reported screenshots.
Jul 2022	GameStop executes 4-for-1 stock split via stock dividend (record date Jul 18, distribution Jul 21). Community discourse intensifies around settlement mechanics.
2022–2023	Quiet accumulation period. r/Superstonk reaches ≈800,000 members. DRS counts rise from 35.6M (Jan 2022, split-adjusted) to peak of ≈76.6M (Jun 2023, split-adjusted). Community produces ongoing DD around SEC filings, options mechanics, and corporate governance. A significant fraction of GME shareholders also held positions in Bed Bath & Beyond (BBBY), linked in part by Ryan Cohen's disclosed BBBY stake (March 2022). BBBY filed for Chapter 11 bankruptcy on April 23, 2023 and was delisted from Nasdaq on May 3, 2023; shares were cancelled in October 2023. After the bankruptcy, displaced BBBY holders became more active on X/Twitter, where—unlike Superstonk, whose content rules restrict discussion to GME—other stocks, speculative cross-asset connections, and political commentary face no restrictions. The GME community on X grew into a parallel venue with substantial overlap with Superstonk, broadening the ecology's interpretive scope.
May 13, 2024	Roaring Kitty returns to X/Twitter after three-year silence. GME opens +50.6% the following session.
Jun 2–7, 2024	Roaring Kitty posts portfolio screenshots on r/Superstonk showing $180M+ GME position (5M shares + 120,000 call contracts). Roaring Kitty conducts YouTube livestream Jun 7; GameStop issues surprise early earnings release same day.
May–Sep 2024	GameStop conducts three ATM equity offerings raising ≈$3.5B total (45M shares in May, 75M shares in Jun–Jul, 20M shares in Sep).
2025	r/Superstonk at ≈930,000 members. Community continues to produce research and monitor corporate actions.

Table 8: Platform migration and collective timeline, 2021–2025. Sources: subreddit records, SEC filings [9, 16, 17], contemporaneous reporting [27, 28, 29].

E.3 Exemplar community artefacts

The claims in Section 5 are grounded in observable community artefacts. This subsection documents representative examples; all are publicly accessible as of early 2026.

Canonical DD. Three examples illustrate the range. "A House of Cards" [38] (April 2021; three parts) examined DTCC custody mechanics and naked-short-selling incentives; "The Dollar Endgame" [39] (June–September 2021; four parts) situated GME within a broader macro-financial fragility thesis; u/Criand's posts on FTD cycles and options mechanics [40] (mid-2021) connected failure-to-deliver patterns to recurring price movements and proposed trading-day cycle lengths that provided testable hypotheses for the community's ongoing analysis. The community-curated SuperStonk Library [41] catalogues dozens of additional DD contributions by topic and date, functioning as the community's institutional memory.

DRS campaign. The direct-registration campaign emerged organically in September–October 2021 after community members identified Computershare as GameStop's transfer agent and began posting confirmation screenshots—displaying the distinctive purple circle of the Computershare portfolio interface—as public proof of registration. A community-maintained bot tracked self-reported DRS totals from screenshot posts; issuer disclosures beginning in late 2021 provided official confirmation. The GME DRS Discovery Timeline [42] documents the campaign's emergence and milestones. A volunteer-run educational site, DRSGME.org [43], aggregates broker-specific transfer guides, publicly verifiable DRS statistics, and advocacy resources, functioning as the campaign's primary public-facing infrastructure. External coverage describes the campaign as unprecedented in scale for a retail direct-registration effort [44].

Persistence rituals. A handful of running jokes have outlasted every news cycle. "MOASS is tomorrow" gets repeated daily as a running joke. The German-market pre-open thread serves a similar role, with European members posting Frankfurt prices hours before New York opens. None of these posts contain analysis or even expect replies; they are roll-call signals, proof that the poster is still around and still holding. That the same phrases have recurred for years, largely unchanged, is itself a

Rule category	Mechanism and collective function
Access barriers	Post: 240-day account age, 4,800 karma. Comment: 120-day account age, 1,200 karma. Filters transient and adversarial accounts; thresholds raised during high-attention periods.
Content relevance	All posts must relate to GME or GameStop. No political content unless directly GME-related. Removes off-topic dilution of the epistemic infrastructure.
No gains/losses	Screenshots of exited positions (gains or losses from sales) removed on sight. Reduces social salience of exits.
No brigading	Adopted by moderators after Reddit's sitewide brigading policy was applied disproportionately against GME shareholders. Automod prevents cross-subreddit linking entirely.
No monetisation	Links to monetised Discord, YouTube, or similar platforms prohibited. Prevents capture of community attention by individual profit motives.
Civility	No intentional rudeness or insults. Maintains the cooperative tone that sustains collective contribution to the DD canon.

Table 9: r/Superstonk moderation architecture and collective function. Rules sourced from subreddit wiki and community documentation.

low-frequency persistence indicator. External coverage has noted the pattern as a defining feature of the post-2021 ecology [45].

References

[1] O. Peters and A. Adamou. The ergodicity solution of the cooperation puzzle. *Philosophical Transactions of the Royal Society A*, 380:20200425, 2022. doi: 10.1098/rsta.2020.0425.

[2] O. Peters. Optimal leverage from non-ergodicity. *Quantitative Finance*, 11(11):1593–1602, 2011. doi: 10.1080/14697688.2010.513338.

[3] O. Peters. The time resolution of the St Petersburg paradox. *Philosophical Transactions of the Royal Society A*, 369(1956):4913–4931, 2011. doi: 10.1098/rsta.2011.0065.

[4] O. Peters. The ergodicity problem in economics. *Nature Physics*, 15(12):1216–1221, 2019. doi: 10.1038/s41567-019-0732-0.

[5] O. Peters and M. Gell-Mann. Evaluating gambles using dynamics. *Chaos*, 26(2):023103, 2016. doi: 10.1063/1.4940236.

[6] O. Peters and M. Gell-Mann. Evaluating gambles using dynamics (Santa Fe Institute working paper page). santafe.edu.

[7] F. Gadenne. Ergodicity Economics in Plain English. *Retirement Management Journal*, 9(1):61–65, 2020. Available at SSRN: ssrn.com.

[8] N. Gârleanu, L. H. Pedersen, and A. M. Poteshman. Demand-based option pricing. *Review of Financial Studies*, 22(10):4259–4299, 2009. doi: 10.1093/rfs/hhp005.

[9] U.S. Securities and Exchange Commission. *Staff Report on Equity and Options Market Structure Conditions in Early 2021*. October 14, 2021. sec.gov.

[10] D. Duffie, N. Gârleanu, and L. H. Pedersen. Securities lending, shorting, and pricing. *Journal of Financial Economics*, 66(2–3):307–339, 2002. doi: 10.1016/S0304-405X(02)00226-X.

[11] G. Calhoun. GameStop/Gamestonk has nothing to do with the madness of crowds. *Forbes*, March 5, 2021. forbes.com.

[12] M. Burry. *Foundations: The Big Short Squeeze — GameStop, The Prequel*. Cassandra Unchained (Substack), Dec. 16, 2025. https://michaeljburry.substack.com/p/foundations-the-big-short-squeeze. Accessed: 2026-01-04.

[13] M. Burry. *Final Stop GameStop: The Jig Is Up*. Cassandra Unchained (Substack), Jan. 26, 2026. https://michaeljburry.substack.com/p/final-stop-gamestop-the-jig-is-up. Accessed: 2026-03-09.

[14] J. E. Fisch. GameStop and the reemergence of the retail investor. *Boston University Law Review*, 102:1799–1858, 2022. ssrn.com.

[15] S. Warkulat and M. Pelster. Social media attention and retail investor behavior: Evidence from r/wallstreetbets. *International Review of Financial Analysis*, 96(B):103721, 2024. doi: 10.1016/j.irfa.2024.103721.

[16] GameStop Corp. Form 10-K for the fiscal year ended January 29, 2022 (includes directly registered share count). U.S. SEC EDGAR, 2022.

[17] GameStop Corp. Form 10-Q for the quarter ended July 30, 2022 (includes directly registered share count). U.S. SEC EDGAR, 2022.

[18] U.S. Securities and Exchange Commission (via Cornell Law School). 17 CFR §242.204 — Close-out requirement (Regulation SHO Rule 204). law.cornell.edu.

[19] U.S. Securities and Exchange Commission. Key Points About Regulation SHO (Investor publication). sec.gov.

[20] FINRA. Rule 11810: Buy-In Procedures and Requirements. finra.org.

[21] Reuters. Panic to close VW shorts as Porsche move surprises. October 27, 2008. reuters.com.

[22] Reuters. VW shares halve as Porsche eases short squeeze. October 29, 2008. reuters.com.

[23] FINRA. FAQ: MMTLP Corporate Action and Trading Halt. March 16, 2023. finra.org.

[24] FINRA. Uniform Practice Advisory (UPC #35-22): Trading and Quotation Halt for Meta Materials PFD SER A (MMTLP). December 9, 2022. finra.org.

[25] Congressional Research Service. Meme Stock MMTLP and FINRA Trading Halt. IN12228, August 21, 2023. congress.gov.

[26] D. Sornette, F. Ulmann, and A. Wehrli. On the Directional Destabilizing Feedback Effects of Option Hedging. Swiss Finance Institute Research Paper Series No. 22–34, 2022.

[27] Reuters. GameStop shares surge as "Roaring Kitty" returns to social media. Reuters, May 13, 2024. https://www.reut

ers.com/technology/gamestop-shares-surge-roaring-kitty-returns-social-media-2024-05-13/. Accessed: 2025-12-15.

[28] Reuters. GameStop shares jump as Keith Gill discloses large position. Reuters, June 2, 2024. https://www.reuters.com/markets/us/gamestop-shares-jump-keith-gill-reveals-large-position-2024-06-02/. Accessed: 2025-12-15.

[29] Reuters. GameStop raises $2.14 billion in stock sale as meme frenzy fades. Reuters, June 11, 2024. https://www.reuters.com/markets/us/gamestop-raises-214-bln-stock-sale-meme-frenzy-fades-2024-06-11/. Accessed: 2025-12-15.

[30] C. Long, B. Lucey, Y. Xie, and L. Yarovaya. "I just like the stock": The role of Reddit sentiment in the GameStop share rally. *Financial Review*, 58(1):19–37, 2023. doi: 10.1111/fire.12328.

[31] V. Semenova and J. Winkler. Self-induced consensus of Reddit users to characterise the GameStop short squeeze. *Scientific Reports*, 12:13780, 2022. doi: 10.1038/s41598-022-17925-2.

[32] L. Lucchini, L. Aiello, L. Alessandretti, G. De Francisci Morales, M. Starnini, and A. Baronchelli. The dynamics of the Reddit collective action leading to the GameStop short squeeze. *npj Complexity*, 2:5, 2025. arXiv:2401.14999.

[33] J. L. Kelly, Jr. A new interpretation of information rate. *Bell System Technical Journal*, 35(4):917–926, 1956. doi: 10.1002/j.1538-7305.1956.tb03809.x.

[34] E. O. Thorp. The Kelly criterion in blackjack, sports betting, and the stock market. In S. A. Zenios and W. T. Ziemba, editors, *Handbook of Asset and Liability Management*, volume 1, pages 385–428. North-Holland, 2006.

[35] T. M. Cover and J. A. Thomas. *Elements of Information Theory*. Wiley-Interscience, 2nd edition, 2006.

[36] M. Burawoy. The extended case method. *Sociological Theory*, 16(1):4–33, 1998. doi: 10.1111/0735-2751.00040.

[37] B. G. Glaser and A. L. Strauss. *The Discovery of Grounded Theory: Strategies for Qualitative Research*. Aldine, Chicago, 1967.

[38] u/atobitt. A House of Cards—Part 1. r/Superstonk, April 21, 2021. https://www.reddit.com/r/Superstonk/comments/mvk5dv/a_house_of_cards_part_1/. Accessed: 2025-12-15.

[39] u/peruvian_bull. Hyperinflation is Coming—The Dollar Endgame (series). r/Superstonk, June–September 2021. https://www.reddit.com/r/Superstonk/comments/o4vzau/. Accessed: 2025-12-15.

[40] u/Criand. The Puzzle Pieces of Quarterly Movements, Equity Total Return Swaps, DOOMPs, ITM CALLs, Short Interest, and Futures Roll Periods. Or, "The Theory of Everything." r/Superstonk, August 2021. https://www.reddit.com/r/Superstonk/comments/pb22oj/the_puzzle_pieces_of_quarterly_movements_equity/. Accessed: 2026-04-02.

[41] u/zedinstead. The SuperStonk Library of DD, Art Books, and Periodicals. r/Superstonk, community-curated archive, continuously updated since 2021. https://fliphtml5.com/bookcase/kosyg. Accessed: 2026-01-10.

[42] GME Timeline. DRS Discovery Timeline. Community-maintained chronology, continuously updated. https://www.gmetimeline.org/drs-timeline/. Accessed: 2026-01-10.

[43] DRSGME. Direct Register Your Shares to Protect Your Investment. Volunteer-maintained educational resource, continuously updated. https://www.drsgme.org. Accessed: 2026-04-04.

[44] Upside Chronicles. GameStop and the Great Direct Registration Experiment. Upside Chronicles, December 11, 2022. https://upsidechronicles.com/2022/12/11/gamestop-and-the-great-direct-registration-experiment/. Accessed: 2025-12-15.

[45] F. Manjoo. The pious Reddit conspiracists holding out for millions. *Slate*, October 2024. https://slate.com/technology/2024/10/reddit-gamestop-stock-wall-street.html. Accessed: 2025-12-15.

[46] U.S. House Committee on Financial Services. *Game Stopped? Who Wins and Loses When Short Sellers, Social Media, and Retail Investors Collide*. Hearing, 117th Congress, February 18, 2021.

[47] GameStop Corp. Form 8-K: Entry into Definitive Agreement (warrant and convertible note offering). U.S. SEC EDGAR, October 2025.

[48] GameStop Corp. Form 10-K for the fiscal year ended February 1, 2025 (capital structure, share counts, equity offerings). U.S. SEC EDGAR, 2025.

[49] D. Abreu and M. K. Brunnermeier. Bubbles and crashes. *Econometrica*, 71(1):173–204, 2003. doi: 10.1111/1468-0262.00393.

[50] A. Barbon and A. Buraschi. Gamma fragility. University of St. Gallen, School of Finance Research Paper, 2021. SSRN 3725454.

[51] L. C. MacLean, E. O. Thorp, and W. T. Ziemba, editors. *The Kelly Capital Growth Investment Criterion*. World Scientific, 2011.

[52] J. D. Hamilton. A new approach to the economic analysis of nonstationary time series and the business cycle. *Econometrica*, 57(2):357–384, 1989.

[53] R. Killick, P. Fearnhead, and I. A. Eckley. Optimal detection of changepoints with a linear computational cost. *Journal of the American Statistical Association*, 107(500):1590–1598, 2012.

[54] V. Kremnev. Critical volatility threshold for log-normal to power-law transition. *arXiv preprint*, arXiv:2601.01269, 2026. https://arxiv.org/abs/2601.01269.

[55] J. E. Hilliard and J. Hilliard. The GameStop short squeeze: Put–call parity and the effect of frictions before, during and after the squeeze. *Journal of Futures Markets*, 43(5):635–661, 2023. doi: 10.1002/fut.22405.

[56] A. Shleifer and R. W. Vishny. The limits of arbitrage. *Journal of Finance*, 52(1):35–55, 1997. doi: 10.1111/j.1540-6261.1997.tb03807.x.

[57] J. A. Scheinkman and W. Xiong. Overconfidence and speculative bubbles. *Journal of Political Economy*, 111(6):1183–1219, 2003. doi: 10.1086/378531.